Poly(ethylene naphthalate) / Clay Nanocomposites: Preparation, Structures and Properties

Chua Yang Choo

School of Materials Science and Engineering

A thesis submitted to the Nanyang Technological University
in fulfilment of the requirement for the degree of
Doctor of Philosophy

2006

ABSTRACT

Poly(ethylene naphthalate) (PEN) is a high performance engineering thermoplastic which is finding increasing applications in the packaging and electronics industries. In the attempts to further enhance the performance of PEN, the development of PEN nanocomposites based on nanoclay presents a promising approach which has hitherto been relatively unexplored. The ease with which the physical states of PEN can be controlled also provides a unique avenue by which the clay-induced modifications to the matrix crystalline phase and its subsequent impact on materials properties can be better studied, to provide greater insights on the structure-property relationships that govern semicrystalline polymer/clay nanocomposites in general.

In this work, the preparation of PEN/clay nanocomposites via two possible routes – in-situ polymerization and melt intercalation was investigated, and the extent of clay dispersion at various length scales was investigated by a combination of x-ray diffraction (XRD), polarizing optical microscopy (POM) and transmission electron microscopy (TEM). In-situ polymerization was found to be limited in most cases due to the high temperature and long-time exposures required for the polymerization of PEN, which invariably leads to degradation of the organoclays and consequently, a poor dispersion of clay in the PEN matrix. On the other hand, with the use of sufficiently thermally stable organoclays possessing good compatibility with the PEN matrix, the melt intercalation method is able to produce nanocomposites with clay homogeneously dispersed at both the nano- and submicron-scale.

The dynamic mechanical properties and thermal stability of the PEN/clay hybrids indicate that the property enhancements exhibited by the hybrids are related to their level of clay dispersion in the PEN matrix. Furthermore, the nanocomposite was

found to display a greater modulus enhancement over neat PEN after both materials were allowed to crystallize. This suggests that in addition to the direct stiffening effect of clay, the clay-induced modifications to the PEN crystalline phase can also result in additional reinforcement in the nanocomposite. Morphological and structural investigations via atomic force microscopy (AFM) and XRD further provide evidence that the additional reinforcement arises from the alignment of the high-aspect-ratio polymer lamellae (along with the clay) in the injection direction, and the orientation correlation that exists between the PEN naphthalene rings and the clay platelets.

The polymorphism behaviors of the PEN/clay hybrids were also investigated by XRD. It was found that pristine Na-MMT exerts a heterogeneous nucleating effect and enhances the formation of the β-crystal form, over the more common α-crystal phase, while the organoclays tend to favor the β-crystal phase at higher temperatures, but the α-crystal form at lower temperatures. Real-time FTIR spectroscopy and XRD reveals that the temperature-dependent polymorphic behavior of the PEN/organoclay hybrids arises because the organoclays could simultaneously exert a hindered heterogeneous nucleating and plasticizing effect. At higher temperatures, the β-phase is enhanced because the hindrance effect causes the dominance of the β-nuclei at the expense of the thermodynamically less stable α-nuclei; at lower temperatures however, stable nuclei of both crystal phases can develop, the plasticizing effect thus becomes dominant, and the kinetically favored α-crystal phase is preferentially formed instead.

Although this work is focused on PEN/clay nanocomposites, the insights gained on the underlying principles governing structural/morphological changes in the nanocomposites, and the subsequent impact on nanocomposite properties may also be applicable to a wider class of semicrystalline polymer/clay nanocomposites.

ACKNOWLEDGEMENTS

I would especially like to thank A/P Lu Xuehong for her amazing patience towards me throughout the course of my PhD, for always being available to assist me, and for making all decisions according to my best interest. It has been a truly rewarding experience doing my PhD under her supervision.

I am much indebted to Dr Daniel Schmidt (University of Massachusetts at Lowell) for graciously offering me so much precious advice on the preparation and characterization of polymer/clay nanocomposites. Thank you for all the insightful discussions and for being a model of optimism and scientific dedication to me.

My greatest appreciation towards the technicians in the School of Materials Science and Engineering (MSE) who have rendered me so much assistance throughout the course of my PhD – Ms Toh Swee Sing, Mr. Wu Shucheng and Mr. Wilson Lim (Polymer Laboratory); Ms Wang Lee Chin, Ms Guo Jun, Mrs Irene Heng and Mr. Maung Zaw Tun (Electron Microscopy and X-ray Diffraction Laboratory), as well as Ms Sandy Leong, Ms Mastura Aidel and Ms Heryani Binte Ahmad (Microelectronics Materials Laboratory).

This work would also not be possible without the facilities and equipment provided by the Institute of Materials Research and Engineering (IMRE). Specifically, I would like to thank Mr. Lim Poh Chong (high-temperature x-ray diffraction), Dr Pramoda Kumari Pallathadka (high-temperature FTIR) and Mr. Chen Ling (ultramicrotomy and microinjection molding) for their kind assistance in the use of these equipment.

Heartfelt thanks also to the research fellows who have imparted to me so much of their technical knowledge – Dr Chen Yu (organic synthesis), Dr Lee Mun Wai

(polymer processing and characterization), Mr. Goh Chin Foo (mechanical testing) and Dr Jacques Plevert (x-ray diffraction).

I am grateful to Lay Kuan, Yeong Huey, Lixin, Hui Tong, Joey, Kit Yan, Mary, Zhang Yan and Joan for their companionship and support throughout the course of my PhD - your friendships have been one of the most valuable rewards of my PhD studies here.

I am indebted to my mother and sister, for all their love, support and understanding. I thank God also, for His bountiful providence in these years, and for demonstrating to me, that His grace is truly made perfect in my weakness.

Finally, I am grateful to the Agency for Science, Technology and Research for awarding me the Local Graduate Scholarship so that I am able to pursue my PhD studies.

TABLE OF CONTENTS

LIST OF TABLES

LIST OF FIGURES

CHAPTER 1

Introduction

1.1 Background

Nanocomposites are composites in which the reinforcement phase has one or more of its dimensions in the nanometer length scale. Polymer/clay nanocomposites are so-called because of the nanoscopic thickness of the high aspect ratio clay sheets when they are delaminated into individual layers in the polymer matrix.

The reason for the burgeoning interest in polymer/clay nanocomposites in the past decade is two-fold. From the engineering point of view, polymer/clay nanocomposites offer an attractive alternative to conventional microcomposites because they often exhibit a quantum leap in performance, such as enhanced mechanical, physical and thermal properties, at relatively low inorganic loadings. Furthermore, in some cases, property changes, such as stiffness and toughness, which are traditionally considered to be inversely related, have been found to improve cooperatively in such systems. From the scientific point of view, this new class of materials often exhibits interesting modifications in their structures and behaviors, which are hitherto unobserved in conventional composite systems. The unique morphology that results when clay particles are dispersed uniformly at the nanometer length scale, where the size of the clay particles is comparable to the spacing between them, coupled with the ultra-large interfacial area, gives rise to a level of interaction that is previously not achievable in traditional microcomposites. This points to the possibility that in addition to their direct reinforcing effect, nanoclays may also direct

the structure and morphology of the polymer matrix. In ideal cases, the unique structural modifications induced by nanoclays can be exploited to work in synergism to the nanoscale dispersion of clay, in improving the properties exhibited by the polymer [1,2].

The key to the unique behaviors and exceptional properties exhibited by polymer/clay nanocomposites is the dispersion of clay into its nanometer-thick layers within the polymer matrix [3,4]. The complete exfoliation of the hydrophilic clay in the typically hydrophobic polymer, however, remains an unresolved issue for many polymer systems. In addition, it remains unclear how specific molecular interactions can be employed to control the structure and morphology of the nanocomposites. The prediction of material properties, based on the nanostructure and dynamics, is also limited by a dearth of structure-property relationships. Without such models, progress in polymer/clay nanocomposites has remained largely empirical.

1.2 Motivation

This work is focused on the preparation of poly(ethylene naphthalate) (PEN) / clay nanocomposites and the characterization of their structures and properties. PEN (Figure 1.1) is a high-performance polyester that is attracting increasing commercial attention after its price is made more accessible following the development of a major facility for the large-scale production of its monomer dimethyl naphthalene-2,6-dicarboxylate (DMN) [5]. The naphthalene ring in PEN provides greater rigidity to the polymer backbone than the benzene ring in the closely related system of poly(ethylene terephthalate) (PET). This imparts to PEN, a higher melting and glass transition temperature, and enhances its mechanical properties, dimensional stability and barrier properties with respect to PET. These properties make PEN more suitable

than PET for higher temperature or more demanding engineering applications, for instance as base dielectric films for flexible electronic substrates, ultrathin data storage tapes, high-performance tire-cord yarn, and hot-filled plastic containers. At the same time, the performance characteristics, thermal stability, transparency and ease of processing of PEN also make it a strong contender as a potential cost-effective substitute for other engineering thermoplastics and thermosets.

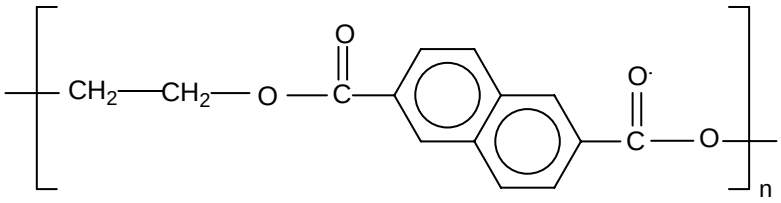

Figure 1.1 Structural formula of PEN

Although there have been numerous attempts in the preparation of polymer/clay nanocomposites based on a wide variety of polymers, including semi-rigid polyesters such as PET and PBT (poly(butylene terephthalate)), the PEN polymer system has been relatively unexplored. In the attempts to improve the performance of PEN in its current applications, or in extending its use to more demanding engineering applications, the development of PEN nanocomposites based on nanoclay fillers presents a promising approach by which the desired property enhancements may be realized. It is hoped that the incorporation of clays into PEN at the nanoscale may further enhance its mechanical, thermal and barrier properties, without sacrificing other properties (such as toughness and transparency).

In the field of polymer/clay nanocomposites, substantial fundamental efforts have also been expended in understanding the origins of the unique combinations of properties exhibited by this class of materials. For semicrystalline polymers in particular, nanoclay-induced modifications to the polymer crystalline phase, such as alterations to the crystalline morphology, crystallite orientation, crystal structure and degree of crystallinity, have often been highlighted as an important reason contributing to the property enhancements in the materials [1,2]. In this context, the PEN polymer serves as a useful model system by which the influence of nanoclay on the development of the polymer crystalline phase, and its subsequent impact on material properties can be better understood. As a slow-crystallizing semicrystalline polymer, PEN can be easily quenched into the completely amorphous state. This characteristic provides PEN with the unique advantage in that the effects of the modified crystalline phase on the nanocomposite properties may be more easily isolated and determined. Insights gained from studying the PEN system may also help to elucidate general principles by which changes in the matrix crystalline structure can alter the properties of the nanocomposites - an understanding of which is essential in order for nanocomposite properties to be more precisely predicted and controlled.

The ease with which the physical states of PEN can be controlled also points to the possibility that it can serve as a useful system by which additional insights may be gained on the underlying principles governing polymorphic and mesostructural changes in semicrystalline polymer/clay nanocomposites. Knowledge gained on the PEN system can serve as a platform by which similar structural modifications may be more precisely engineered in other semicrystalline polymer systems so that they can be exploited to achieve property enhancements.

1.3 Thesis Scope and Organization

Due to the current lack of success in the preparation of PEN/clay nanocomposites, the first issue that this thesis aims to address is the development of PEN/clay nanocomposites. In this respect, two preparation routes – in-situ polymerization and melt intercalation were investigated, and their merits and limitations for the preparation of PEN/clay nanocomposites evaluated.

The second objective of this thesis is to gain a fundamental understanding of the structure-property relationship in the newly developed PEN/clay nanocomposites. Specifically, the dynamic mechanical behaviors and thermal stability of the hybrids were examined and correlated with the hierarchical structures of the materials.

Finally, the polymorphism behavior of the PEN/clay nanocomposites was examined. The investigation was directed towards providing a more fundamental understanding of the origins of clay-induced polymorphism, which is not only specific to the PEN system but may also be extended to other semicrystalline polymers.

It is hoped that this series of investigations on the PEN/clay nanocomposite system may reveal additional insights on the underlying principles governing the structural modifications commonly observed in semicrystalline polymer/clay nanocomposites, as well as provide a greater understanding on how some of these structural alterations may eventually be translated into the properties of the nanocomposites.

This thesis begins with the background which provides the motivation for the preparation and study of PEN/clay nanocomposites. Chapter 2 reviews the structures, preparation and properties of polymer/clay nanocomposites. The routes that have been explored for the preparation of the PEN/clay hybrids are described in Chapter 3. In particular, the strategies employed, critical issues involved, as well as the important

conclusions that were made about the approaches employed are presented. Chapter 4 presents the dynamic mechanical and thermal properties of the PEN/clay nanocomposites. Possible mechanisms for property enhancements in the materials were also proposed based on their morphological organization. Chapter 5 examines the effects of nanoclay on the type of crystal structure developed in PEN. The in-situ crystallization behaviors of the hybrids were also discussed toward providing insight into the origins of the clay-induced polymorphism behavior observed. Finally, Chapter 6 summarizes the important findings that have been made in this work, and Chapter 7 proposes potential areas for future research.

CHAPTER 2

Morphologies, Preparation and Properties of Polymer/Clay Nanocomposites – A Review

2.1 Introduction

The formation of polymer/clay nanocomposites relies on the ability of monomers or polymers to intercalate into the spaces between the layered structures of clay. In this chapter, the structure and properties of clay will first be briefly described to gain an understanding of the basis for the design of synthetic routes for the preparation of such nanocomposites. The possible morphologies that can be exhibited in polymer/clay nanocomposites will then be introduced, as the morphology of a nanocomposite is a crucial factor in determining the final structures and properties of the material. The main approaches of nanocomposite preparation will next be reviewed. Particular focus will be given to the approaches by which the chemistries of the clays and the polymers were fine-tuned to improve compatibility and interaction with the polymer phase, as this forms the key by which clay can be dispersed in the polymer matrix at the nanoscale. Finally, the outstanding improvement in properties exhibited by this new class of materials, which provides the main motivation for its development, will be reported.

2.2 Structure of Clay

Clays or layered aluminosilicates are crystalline materials consisting of layers made up of an octahedral sheet of alumina fused to two tetrahedral sheets of silica (refer to

Figure 2.1). Stacking of the layers leads to a regular van der Waals' gap between the layers called the interlayer or gallery. Although the thickness of each layer is only 1 nm, the lateral dimensions of the layers may range from 30 nm to as large as several microns [4,6].

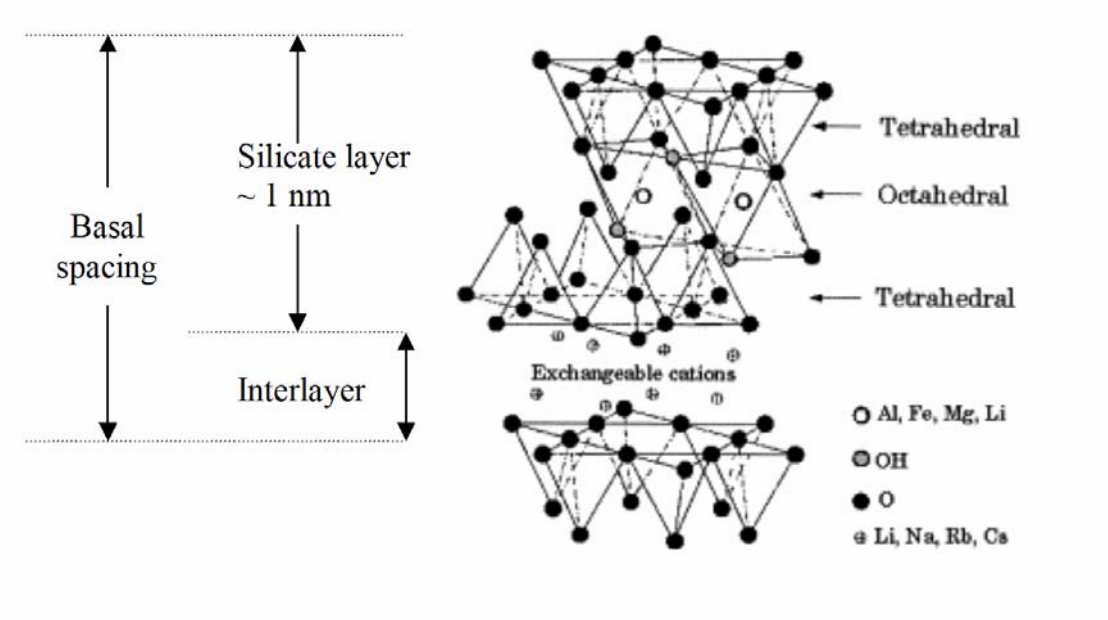

Figure 2.1 Structure of clay [6]

Isomorphic substitutions (for example, Al^{3+} replaced by Mg^{2+}, or Mg^{2+} replaced by Li^{+}) within the layers lead to a net negative charge which must be counterbalanced by cations that are situated in the interlayer space, such as Na^{+} or K^{+} ions. These interlayer cations can be exchanged by organic cations such as alkylammonium ions. The exchange reaction is the basis by which the originally hydrophilic clay surface can be rendered organophilic. The presence of organic ions in the interlayers lowers the surface energy of the clay surface, so that they can be more easily wetted by a polymer [3,4,6].

Montmorillonite (MMT) is the most common type of clay used in polymer/clay nanocomposites. Its chemical structure is given by $(Na,Ca)_x(Al_{4-}$

$_xMg_x)Si_8O_{20}(OH)_4$ where x refers to the degree of isomorphous substitution (between 0.5 and 1.3).

2.3 Properties of Clay

Clays are good candidates for the preparation of inorganic-organic nanocomposites. They are abundant in nature, inexpensive, chemically stable and possess both high aspect ratio and high strength – all of which are important indices for application as reinforcing agents.

On top of the above properties, two important characteristics of clay make them a natural choice of selection for the preparation of nanocomposites [3,4]. Firstly, their layered structure means that it is possible to separate them into individual sheets, each of which is only 1 nm thick. For fully-dispersed clays, an aspect ratio of as high as 1000 can be achieved. Secondly, the possibility of ion-exchange within the interlayers provides clay with a rich intercalation chemistry. The surface chemistry of clays can be fine-tuned through ion exchange with various organic or inorganic cations to make them compatible with a wide range of polymers.

2.4 Structures of Polymer/Clay Composites

When clays are added to a polymer matrix, three types of structures can be expected – a phase-separated microcomposite, an intercalated nanocomposite and an exfoliated nanocomposite (refer to Figure 2.2) [4].

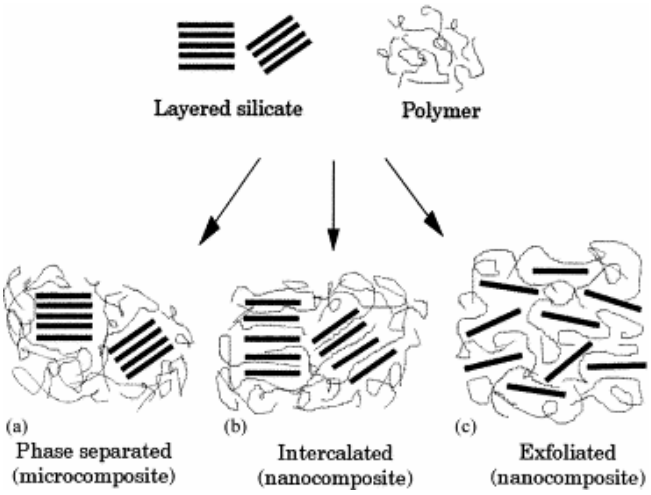

Figure 2.2 Schematic illustration of terminologies used to describe composites arising from the addition of clay to polymer: (a) phase-separated microcomposite; (b) intercalated nanocomposite; and (c) exfoliated nanocomposite [4].

When the polymer is unable to enter the spaces between the clay layers, and the clays still remain in the form of large stacks known as tactoids, a phase-separated microcomposite results. The properties of such composites remain in the same range as conventional microcomposites.

When the extended polymer chains are inserted into the spaces between the clay layers, an intercalated nanocomposite is obtained. In this state, the clay preserves its well-ordered multilayered morphology, although the separation between the individual layers is often increased due to the presence of the polymer which is sandwiched between the clay layers.

With extensive penetration of the polymer chains into the clay galleries, the clay can be completely delaminated into individual nanometer-thick layers. When the clay loses its regular layer register and becomes disordered and uniformly suspended in a continuous polymer matrix, an exfoliated nanocomposite results.

At this point, it is important to note that very often, more than one type of morphologies will be present in a nanocomposite.

2.5 Preparation of Polymer/Clay Nanocomposites

The successful preparation of a polymer/clay nanocomposite, in which the clay layers are uniformly dispersed into its nanometer thick layers, hinges on the satisfaction of two conditions - suitable compatibilization of the originally hydrophilic clay layers with respect to the polymer matrix of interest, and effective mixing and dispersion of the clays to take advantage of such compatibility.

2.5.1 Clay Modification

Clays are polar and hydrophilic; polymers are in most cases, much more hydrophobic, and therefore incompatible with clays. For this reason, the clays must be made compatible with the polymer matrix of interest, to allow the intercalation of the polymer – only when the two components are thermodynamically compatible, will they form and retain the desired nanoscale dispersion state.

Modification of clays is most commonly achieved by ion-exchange reactions with cationic surfactants, such as alkylammonium ions. The substitution of the interlayer cations with organic cations lowers the surface energy of the clay surface, so that they can be more easily wetted by a polymer. At the same time, it enlarges the interlayer spacing of the clay, and reduces the attractive forces felt by the clay layers. Additionally, the surfactants may be tailor made so that they contain functional groups that are able to react with the polymer matrix, or initiate/catalyze the polymerization of the monomers.

The specific ways in which the chemical structure of the surfactant ions may be custom-made to enhance thermodynamic compatibility with the polymer, and/or enhance dispersion in the polymer matrix, will be discussed, with the help of salient examples, in the following section.

2.5.2 Nanocomposite Production

2.5.2.1 Solution Intercalation

Due to the weak forces that stack the layers together, clays can be easily dispersed in an adequate solvent. Solution intercalation is based on a solvent system in which the polymer is soluble and the clay is swellable in [4]. When the polymer and clay solutions are mixed, the polymer chains can intercalate and displace the solvent within the interlayer of the silicate. The driving force for the intercalation of the polymer into the clay layers is the entropy gained by the displaced solvent, which compensates for the entropy loss of the polymer chains when they become confined within the clay interlayers. In the wet state, the clay may be dispersed into individual layers in the solution. Upon solvent removal however, the clay layers tend to reassemble again and sandwich the polymer to form at best, an intercalated nanocomposite.

Solution intercalation has been used to prepare intercalated nanocomposites for water-soluble polymers, such as poly(vinylpyrrolidone) (PVP) [8,9], poly(ethylene oxide) (PEO) [10,11], poly(vinyl alcohol) (PVA) [11,12] and poly(acrylic acid) (PAA) [13]. Solution intercalation can also be applied to non-aqueous solvent systems. For example, polylactide (PLA) [14] and poly(ε-caprolactone) [15] nanocomposites have been prepared by dissolving the polymer in hot chloroform in the presence of a given amount of clay modified with distearyldimethylammonium

cations. High-density polyethylene (HDPE)-based nanocomposites have also been prepared by dissolving the polymer in a mixed solvent system of xylene and benzonitrile with 20 wt% of dodecylamine-modified clay dispersed within [16].

Solution intercalation is a useful way of preparing nanocomposites for polymers that have little or no polarity into layered structures, and facilitates the production of thin films with oriented clay layers. It is however, often not feasible from a commercial point of view, due to the need for large amounts of organic solvents, which is both economic prohibitive and environmentally unfriendly.

2.5.2.2 In-situ Polymerization

In-situ polymerization involves the dispersion of clay in a suitable monomer, followed by polymerization. Monomers, being smaller in size, tend to undergo a smaller entropic loss when they diffuse into the clay galleries. They are therefore, expected to intercalate more easily compared to the corresponding polymer. The monomers are then polymerized within the clay layers. Ideally, as polymerization inside the clay gallery progresses and the polymer chain density increases, the clay layers can be gradually pushed apart and eventually delaminate, resulting in a well-dispersed nanocomposite.

In order for the clay layers to be delaminated during the polymerization process, the intragallery polymerization needs to proceed faster than the extragallery polymerization. To achieve this, the clay is often intercalated with modifiers that possess functional groups which are able to catalyze the polymerization reaction [17-19]. Another important factor is the accessibility of the monomers to the clay galleries. Before the polymerization can take place at the clay galleries, the monomers must first be present in the gallery spaces. After the polymer chains start to grow,

additional monomers must be able to enter the galleries. Delamination of clay is often limited when monomer diffusion into the clay galleries is not facilitated by proper modification of the clay surface [18,19].

In-situ polymerization may also make use of reactive surfactants which possess functional groups that are able to form covalent bonds with the intercalated monomers [20,21]. In the same way, a polymerization initiator may be ion-exchanged into the clay galleries. In this case, if no other source of initiation is present, the polymerization will be forced to take place inside the clay galleries. As the polymer chain density within the clay galleries increases, the clay layers can eventually be delaminated [22,23].

2.5.2.3 Melt Intercalation

Melt intercalation involves mixing the clay with the polymer and heating the mixture above the softening point of the polymer [24,25]. Shear forces, encountered using conventional compounding equipment, are often employed to facilitate the mixing of the polymer and the clay. In addition, the clays are often organically-modified, for instance, via ion exchange reactions with organic cations, to improve its compatibility with polymers.

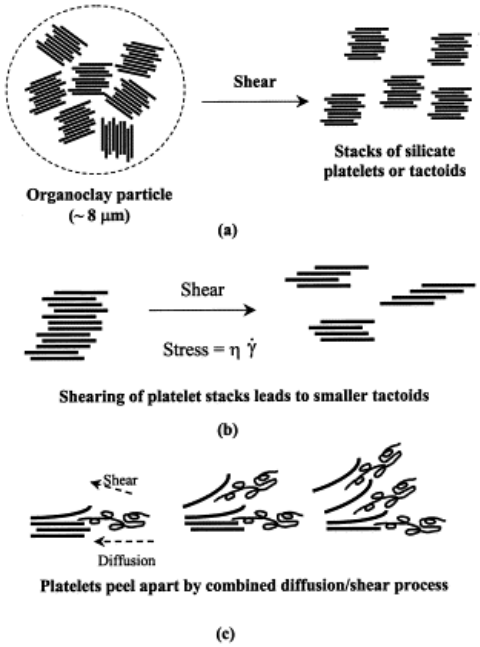

Figure 2.3 Stepwise mechanism of clay platelet exfoliation during melt intercalation: (a) breakup of organically-modified clay, (b) breakup of intercalated organically modified clay and (c) platelet exfoliation [26].

Melt intercalation offers great potential industrially because it is extremely compatible with current mixing and processing techniques used in industries. It offers the prospect of producing nanocomposites using conventional industrial processes such as extrusion and injection molding. It is more versatile than in-situ polymerization because it does not require the involvement of resin producers. In addition, the process is more environmentally benign compared to solution intercalation due to the absence of organic solvents.

Several studies have been attempted to generalize the relationship between organoclay structure and the degree of clay dispersion achieved in the polymer matrix. Vaia and Giannelis [24,25] have developed a mean-field lattice-based model for the selection of potentially compatible polymer-organoclay systems. Based on the model, the success of melt intercalation in delaminating the clay depends on an

interplay of both entropic and enthalpic factors. Although confinement of the polymer within the clay interlayers results in a decrease in the overall entropy of the polymer chains, this entropic penalty may be compensated by the greater conformational freedom of the tethered surfactant chains when the clay layers separate. For small increases in interlayer spacing, the total entropy change is expected to be small, thus changes in the system's total enthalpy plays a crucial role in determining whether intercalation is thermodynamically possible. Complete delamination of the clay layers thus hinges strongly on the maximization of the amount of favorable polymer-clay interactions and the minimization of unfavorable non-polar interactions between the polymer and the aliphatic surfactants on the clay.

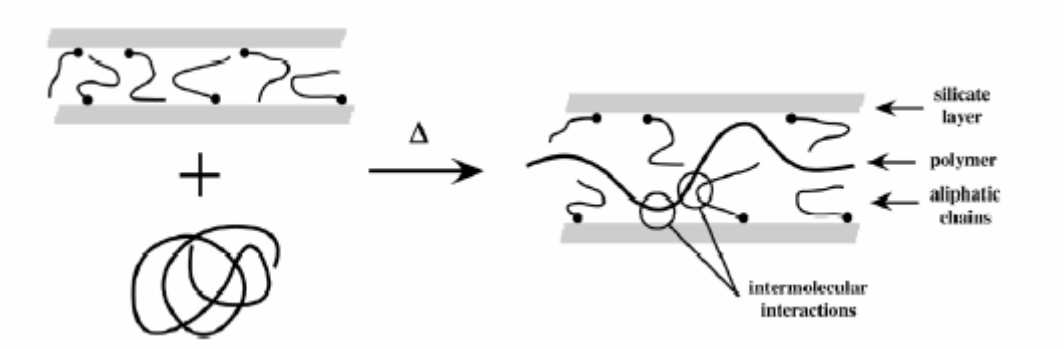

Figure 2.4 Schematic representation of the system components before and after intercalation takes place [6].

The importance of polymer-organoclay thermodynamic interactions during melt intercalation was also investigated experimentally by Paul *et al*. In particular, the effect of the number of alkyl tails attached to the nitrogen of the organoclay on clay dispersion was examined. For nylon-6, it was found that organoclays made from amines containing one long alkyl group lead to better exfoliation than surfactants

containing two long alkyl groups. As nylon-6 is a relatively polar polymer, it has a relatively good affinity for the polar clay surface. The better dispersion observed with only one alkyl tail is attributed to the better accessibility of the nylon-6 segments to the clay surface for favorable nylon-6-clay interactions to take place [27,28]. On the other hand, linear low-density polyethylene (LLDPE)/clay nanocomposites exhibit better dispersion with organoclays possessing two rather than one alkyl tails [29]. This is due to the non-polar nature of LLDPE, which means that it will require a more non-polar modifier for it to be energetically favorable to displace the modifier from the clay surface.

For polymers which do not possess any polar groups, dispersion of clay could not be achieved even with the use of organically-modified clay. For these polymers, polar functionalities are often grafted onto the polymer to improve its ability to interact with the organoclays during the melt intercalation process. This approach is most commonly employed for the production of polyolefin/clay nanocomposites. For instance, maleic anhydride grafted polypropylene (PP-g-MA) is often introduced as a compatibilizer to mediate the polarity difference between polypropylene and the clay surface. Exfoliated and homogeneous dispersion of clays in the polymer can be achieved by optimizing the content of polar functional groups in the oligomers (to allow sufficient interaction with the clay layers via hydrogen bonding), whilst maintaining a good miscibility with the polymer matrix [30].

The effect of the incorporation of ionic groups on the backbone of the polymer on clay dispersion has also been investigated for the system of poly(butylene terephthalate) (PBT) [31]. In this study, ionic groups were incorporated into the polymer by melt copolymerization of dimethyl terephthalate and 1,4-butanediol with dimethyl-5-sodiosulfoisophthalate. The presence of low levels of sodium sulfonate

(SO_3Na) groups (1.0 - 5.0 mole %), coupled with the use of an organically-modified clay results in the formation of highly exfoliated nanocomposite by simple melt compounding. The negatively charged SO_3Na groups help to enhance interactions between the polymer and the positively-charged edge surfaces of the clay platelets. With attachment of the polymer chains at the site of entrance to the galleries, diffusion of the mobile chain segments into the organically-modified clay galleries is facilitated. This intercalation, driven by favorable enthalpic interactions between the organic modifiers and the organic polymer chains, provides the force to peel apart the individual clay layers to produce an exfoliated structure.

2.5.2.4 Other Critical Issues

(I) Organoclay Degradation

Elevated temperatures are generally required for the production and/or subsequent bulk processing of nanocomposites. When high temperatures are used however, another complication arises – degradation of the organic clay modifiers. Most conventional alkylammonium-treated clays have an onset thermal decomposition temperature of about 200^{o}C or below [32], way below the processing temperatures required for many polymers. The issue of modifier degradation during nanocomposite preparation is not trivial, as it often has a detrimental effect on the carefully tailored interface between the clay surface and the polymer matrix. Clay surfactant degradation often leads to a loss of favorable interactions between the clay and the polymer, as well as irreversible layer collapse [32]. The result is a poor dispersion of clay in the hybrids. In addition, the decomposition of the modifiers may initiate degradation reactions within the polymer matrix itself, resulting in molecular weight reduction, discoloration, and loss of mechanical properties [33,34].

The limited thermal stability of the alkylammoniums that are commonly used to modify the surface of clay has motivated the development of new organic modifiers, such as phosphonium, pyridinium, iminium, and imidazolium cations [34] which possess greater thermal stability. The use of these thermally stable systems should enable the preparation of polymer/clay nanocomposites based on thermoplastic polymers with high processing temperatures and themoset polymers with high cure temperatures, which are hitherto inaccessible.

(II) Processing Conditions

Although not discussed in great detail in this review, it is essential to note that in addition to the compatibilization strategy, processing conditions also play a very important role in the preparation of polymer/clay nanocomposites [35]. For example, the shearing profile used in melt compounding must be optimized to ensure that all agglomerates are broken up, and multilayer stacks separated (as even the presence of a single micron-sized agglomerate can lead to premature failure under load), without fracturing them along their lateral dimensions (which will reduce the aspect ratio of the clay particles) [36]. Similarly, to achieve good mixing, a longer mixing time is preferred, but this must be balanced against the thermal degradation of the organic modifiers and/or polymers, which becomes more serious when the materials are subjected to high temperatures for extended times.

With that said though, optimization of processing conditions alone cannot compensate for a lack of compatibility between the polymer and the clay, to bring about nanoscale dispersion of clay.

2.5.3 Previous Work on PEN and PET/Clay Nanocomposites

In this section, the various approaches that have been employed for the preparation of PEN/clay nanocomposites, as well as the closely related PET/clay nanocomposite system will be reviewed to provide the background against which the potential issues that will be involved in the preparation of PEN/clay nanocomposites can be better anticipated.

2.5.3.1 PEN/Clay Nanocomposites

Little has been reported on the preparation of PEN/clay nanocomposites prior to this study. The closest attempt was based on a copolymer system based on poly(ethylene terephthalate-co-ethylene naphthalate) (PETN) with the solution intercalation method [37,38]. In the preparation of the nanocomposites, PETN was dissolved in N,N-dimethylacetamide (DMAc) in which the organoclay had been dispersed in. Mixing and dispersion was achieved by vigorous stirring before the suspension was cast into films. X-ray diffraction and transmission electron microscopy indicates that with a Cloisite 25A organoclay (dimethyltallow-2-ethylhexyl-modified clay), an exfoliated nanocomposite can be produced, whereas organoclays based on hexadecylammonium, dodecyltrimethylammonium or Cloisite 30B (bis(2-hydroxyethyl)methyl tallow ammonium-modified clay) yielded only intercalated structures. As discussed earlier however, the commercial viability of the solution intercalation method is very limited. The preparation of nanocomposites based on PEN (rather than the copolymer) with the solution intercalation method is further restricted by the absence of good non-toxic solvents for PEN.

A very recent effort in the preparation of PEN/clay nanocomposites made use of clays that have been modified by n-hexadecyl trimethylammonium bromide

(CTAB) cations and which were subsequently polymerized with a mixture of styrene and methyl methacrylate monomers [39]. The polymerization of the exchanged clays was performed to enhance the compatibility between the rigid PEN polymer and the organoclay. The PEN/clay nanocomposite was then formed by direct melt intercalation. In the report however, the ability of the PS/PMMA polymer to intercalate into the clay sheets during polymerization, as well as the ability of the organically-treated clay to withstand the melt compounding conditions have not been addressed.

2.5.3.2 PET/Clay Nanocomposites

Because of the limited prior efforts on the preparation of PEN/clay nanocomposites, the approaches for the preparation of PET/clay nanocomposites will also be reviewed in this section. Due to the great similarity in the chemistry and preparation of PEN and PET, the previous work on PET/clay nanocomposites shall serve as a useful guideline from which the strategies for the preparation of PEN/clay nanocomposites in this work can be more appropriately determined.

Imai *et al* prepared PET/clay nanocomposites based on a novel reactive clay modifier 10-[3,5-bis(methoxycarbonyl)phenoxy]decyltriphenylphosphonium] [20]. The dimethyl isophthalate groups provide opportunity for covalent bond formation with PET via transesterification reactions during in-situ polymerization, while the triphenylphosphonium group provides additional thermal stability for the modifier to withstand the polymerization conditions of PET without degrading severely. Although complete exfoliation was not achieved, the flexural modulus of the nanocomposites was increased by 170%.

To address the issue of organoclay degradation, Davis *et al* employed a 1-hexadecyl-2,3-dimethylimidazolium-modified clay for the preparation of PET/clay nanocomposites via melt blending [33]. The resulting PET/clay nanocomposites exhibited a high degree of dispersion with no micron-sized particles, while nanocomposites prepared with the conventional dimethyldioctadecylammonium-modified clay reference were black, brittle and tarlike.

Tsai and co-workers recently reported on a different approach for the preparation of exfoliated PET/clay nanocomposites via an in-situ polymerization process [19]. In their work, clays were treated with a combination of antimony (III) acetate and acidified sodium cocoamphohydroxypropylsulfonate (SB). Antimony (III) acetate, which can act as the polycondensation catalyst for the polymerization of PET, helps to create active sites within the clay layers for polymerization to take place, while the organic modifier SB helps to improve the compatibility as well as the opportunity for bond formation between the clay and the polymer. The exfoliated clay structure achieved with this method was attributed to the occurrence of polymerization within the clay galleries, which provides the driving force by which the clays can be broken down into individual disordered layers.

2.6 Properties of Polymer/Clay Nanocomposites

The presence of clay dispersed at the nanometer scale often results in a dramatic improvement in properties, far greater than what is expected from such a small addition (within a few weight percent) of inorganic fillers. In particular, polymer/clay nanocomposites have been reported to trigger tremendous enhancements in mechanical, thermal and barrier properties. These will be reviewed in the following

section to gain a better insight of the important factors that contribute to the great improvement in properties observed in this class of materials.

2.6.1 Mechanical Properties

(I) Tensile Modulus

Tensile modulus, or Young's modulus is the stiffness of a material, as measured at the beginning of a tensile test. Exfoliated nylon-6/clay nanocomposites demonstrated a drastic improvement in tensile modulus, at relatively low filler concentrations [1]. The dramatic improvement in tensile modulus is attributed to the strong interaction between the matrix and the clay layers via the formation of hydrogen bonds (Figure 2.5). Furthermore, the extent of improvement of the modulus is found to be directly dependent on the aspect ratio. The reduction in tensile modulus with a reduction in clay exfoliation indicates that the presence of exfoliated layers is the main factor responsible for the improvement in stiffness, while intercalated particles, having a smaller aspect ratio, tend to play only a minor role.

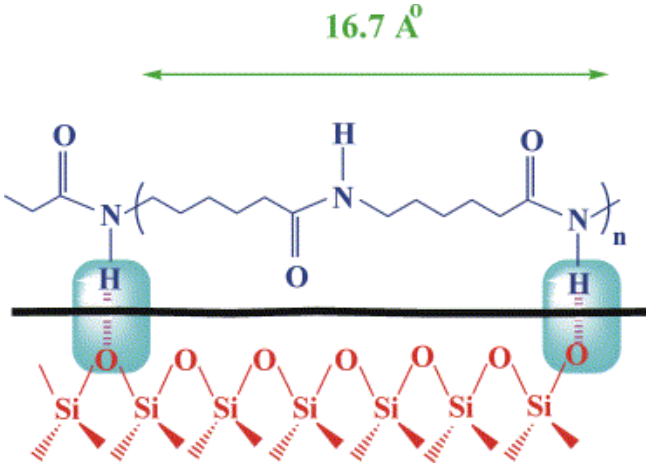

Figure 2.5 Schematic illustration of hydrogen bond formation in a nylon-6/clay nanocomposite [3].

The same reasons account for the evolution in Young's modulus observed in PP/clay nanocomposites [40]. Increasing the amount of PP-g-MA helps to improve interactions between the PP matrix and the organoclay. The tensile modulus increases with PP-g-MA content, as the dispersion of clay in the polymer matrix is improved, and the stress can be much more efficiently transferred from the polymer matrix to the inorganic filler. (The lower Young's modulus for pure PP-g-MA ruled out any possibility of matrix stiffening due to the increasing amounts of PP-g-MA.)

In contrast, for simply intercalated structures (without any exfoliation), such as PMMA [41] or PS [42] based nanocomposites, the Young's modulus increased only slightly. This result again attests for the inefficiency of intercalated structures in improving the stiffness of the polymer matrix.

Dispersion is however, not the only factor that determines the tensile modulus of the resulting nanocomposites. Nanocomposites of an elastomeric epoxy matrix were prepared using different kinds of layered silicates [43]. It was found that a much more significant increase of the tensile modulus was observed for the montmorillonite-based nanocomposites for filler contents greater than 4 wt%. The authors explained this behavior by the difference in layer charge density for magadiite and montmorillonite. Organomagadiites have a higher layer charge density and consequently, higher alkylammonium content than organomonmorillonite. As the alkylammonium ions interact with the epoxy resin during polymerization, dangling chains are formed. More of these chains are thus formed in the presence of organomagadiites. These dangling chains are known to weaken the polymer matrix by reducing the degree of network crosslinking. As a result, the reinforcement effect of the silicate layer exfoliation is compromised.

In addition, Zilg and co-workers [44] reported about rather weak improvements in stiffness for anhydride-cured epoxy-based nanocomposites, even though true exfoliated structures were observed. For these authors, the real key for the matrix stiffness improvement lies in the formation of supramolecular assemblies obtained by the presence of dispersed anisotropic laminated nanoparticles. Furthermore, the importance of interaction at the clay-polymer interface is emphasized, as a stiffening effect is observed when the montmorillonite is modified by a functionalized organic cation (carboxylic acid or hydroxyl groups) that is able to interact with the matrix during curing.

(II) Stress at Break

Stress at break refers to the ultimate strength that a material can bear before failure. Stress at break of nanocomposites has been demonstrated to vary strongly, depending on the nature of the interactions between the matrix and the filler.

Exfoliated nylon-6-based nanocomposites [1] exhibit an increase in their stress at break. This is attributed to the exfoliated nanocomposite structure formed, as well as the presence of ionic interactions between the polymer and clay layers. On the other hand, for PP-based nanocomposites [40], no or only very slight tensile stress enhancement is observed. This effect can be partially explained by the lack of interfacial adhesion between the apolar PP and the polar clays.

(III) Dynamic Mechanical Analysis

Dynamic mechanical analysis (DMA) measures the response of a material to an oscillatory deformation (usually tension or three-point flexion type deformation) as a function of temperature. Three important parameters can be obtained from DMA: (1)

the storage modulus (E') which indicates the elastic response to the deformation; (2) the loss modulus (E'') which indicates the plastic response to the deformation; and (3) the loss tangent (tan δ), which is given by the E''/E' ratio.

DMA of a series of PP/clay hybrids [40] displayed a corresponding increase in the storage modulus when the amount of maleic anhydride added was increased. This is again attributed to the better dispersion of clay when better compatibility between the clay and the PP matrix is achieved.

The effect of dispersion and length of the layered particles on the storage modulus was also demonstrated in a study based on poly(imide)/clay nanocomposites [45]. At a given temperature, a higher storage modulus was obtained from better clay dispersion. In addition, the higher storage modulus for the exfoliated montmorillonite nanocomposite, as compared to the exfoliated mica-based nanocomposite, was attributed to the higher aspect ratio of the dispersed silicate layers, as observed under the TEM.

Finally, DMA studies on organoclays exfoliated within an epoxy matrix revealed a dramatic improvement in the storage modulus, especially above T_g [46] – with the addition of 4 vol% clays, a 58% increase in modulus was observed below T_g. Above T_g however, the storage modulus increased by a factor of 4.5. Above T_g, the polymer matrix softens, the reinforcement effect of the clay particles thus becomes more prominent due to the restricted movement of the polymer chains.

The above results suggest that an exfoliated structure is the key to the dramatic improvement in storage modulus observed in polymer/clay nanocomposites. A possible mechanism by which exfoliated clay achieves this is by the creation of a three-dimensional network of long interconnected silicate layers through strong edge-edge interaction of the clay particles. Due to this flocculation, the length of the clay

particles increases enormously, resulting in a corresponding increase in the overall aspect ratio [3,4].

(IV) Toughness

Toughness is the energy absorbed by a material as it fractures. The addition of reinforcing elements usually leads to a reduction in the toughness of the material, however, a simultaneous improvement in both stiffness and toughness has been observed in several polymer/clay nanocomposite systems.

Shah *et al* reported an order-of-magnitude increase in the toughness of polyvinylidene fluoride (PVDF), with a concurrent increase in stiffness after the addition of nanoclay [2]. The dramatic improvement in toughness is attributed to structural and morphological changes induced by the presence of nanoclay, which contributes to new energy dissipation mechanisms during deformation. It was postulated that the nucleation of the fiber-like β phase on the surface of the clay leads to a structure that is much more conducive to plastic flow under applied stress. Furthermore, nanoclays can act as temporary crosslinks between polymer chains and provide localized regions of enhanced strength. These modifications contribute to a more efficient energy-dissipation mechanism in the nanocomposite, which helps to retard the growth of cracks and cavities.

A study on the fracture behavior of PP/clay nanocomposites also reported a more than four times increase in toughness upon introduction of 2.5 wt% organoclay [47]. This toughness increase was again attributed to plastic deformation in the reinforced matrix. Similar to the case of PVDF/clay nanocomposites, nanoclays toughen the PP matrix by enhancing the energy-absorbing mechanisms in front of the crack tip.

Characterization of the fracture behavior of a highly exfoliated epoxy/clay nanocomposite [48] however shows neither plastic deformation nor crack pinning effect. Instead, the initiation of massive microcracks and the increase of the fracture surface area due to crack deflection are the major toughening mechanisms.

In conclusion, although toughness improvements have been reported for both glassy and rubbery polymers, the mechanism of toughness improvement cannot be generalized, but is instead specific to the deformation mechanisms in the polymer system, as well as the degree of polymer/clay interactions.

2.6.2 Heat Distortion Temperature (HDT)

Heat distortion temperature (HDT) of a polymeric material is the temperature at which it undergoes an arbitrary deformation under a constant load. HDT is one of the key indicators of the load-bearing capabilities of the polymer at elevated temperatures. Kojima *et al* reported the dependence of the HDT of nylon-6/clay nanocomposites as a function of clay content [49]. It was found that there is a marked increase of almost 90^{o}C in the HDT of a 4.7 wt% nanocomposite, but with higher levels of clay loading, the HDT of the nanocomposite was found to level off. The huge improvement in the HDT is attributed to the existence of strong hydrogen bonds between the matrix and the clay surface. Furthermore, TEM observations of the morphology of the nylon-6 nanocomposite reveal that the nanocomposite has a sandwiched structure, where each silicate layer is strongly covered by polymer crystals [50]. The additional rigidity provided by such an internal structure probably also makes an important contribution to the large increase in the HDT of the polymer.

The incorporation of nanoclay in PP also results in a higher HDT in the polymer, from 109^{o}C for the neat polymer to 152^{o}C for a 6 wt% clay nanocomposite

[51]. The improvement in the HDT originates from the more enhanced mechanical stability of the nanocomposite, as there is no increase in the melting point in the neat PP after nanocomposite preparation.

As a final point, it is essential to note that the increase in the HDT due to the addition of dispersed clay layers is a very important property improvement for polymer/clay nanocomposites, because it is very difficult to achieve similar HDT improvements by chemical modifications or reinforcement by conventional fillers.

2.6.3 Thermal Stability

Polymer/clay nanocomposites often exhibit enhanced thermal stability at much lower filler contents compared to conventional composites. This is an important advantage offered by this class of materials, as it enables the polymer to withstand higher temperatures without a compromise in cost, weight and ease of processibility. Generally, clays enhance the thermal stability of the matrix polymer by acting as an effective heat insulator and a superior mass transport barrier to the volatile products generated during decomposition [3].

The thermal stability of crosslinked poly(dimethylsiloxane) was studied by means of thermogravimetric analysis (TGA) under nitrogen flow [52]. A stabilization of 140^{o}C at 50% weight loss was observed when 10 wt% of organoclay was exfoliated in the polymer matrix. It was proposed that the enhanced thermal stability was due to hindered out-diffusion of the volatile decomposition products (mainly cyclic silicates) – a mechanism related to the lower permeability usually observed in exfoliated nanocomposites.

The thermal stability of poly(ε-caprolactone) (PCL) /clay nanocomposites has also been studied by TGA [3,53]. Both intercalated and exfoliated nanocomposites

display a higher thermal stability, as compared to the neat PCL or the corresponding microcomposites. The enhanced thermal stability is attributed to the decrease in the permeability/diffusivity of oxygen and volatile degradation products with the addition of clay, the barrier imposed by the high-aspect ratio clay fillers, as well as the formation of char (which acts as a physical barrier between the polymer matrix and the combustion site).

Although an improvement in thermal stability is often observed in polymer/clay nanocomposites, it is important to note that the extent of thermal stabilization achieved is not only dependent on the clay loading and clay dispersion. Also of key importance are the chemical nature of the polymer matrix and its degradation mechanism [3]. For example, Zanetti *et al* [54] found that the deacylation of EVA in nanocomposites is accelerated, and may even occur at temperatures lower than those for the pure polymer or the corresponding microcomposites, because the strongly acidic sites created by the thermal decomposition of the silicate modifier has a catalytic effect on the decylation reaction.

2.6.4 Barrier Properties

The fine dispersion of clay layers in polymer/clay nanocomposites has been found to greatly reduce the gas permeability in films made from such materials. This has been widely attributed to the increased tortuosity of the diffusing paths (which translate into a longer diffusing path) that must be undertaken by the gas molecules. The sheet-like morphology of clay is particularly efficient at maximizing the path length, due to the large length-to-width ratio, when compared to other filler shapes, such as spheres or cubes. This effect is expected to be more pronounced in exfoliated nanocomposites due to the extremely high aspect ratio presented by the delaminated clay layers.

The permeability to carbon dioxide for partially exfoliated poly(imide)-based nanocomposites has been measured [55]. It was found that the relative permeability dropped exponentially with increased volume fraction of clay. When 8 vol% of clay was added, the permeability to carbon dioxide dropped to one-fifth of the permeability of the neat matrix.

In addition, the permeabilty to water vapour has also been investigated for exfoliated nanocomposites based on poly(ε-caprolactone) (PCL) [56]. Again, a dramatic drop in the relative permeability was observed by dispersing increasing amounts of the layered nanofillers. In particular, a relative permeability of 0.2 (where the permeability of the unfilled PCL was taken to be 1) was reported at a clay loading of 4.8 vol%.

Of special interest is a nylon-6-based exfoliated nanocomposite that exhibits an oxygen transmission rate that is halved compared to that of the pure polymer. The improved gas barrier properties, combined with the enhanced transparency and gloss, and increased tensile modulus, has led to its recent commercialization under the tradename Durethan® LPDU 601 [57].

2.7 Conclusions

The extent of property enhancements achieved in polymer/clay nanocomposites is found to be dependent on a combination of several factors, including the extent of delamination of clay (that is, whether an exfoliated, intercalated or partially exfoliated structure has been formed), the presence of polymer-clay interactions, and the nature of the polymer matrix itself. In particular, many studies point towards an exfoliated structure as the key to the vast improvement in properties observed in this class of materials. A survey of the literature pertaining to the preparation of polymer/clay

nanocomposites however indicates that an exfoliated structure is also the most challenging to achieve. The lack of success in the PEN/clay system necessitates a systematic investigation on the critical factors that affect the delamination of clay layers in PEN – this will form the motivation for the study that will be detailed in the following chapter.

CHAPTER 3

Preparation of PEN/Clay Hybrids

3.1 Introduction

As reports on the preparation of PEN/clay nanocomposites prior to this work are very limited, the two approaches of nanocomposite preparation - in-situ polymerization and melt intercalation were explored in this work to gain an understanding of their relative merits and limitations for the production of PEN/clay nanocomposites. In this chapter, the strategies employed, critical issues involved, as well as the important conclusions that can be made about the two preparation routes will be discussed.

3.2 Materials

Table 3.1 lists the materials that were used for the preparation of the PEN/clay hybrids and their sources. All chemicals were used without further purification.

Table 3.1 Materials used for the preparation of PEN/clay hybrids and their sources.

	Chemical Name	Supplier
Clay	PGW grade sodium montmorillonite (Na-MMT) (cation exchange capacity (CEC) = 145 meq/100g)	Nanocor
	1.34 TCN (methyl dihydroxyethyl hydrogenated tallow ammonium-modified clay)	Nanocor
Clay Modifier	12-aminododecanoic acid	Tokyo Kasei
	Ethyl-4-dimethylaminobenzoate (>99%)	Merck
	P-xylylene bis(triphenyl phosphonium) bromide (95%)	Lancaster Synthesis
	1,3-didecyl-2-methylimidazolium chloride (96%)	Aldrich
	1-hexadecyl-2,3-dimethylimidazolium chloride	Merck
Monomer	Dimethyl naphathalene-2,6-dicarboxylate (99.95%) (DMN)	BP
	Ethylene glycol (analytical grade)	Merck
Catalyst / Stabilizer	Manganese (II) acetate (98%)	Aldrich
	Triphenyl phosphate (99+%)	
	Antimony (III) acetate (99.99%)	
Polymer	PEN resins	Goodfellow Cambridge

3.3 Materials Preparation

3.3.1 Synthesis of Ammonium Salt

12-carboxyl dodecanoic ammononium chloride (CDA) was prepared by reacting stoichiometric amounts of 1 M hydrochloric acid with 12-aminododecanoic acid at a temperature of 80°C for 2 hours.

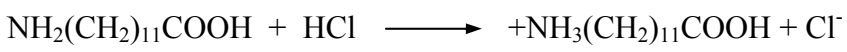

Figure 3.1 Synthesis route of CDA

Ethyl-4-trimethylammoniobenzoate iodide (ETMAB) was prepared by methylation reaction of ethyl-4-dimethylaminobenzoate with 5 mole equivalents of methyl iodide at room temperature for 4 days.

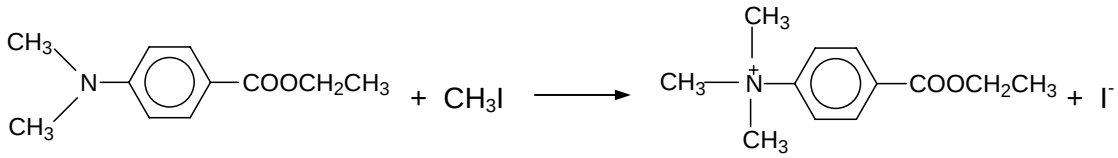

Figure 3.2 Synthesis route of ETMAB

3.3.2 Clay Modification

The modified clays in this work were prepared by a standard aqueous ion-exchange procedure, in which the compatibilizer salt of choice was introduced to the clay suspension and the system was thoroughly mixed to allow the compatibilizer cations to exchange with the interlayer Na^+ ions. Specific procedures that were employed for the preparation of the various modified clays were detailed below.

(I) Preparation of Organoclay

1.5L of distilled water was added to 15 g of sodium montmorillonite (Na-MMT) in a beaker, and the resulting mixture was stirred vigorously at 80^{o}C with a mechanical stirrer to form a uniform suspension. Separately, 1.2 mole equivalent of the organic modifier, with respect to the clay C.E.C value, was dissolved in 300 ml of ethanol. (In the case where divalent organic modifiers were used, the amount of modifier salt added was simply halved.) Upon complete dissolution, the modifier solution was added drop by drop into the clay suspension. Immediate precipitation of the organically modified clay was observed, but the reaction mixture was left to stir for a further 7 hours at 80^{o}C to ensure complete reaction. The ion-exchanged clay was then separated from the solution by centrifugation and subsequent removal of the supernatant. The clay was subsequently washed by redispersing it in ethanol. Washing was repeated at least 4 times to ensure complete removal of the excess surfactants. After each washing step, the clay was separated from the ethanol by centrifugation. Although excess modifiers may also be removed by vacuum filtration or Soxhlet extraction, previous studies [58] have found that centrifugal extraction is the most effective means of removing the excess modifiers. The clay was then dried under vacuum at 80^{o}C for at least 48 hours and subsequently ground into fine powder using a Fritsch Pulverisette 14 and an 80-μm sieve.

(II) Preparation of Catalyst-Intercalated Clay

1.16 g of antimony (III) acetate was added to 100 g of ethylene glycol. The ethylene glycol was heated to 60^{o}C to completely dissolve the antimony (III) acetate. 16 g of untreated clay was added to the solution and the mixture was stirred for 5 hours to allow antimony (III) acetate to intercalate into the clay layers. The clay was then

separated from the ethylene glycol by centrifugation and subsequent removal of the supernatant. The clay was subsequently washed by redispersing it in ethylene glycol. Washing was repeated at least four times to ensure that most of the catalysts remaining on the external surfaces were removed and that the catalyst exists mainly in the clay galleries. The catalyst-intercalated clay was then dried under vacuum at 150^{o}C for 8 hours to completely remove all ethylene glycol.

(III) Preparation of Mixed Intercalant Clay

The same procedure as (I) was employed, except that the ethanolic solution of the modifier salt was added to a suspension of catalyst-intercalated clay for ion exchange.

Table 3.2 lists the modified clays that have been prepared in this work.

3.3.3 Nanocomposite Preparation

(I) In-situ Polymerization

The reaction used for the polymerization of PEN in this work is a two-step process, (Figure 3.3). The first step is the transesterification of dimethyl naphthalene-2,6-dicarboxylate (DMN) with ethylene glycol (EG) to form bis(2-hydroxyethyl) naphthalene-2,6-dicarboxylate (BHEN). The second step involves the polycondensation of BHEN to form the PEN polymer. In the preparation of PEN/clay hybrids, this standard procedure was slightly modified to incorporate the addition of clay in the polymerization reaction.

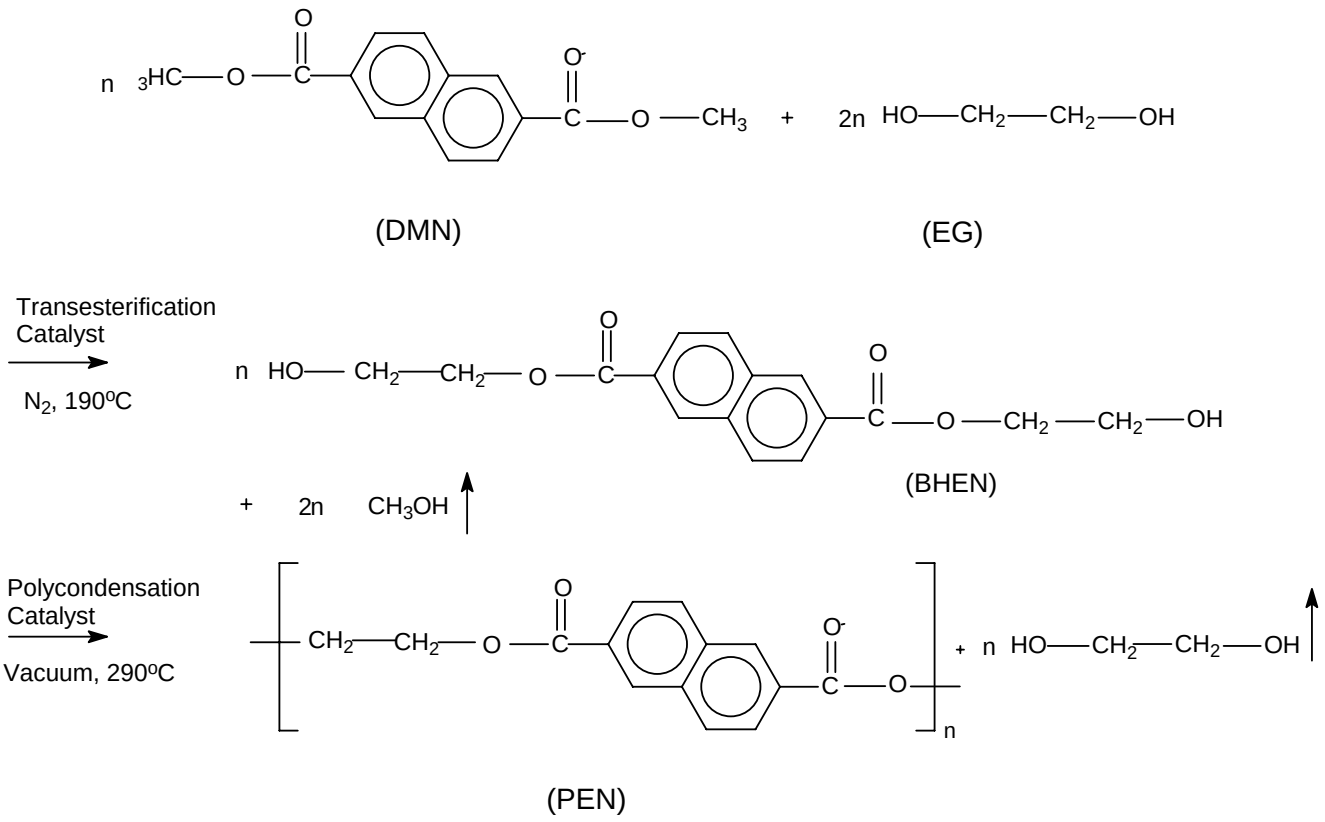

Figure 3.3 Synthesis route of PEN polymerization

A typical procedure employed for the in-situ polymerization of the PEN/clay hybrids is described below.

Preparation of EG/clay suspension

The amount of clay corresponding to ~2 wt% inorganic MMT was added to 38.4 g of EG and stirred at high speed using the homogenizer for 2 hours to form a homogeneous suspension. The suspension was then sonicated under a nitrogen flow for 5 hours. It has been demonstrated that the accessibility of the clay interlayer is dependent upon the size of the primary clay particles. In particular, bigger clay particles tend to be less intercalated than the smaller ones [59]. The above pretreatment of clay prior to the polymerization step was thus carried out in an attempt to reduce the starting size of the primary clay particles.

Polymerization

The EG/clay suspension and 60.5 g of DMN were combined in a 250 ml 3-neck round-bottom flask. 0.28 mol% (120 mg) of manganese (II) acetate transesterification catalyst was also added into the mixture. An excess of EG was added to allow for loss due to vaporization during reaction. The system was heated under nitrogen flow to 190^{o}C to completely melt the DMN. The melt was maintained at 190^{o}C for 90 minutes for the transesterification reaction to take place. Methanol was released as a by-product of the transesterification, and the progress of the transesterification reaction was monitored by the methanol production. A finger filled with warm water was placed above the outlet leading towards the condenser, to allow the methanol (boiling point: 64^{o}C) to escape, while effectively condensing the EG (boiling point: 197^{o}C).

After the transesterification reaction was completed, 0.09 mol% (73 mg) triphenyl phosphate stabilizer and 0.075 mol% (56 mg) antimony (III) acetate polycondensation catalyst was added into the system (in the case where the polycondensation catalyst was incorporated into the clay galleries, no antimony (III) acetate will be added during this step) and the temperature was slowly raised to 290^{o}C for the polycondensation of BHEN to take place to form PEN. The nitrogen flow was then turned off, and the pressure of the system was gradually reduced to less than 0.5 mbar over 45 minutes. The melt was maintained at 290^{o}C at this pressure level for another 90 minutes. After the reaction was completed, the system was allowed to cool to room temperature.

Table 3.3 lists the PEN/hybrids that were prepared in this work by the in-situ polymerization method.

Table 3.3 PEN/clay hybrids prepared via in-situ polymerization. All the hybrids have a nominal 2 wt% inorganic MMT content (as indicated by the suffix "2" in their abbreviations).

Clay Type	Clay Modifier	Abbreviation for Hybrid
Ammonium-modified Clays	12-carboxyl dodecanoic ammonium (CDA)	PEN/CDA-MMT-2
	Ethyl-4-trimethylammoniobenzoate (ETMAB)	PEN/ETMAB-MMT-2
	Methyl dihydroxyethyl hydrogenated tallow ammonium (1.34 TCN)	PEN/1.34 TCN-MMT-2
Phosphonium-modified Clay	P-xylylene bis(triphenyl phosphonium) (TPP)	PEN/TPP-MMT-2
Catalyst-treated Clay	Antimony (Sb)	PEN/Sb-MMT-2
Mixed Intercalant Clay	P-xylylene bis(triphenyl phosphonium) and antimony (TPP-Sb)	PEN/TPP-Sb-MMT-2

(II) Melt Intercalation

To achieve better homogeneity in the polymer/clay premix, the as-received PEN granules were first ground into a finer particle size using the Fritsch Pulverisette 14 and a 2-mm sieve. The PEN and the corresponding amount of clay powder to form a nominal 2 wt% hybrid were then dry-mixed by shaking them in a Ziploc bag. The mixture was then melt compounded in a co-rotating intermeshing twin-screw extruder (Leistritz Micro 18, L/D = 30) with a six-zone barrel. Processing temperatures of 275^{o}C, 275^{o}C, 280^{o}C, 280^{o}C, 290^{o}C and 295^{o}C from Zone 1 to Zone 6 of the barrel, and a screw speed of 30 rpm were used. Pure PEN was also extruded under the same conditions to be used as a reference. All materials were dried under vacuum at 80^{o}C for at least 8 hours prior to melt compounding.

To investigate the effect of clay concentration and a second compounding cycle on the dispersion of clay, a masterbatch containing 4 wt% clay was also prepared. The masterbatch was then diluted with pure PEN using the same processing conditions to produce a 2 wt% hybrid. Table 3.4 lists the PEN/clay hybrids that have been prepared via the melt intercalation route.

Table 3.4 PEN/clay hybrids that were prepared by the melt intercalation method.

Clay Type	Clay Modifier	MMT Content (%)	No. of Extrusion Cycles	Abbreviation
Unmodified Clay	-	2	1	PEN/Na-MMT-2
Trialkylimidazolium-modified Clays	1,3-didecyl-2-methylimidazolium	2	1	PEN/IM2C10-MMT-2
	1-hexadecyl-2,3-dimethylimidazolium	2	1	PEN/IMC16-MMT-2
		2	2	PEN/IMC16-MMT-2B
		4	1	PEN/IMC16-MMT-4

3.4 Materials Characterization

3.4.1 Thermal Analysis of Modified Clays

(I) Thermal Stability and Organic Loading

The thermal stability and organic loading of the modified clays was assessed following the procedure proposed by Xie *et al* [32], which provides a more reproducible estimate of the onset degradation temperature of the modified clays. Thermogravimetric analysis (TGA) was conducted on a TA Instruments Hi-Res TGA 2950 Thermogravimetric Analyzer. The modified clays were heated to 800^{o}C at a heating rate of 2^{o}C/min and under a nitrogen flow rate of 50 cc/min. A predrying step at 140^{o}C for 1 hour, followed by rapid cooling to 60^{o}C, was performed before the thermogravimetric analysis at 2^{o}C/min, to remove physiabsorbed water and gases, to ensure a reproducible estimate of the onset temperature of degradation. The onset degradation temperature was taken as the temperature at which 5% mass fraction loss was observed, while the organic content of the clay was obtained by subtracting the

total mass loss between 150°C and 800°C by the mass loss due to water from the dehydroxylation of the aluminosilicate (5.25%).

(II) Thermal Stability under Polymerization Conditions

To examine the degradation that took place in the modified clay during the polymerization reaction, TGA was also performed simulating the temperature profile of the in-situ polymerization process. A predrying step at 140°C for 1 hour was applied before the clay was heated at 1°C/min to 190°C and held for 90 minutes. The sample was then heated to 290°C at 1°C/min and held at that temperature for a further 90 minutes. The entire TGA procedure was carried out under a nitrogen atmosphere.

(III) Thermal Stability under Melt Compounding Conditions

To assess the ability of the modified clays to survive the melt compounding process, isothermal TGA was performed at the compounding temperature and in an air atmosphere. A predrying step at 140°C for 1 hour was applied before the clay was heated at 20°C/min to 295°C and held at that temperature for 15 minutes.

3.4.2 Energy Dispersive X-Ray (EDX) Analysis of Antimony-Intercalated Clay

The successful ion-exchange of sodium ions in the pristine Na-MMT by antimony ions was verified by scanning electron microscope / energy-dispersive x-ray analysis (SEM-EDX). The EDX data were measured with a JEOL JSM-5600 scanning electron microscope at an accelerating voltage of 15 kV, and the elemental analysis was performed with the Oxford energy EDS software. The sample is coated with a thin layer of carbon prior to analysis.

The amount of antimony that has been exchanged into the clay galleries was determined by taking the difference in the atomic percent of sodium in the clay before and after ion-exchange with antimony (using the atomic percent of silicon as a reference); the actual antimony peak cannot be detected in the SEM-EDX setup because the antimony L line is too weak to be detected, while the antimony K line (which is much stronger) lies beyond 30 keV (which cannot be detected because the maximum allowable accelerating voltage in the SEM-EDX set-up used is only 20 kV).

3.4.3 Morphological Characterization of Nanocomposites

(I) X-ray Diffraction (XRD)

XRD is performed for the materials in Sections 3.5.2(I) and 3.5.3, with a Shimadzu x-ray diffractometer in a Bragg-Brentano θ-2θ geometry with CuK_α radiation (λ = 0.154 nm) generated at 30 kV and 30 mA. The samples were scanned from 2.5° to 10.0° 2θ at a rate of 1°/min. The materials in Sections 3.5.2(II) to 3.5.2(IV) were scanned using a Bruker AXS x-ray diffraction system equipped with a two-dimensional, position-sensitive area detector using CuK_α radiation. An acceleration voltage of 40 kV and a current of 40 mA were employed. As the absolute intensities of the clay peaks could vary according to the experimental conditions, the intensities of the clay peaks were scaled using the amorphous halo from the polymer as a reference, before they were compared.

(II) Polarizing Optical Microscope (POM)

The morphology of the PEN/clay hybrids were observed at a magnification of 100x under crossed polarizers with a Nikon Optiphot-pol Universal Stage polarizing

microscope. A thin piece of the polymer/clay hybrid was sandwiched between two glass coverslips and placed on the digital hotplate. The hotplate was heated at a rate of 50^{o}C/min to 300^{o}C, and kept isothermal at that temperature while the morphology of the sample was observed. A CCD camera was used to snap the morphologies exhibited by the hybrid materials.

(III) Transmission Electron Microscopy (TEM)

Ultrathin sections (~ 80 nm) thick were sectioned from the PEN/clay hybrids using a Leica Ultracut UCT Ultramicrotome. The sections were collected using 200 mesh carbon-coated copper grids, and examined using a JEOL 2010 TEM operating at an accelerating voltage of 200 kV.

3.5 Results and Discussion

3.5.1 General Comments on the Evaluation of Clay Dispersion

In this section, the effectiveness of the preparation procedures employed will be mainly discussed with respect to the clay dispersion that has been achieved. While it is by no means the only criterion by which the materials should be judged, it has been repeatedly demonstrated in previous studies that a certain level of clay dispersion must be achieved in order for significant property enhancements to be observed. In evaluating the degree of clay dispersion that has been achieved in the hybrids, a combination of x-ray diffraction (XRD), polarizing optical microscopy (POM) and transmission electron microscopy (TEM) has been employed in this work.

XRD provides a quick and convenient method for determining the clay interlayer spacing in the original organically modified clays, as well as in intercalated nanocomposites. In particular, the measured diffraction angle (θ) is related to the

average interlayer spacing of clay (d) by Bragg's relation: $\lambda = 2d \sin\theta$, where λ corresponds to the wavelength of the x-ray radiation used. In addition, the width of the peak provides an assessment of the degree of order in the stacked sheets while the intensity of the peak provides statistical information about the number of multilayer stacks.

The clay layers can only be detected by XRD if they remain parallel and evenly spaced. In an exfoliated nanocomposite; the extensive layer separation associated with the delamination of the original clay layers in the polymer matrix results in the eventual disappearance of any coherent x-ray diffraction from the distributed clay layers. (The lack of low-angle XRD peaks (or low peaks), however, cannot be directly correlated to high levels of clay dispersion, as it can also be the result of disordered but poorly dispersed clay layers.) For an intercalated nanocomposite, the intercalation of polymer into the intergallery spaces results in a shifting of the basal reflection to a position corresponding to a larger interlayer spacing. In the case where the clay is incompatible with the polymer matrix, the diffraction peak will be observed at the same position as that seen for the clay in the absence of the polymer. Finally, degradation of the polymer and/or clay modifier results in the collapse of the clay layers. In this case, the interlayer spacing becomes less than that of the original organically modified clay. The clay may exhibit an increase in its width but this is most likely to be due to the disordering of the clay layers caused by the degradation process, rather than an improvement in the clay dispersion. Due to the aforementioned reasons, peak broadening and intensity reduction in XRD patterns are very difficult to study systematically, to provide information about the spatial distribution of the clay layers or any structural inhomogeneities in the nanocomposites.

Because of these inherent limitations of XRD, POM and TEM were used in parallel with XRD in this work to clarify the level of dispersion that has been achieved in the hybrids at the micron- and nanoscale respectively. TEM allows direct visualization of the clay layers at the nanometer length scale. However, because of the small area of inspection, it may not be very representative of the level of dispersion that has been achieved in the whole material. POM helps to fill in this gap, by allowing large clay agglomerates whose size lies within its resolution limit (~ 1 μm) to be observed. These large particles would otherwise not be detected with the TEM due to the small size of the probed area.

3.5.2 In-situ Polymerization

(I) Ammonium-Based Modifiers with a Reactive Functional Group

Principles

Ammonium-based modifiers were the system of choice to begin with, due to their common use for clay modification in the preparation of polymer/clay nanocomposites. Specifically, modifiers possessing functional groups that are able to react and form covalent bonds with the PEN monomers (either ethylene glycol or dimethyl naphthalene-2,6-dicarboxylate (DMN)) were investigated as previous studies have demonstrated that the incorporation of a reactive functional group in the clay modifier not only helps to force apart the clay layers (by ensuring that the polymerization proceeds, at least partially, inside the clay galleries), but may also improve the interaction strength between the polymer chains and the clay.

In this work, several modifier systems that fall into this category have been investigated, in this section however, only a few examples (refer to Tables 3.2 and 3.3) will be described to illustrate the results. In principle, CDA is able to react with

ethylene glycol via esterification, 1.34 TCN with DMN via transesterification, and ETMAB with ethylene glycol via transesterification.

Discussion

Figure 3.4 shows the XRD patterns of the organoclays and the corresponding PEN/clay hybrids prepared.

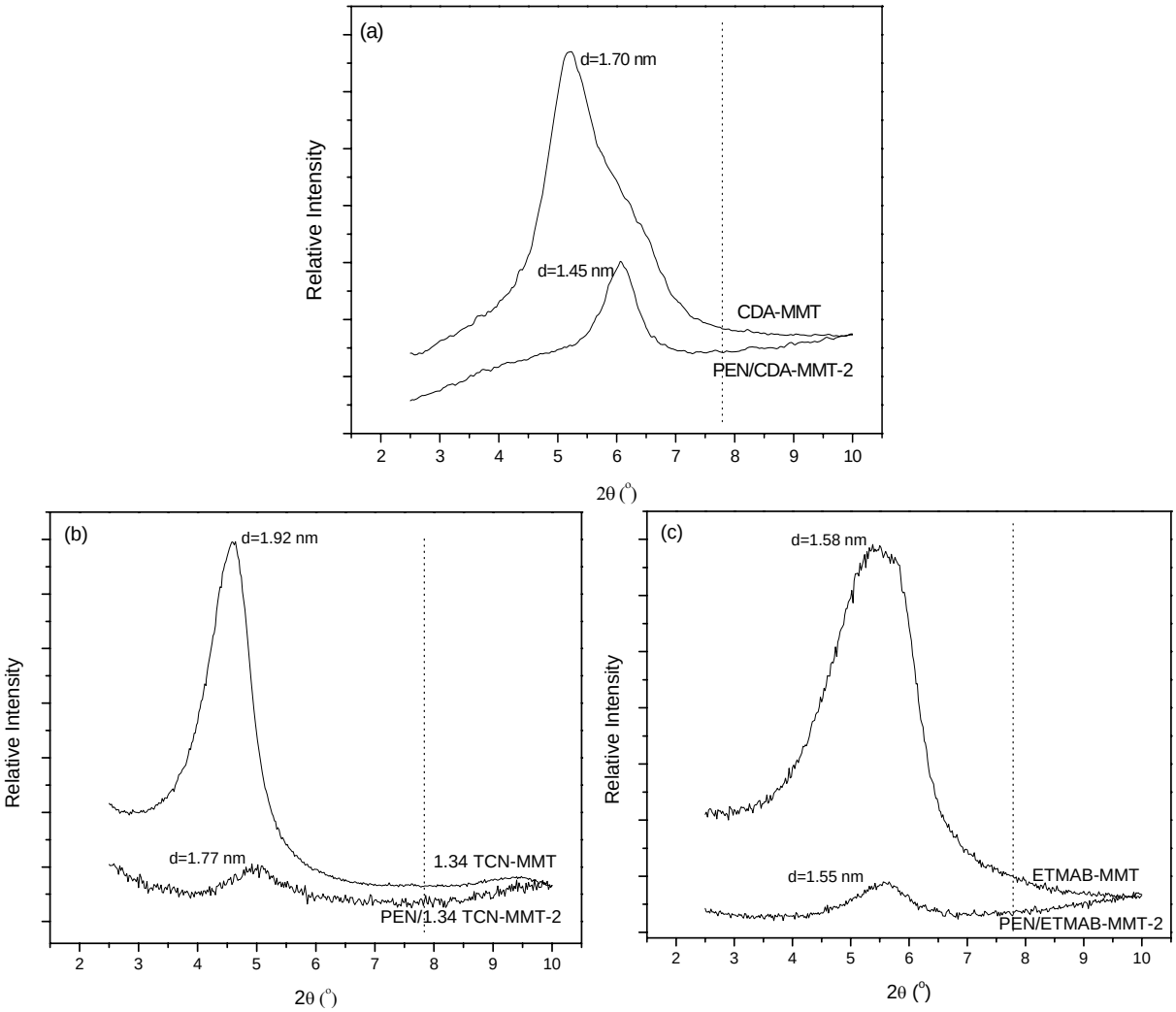

Figure 3.4 XRD patterns of organoclays modified with reactive ammoniums, and the corresponding PEN/clay hybrids for (a) CDA, (b) 1.34 TCN and (c) ETMAB. The d-spacings between the clay layers are indicated. (The dotted line indicates the original position for the (001) basal reflection of untreated Na-MMT.)

The shift of the (001) basal reflection of Na-MMT to lower angles upon modification with the ammonium ions indicates an expansion of the intergallery distance, which confirms the successful exchange of the intergallery Na^+ ions by the ammonium ions.

XRD of the hybrids however indicates that the interlayer spacings in all the organoclays decreased after in-situ polymerization with PEN. The layer collapse suggests that the organic modifiers have degraded during the polymerization process. Degradation of the organic modifiers (and possibly, the PEN polymer too) was corroborated by the severe discoloration observed in the PEN/clay hybrids.

To further confirm the occurrence of degradation, TGA was performed on the organoclays, simulating the temperature profile of the in-situ polymerization process. The TGA results indicate severe weight loss in the organoclays, in the order of 70 wt% of the total organic content or more, after being subjected to the elevated temperature excursion. Figure 3.5 displays as an example, the TGA profile of CDA-MMT under the simulated polymerization conditions.

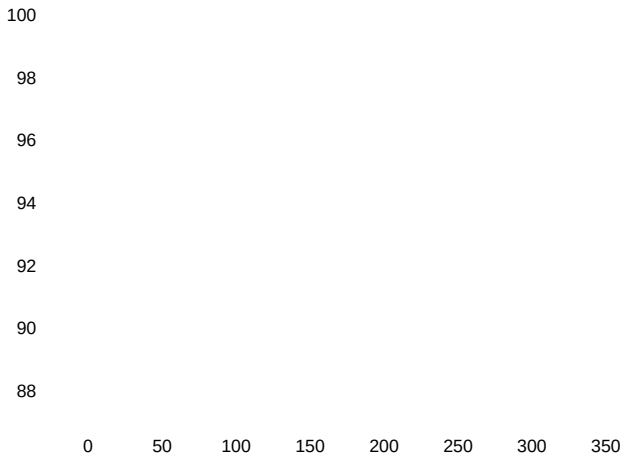

Figure 3.5 TGA profile of CDA-MMT under the simulated polymerization heating profile. Time = 0 min corresponds to the end of the predrying step at 140^{o}C. The TGA curve shows an 11.5% weight loss in the clay at the end of the heating cycle, which corresponds to 69.2% of the total organic content in CDA-MMT.

XRD analysis of the organoclay after the heat treatment in TGA also reveals a collapse of the clay interlayer spacing (Figure 3.6). This verifies that the smaller interlayer spacing observed in the hybrid after in-situ polymerization is predominantly due to the degradation of the organic modifiers.

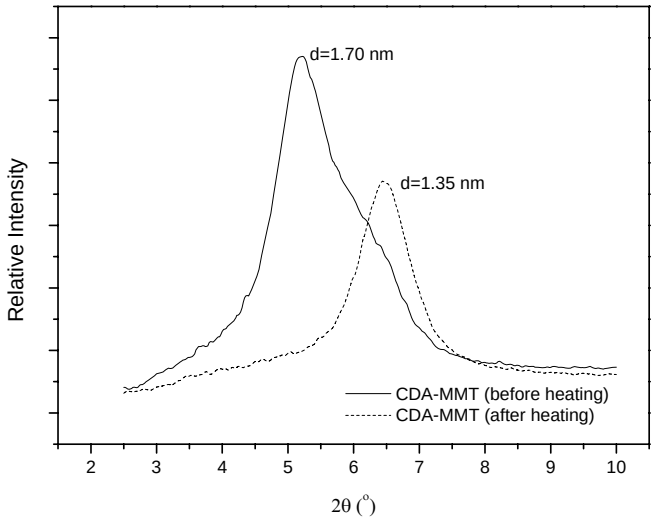

Figure 3.6 XRD pattern of CDA-MMT before and after the simulated polymerization heating profile in the TGA.

Degradation of the organic modifiers alters the carefully tailored chemistry of the polymer and clay interface, and results in the poor dispersion of clay in the PEN matrix, as verified by TEM observations, where many large multilayer clay tactoids (Figure 3.7(a)), with small d-spacings (Figure 3.7(b)) remain.

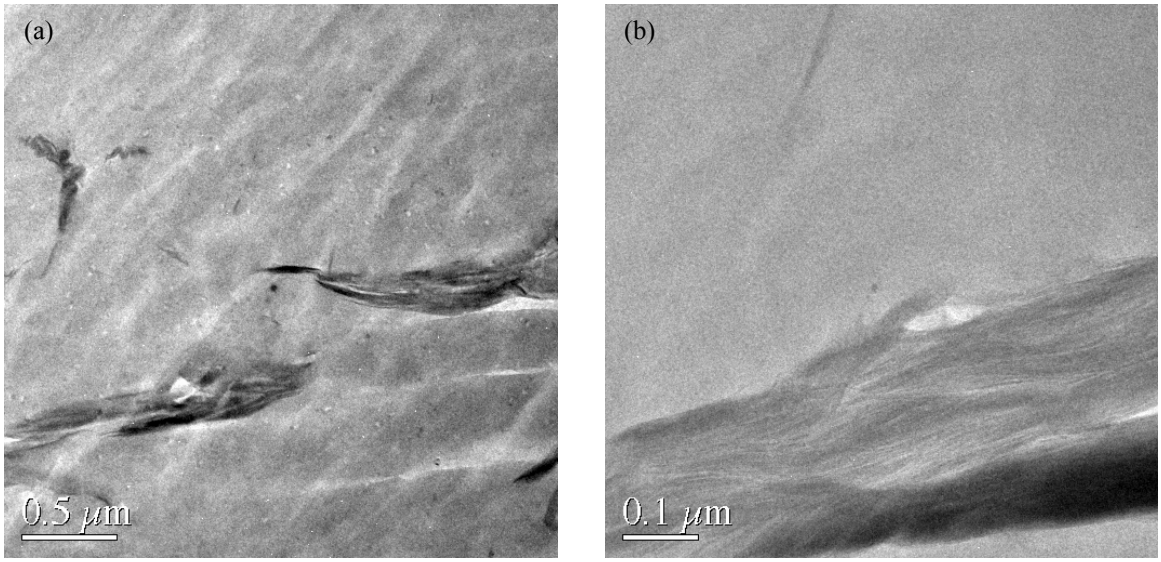

Figure 3.7 TEM images of PEN/CDA-MMT-2

(II) Aryl Phosphonium Modifiers

Principles

Due to the severe thermal degradation that took place in the ammonium-based modifiers, the use of phosphonium surfactants, which could potentially provide greater thermal stability [60], was investigated. In particular, an aryl phosphonium modifier, p-xylylene bis(triphenyl phosphonium) (TPP), was chosen. Due to its inability to undergo elimination reactions, the degradation of aryl phosphonium-clay occurs by alternative decomposition pathways [60]. This imparts greater stability to aryl phosphoniums compared to their alkyl counterparts.

Discussion

Figure 3.8 displays the XRD pattern of TPP-modified clay and the corresponding hybrid. It was observed that there was again a reduction in the clay interlayer spacing upon in-situ polymerization with PEN. TGA simulating the heating profile of the in-situ polymerization process (Figure 3.9) indicates a mass loss of 30.6 wt% after being subjected to the severe heating procedure. Although the mass loss is still significant, the TPP-MMT system represents a vast improvement to the ammonium-based organoclays. This is further confirmed by the much less severe discoloration observed in the resulting PEN/TPP-MMT-2 hybrid. The improved thermal stability of TPP-MMT also helps to achieve a better clay dispersion in the PEN matrix, as evidenced by the presence of smaller clay tactoids based on TEM analysis (Figure 3.10).

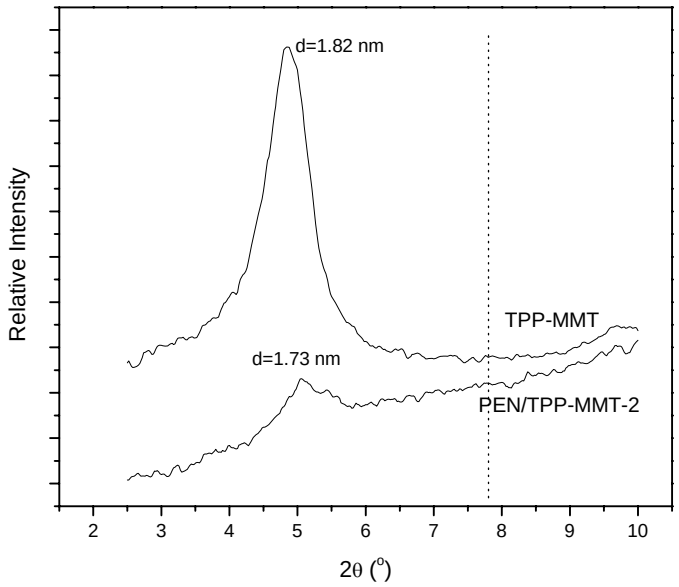

Figure 3.8 XRD patterns of TPP-MMT and the corresponding PEN/TPP-MMT-2 hybrid. (The dotted line indicates the original position for the (001) basal reflection of untreated Na-MMT.)

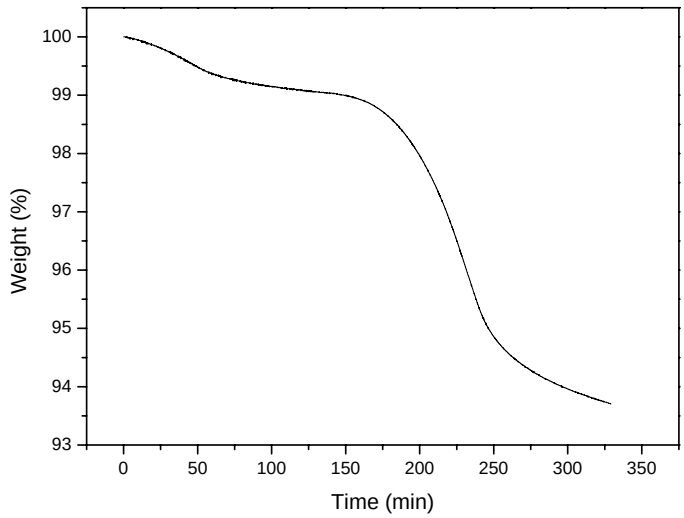

Figure 3.9 TGA profile of TPP-MMT under the simulated polymerization heating profile. The TGA curve shows a 6.3% weight loss in the clay at the end of the heating cycle, which corresponds to 30.6% of the total organic content in TPP-MMT.

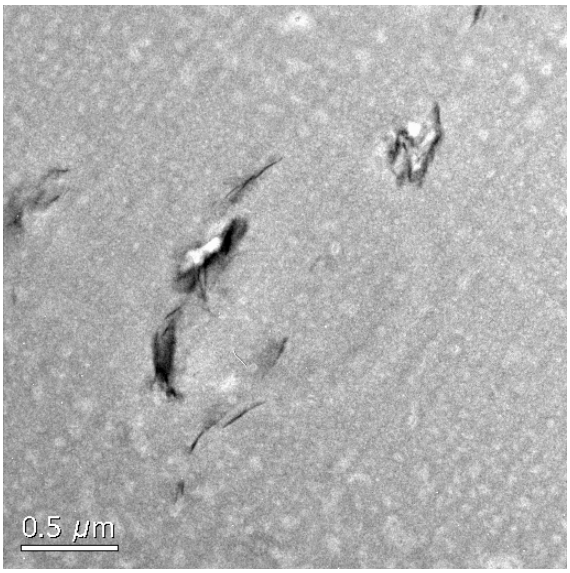

Figure 3.10 TEM image of PEN/TPP-MMT-2

(III) Antimony Cations Having a Catalytic Effect

Principles

Previous studies have demonstrated that by incorporating a modifier with catalytic functional groups into the clay galleries, the intragallery polymerization rates can be increased with respect to the extragallery polymerization rates. Consequently, the dispersion of clay within the polymer matrix can be greatly enhanced [19]. The use of the polycondensation catalyst precursor antimony (III) acetate as an intercalant was thus investigated to make use of the driving force of polymerization within the clay galleries to peel apart the clay layers.

Discussion

The successful intercalation of antimony into the clay galleries in the catalyst-treated clay (Sb-MMT) is verified by energy dispersive x-ray spectroscopy (EDX) (Figure 3.11).

(a)

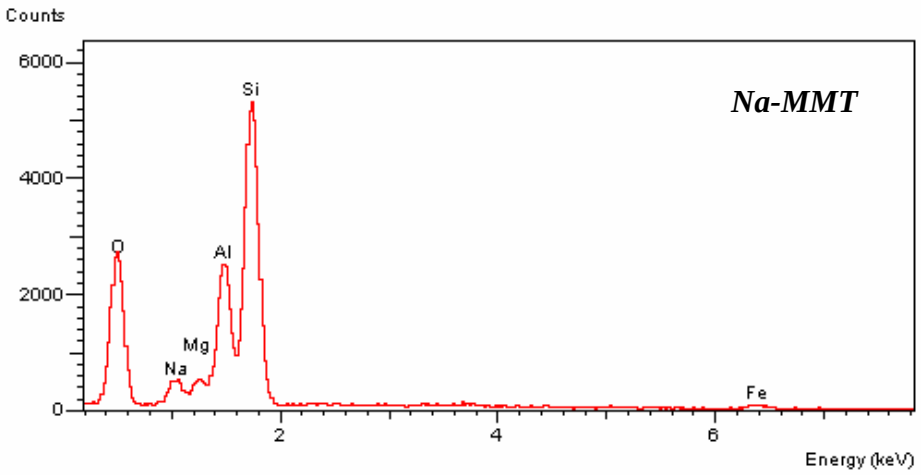

(b)

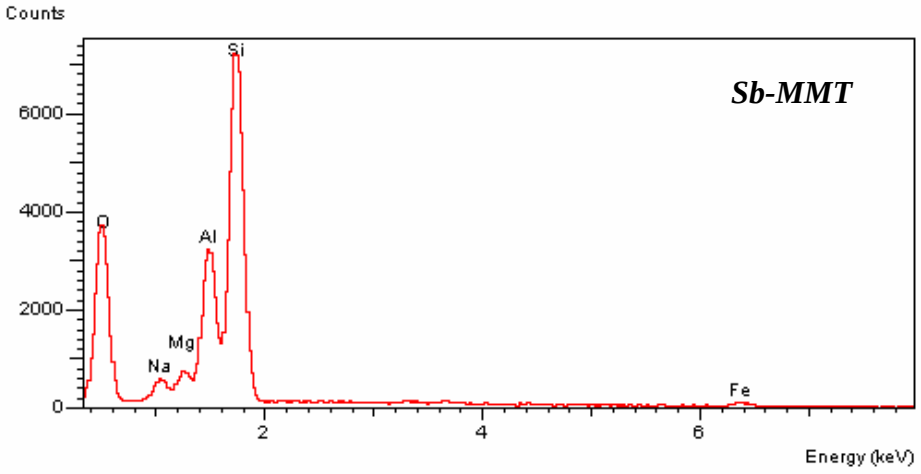

Figure 3.11 Energy dispersive x-ray (EDX) spectra of clay (a) before and (b) after ion-exchange with antimony. The ion-exchange of the intergallery sodium ions by the antimony ions results in a reduction in the intensity of the sodium line with respect to the silicon line. Analysis of the EDX spectra indicates that ~47% of the sodium ions (based on the C.E.C. value of the Na-MMT) have been replaced by antimony ions.

Figure 3.12 shows the XRD patterns of the clay after intercalation with the antimony catalyst (Sb-MMT). The resulting hybrid, PEN/Sb-MMT-2, however, did not show any significant increase in d-spacing compared to the original modified clay, which we would expect if there is an increased amount of materials formed by enhanced intragallery polymerization. Furthermore, observations under the POM (Figure 3.13) indicate that the clay is still present in the form of micron- or submicron-sized particles.

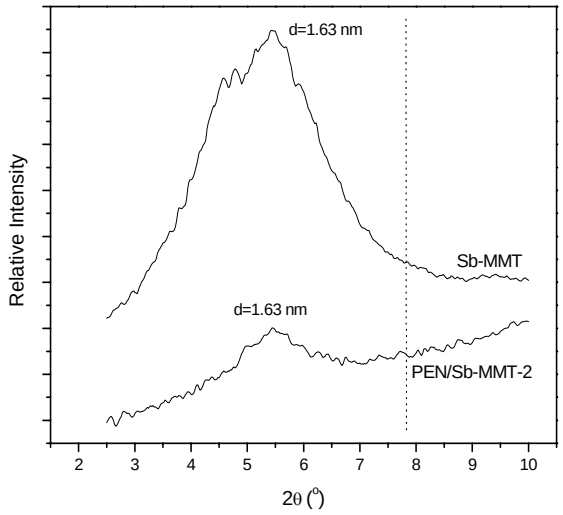

Figure 3.12 XRD patterns of Sb-MMT and the corresponding PEN/Sb-MMT-2 hybrid. (The dotted line indicates the original position for the (001) basal reflection of untreated Na-MMT.)

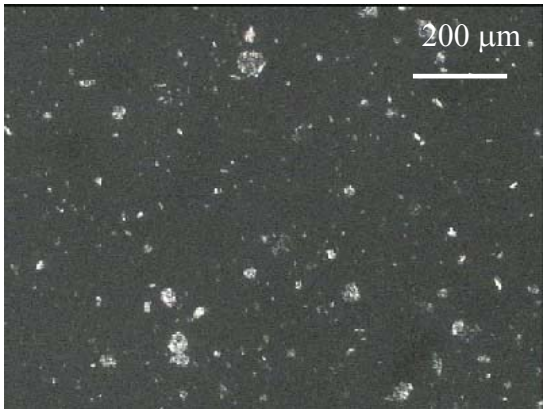

Figure 3.13 POM micrograph of PEN/Sb-MMT-2 under crossed polarizers.

The poor dispersion of clay in PEN/Sb-MMT-2 is attributed to the inorganic nature of the clay surface, which causes it to remain largely hydrophilic. This increases the driving force of the clay to reaggregate. In addition, the poor compatibility of the Sb-MMT with the PEN monomers greatly diminishes the ability of the monomers to intercalate into the clay galleries for polymerization to proceed within the clay interlayers. Consequently, the amount of clay dispersion achieved by this method is very minimal.

(IV) Mixed Intercalant System

Principles

Finally, a mixed intercalant system was investigated, in which the clay was modified with an organic surfactant following catalyst intercalation to enhance its compatibility with the PEN matrix. At the same time, such a system would also allow the effect of intragallery catalysis on the delamination of organically-modified clay to be studied. In particular, TPP was chosen as the organic surfactant to impart compatibility between the clay and the polymer, due to its greater thermal stability.

Discussion

XRD analysis (Figure 3.14) of the mixed intercalant clay system (TPP-Sb-MMT) indicates that the interlayer spacing collapsed after in-situ polymerization. This is attributed to partial degradation of the TPP modifier during the polymerization reaction, as has been previously discussed.

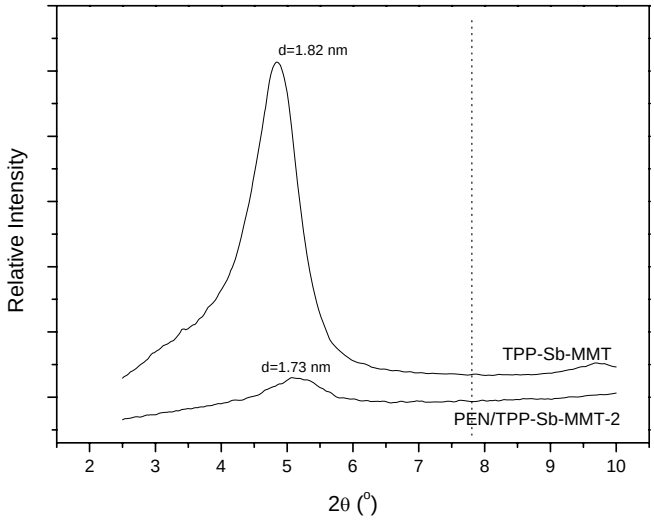

Figure 3.14 XRD patterns of TPP-Sb-MMT and the corresponding PEN/TPP-Sb-MMT-2 hybrid. (The dotted line indicates the original position for the (001) basal reflection of untreated Na-MMT.)

Under the POM however, it was found that the micron- and submicron-sized aggregates observed in PEN/Sb-MMT-2 (Figure 3.13) had been broken down into much smaller stacks in PEN/TPP-Sb-MMT-2 (Figure 3.15(b)), since essentially no clay particles could be observed in PEN/TPP-Sb-MMT-2 at the same magnification. In spite of the partial degradation of the TPP modifier during polymerization, the interfacial compatibility between the polymer and the clay is sufficiently improved by the incorporation of the TPP modifier, which helps to lower the surface energy of the clay, as well as prevent the reaggregation of clay. Furthermore, comparison of the POM images for PEN/TPP-MMT-2 and PEN/TPP-Sb-MMT-2 (Figure 3.15) indicates that although both the hybrids have the same organophilic surface, the occurrence of intragallery polymerization in PEN/TPP-Sb-MMT-2, due to the presence of the polycondensation antimony catalyst, has helped to further delaminate the clay into smaller stacks.

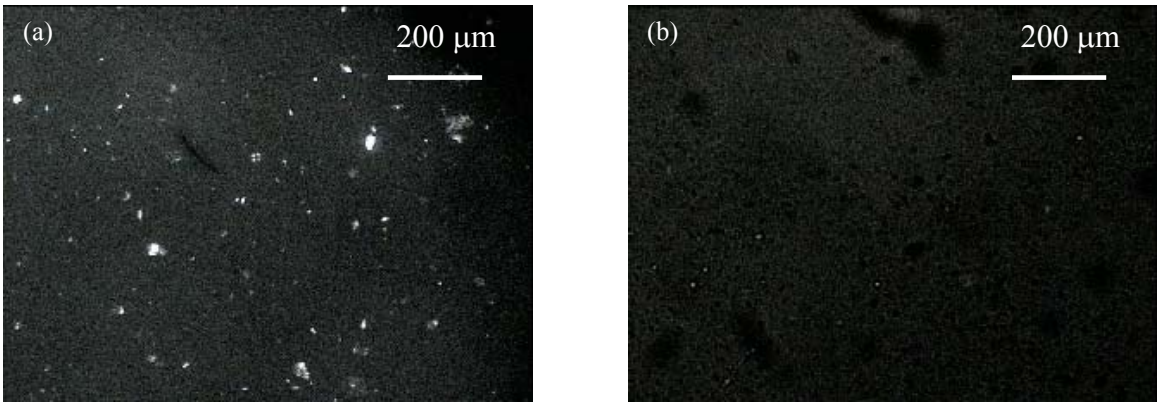

Figure 3.15 POM micrographs of (a) PEN/TPP-MMT-2 and (b) PEN/TPP-Sb-MMT-2 under crossed polarizers.

The presence of thinner clay stacks in PEN/TPP-Sb-MMT-2, as revealed by TEM analysis (Figure 3.16), further confirms the better dispersion of clay that has been achieved by the use of clay that has been modified with a combination of an organic surfactant and a polycondensation catalyst.

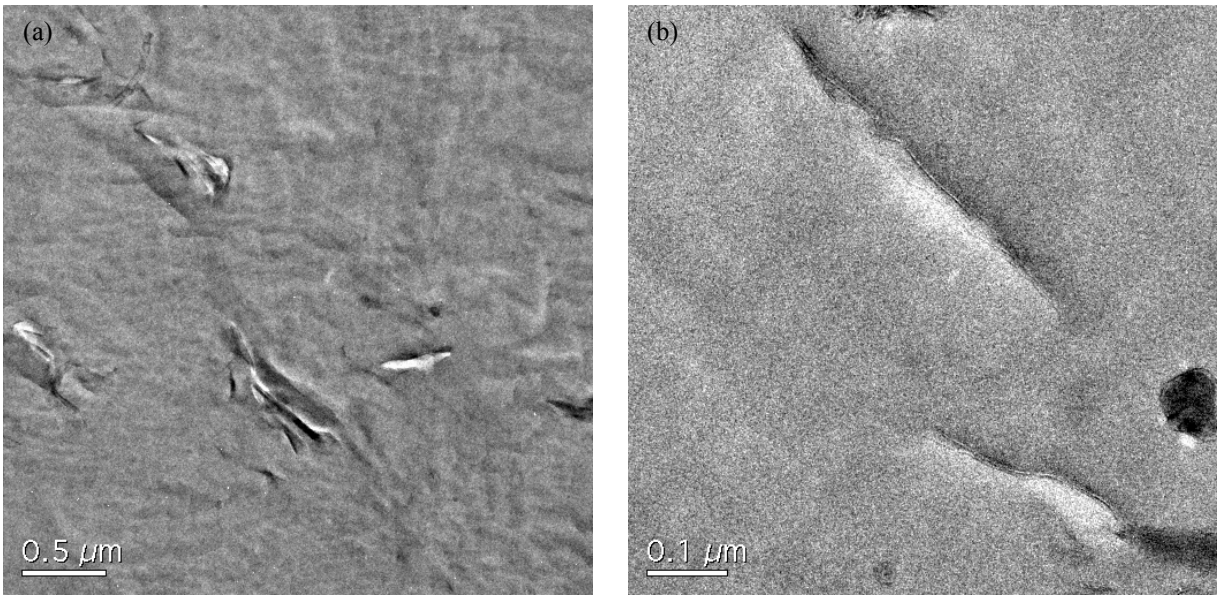

Figure 3.16 TEM images of PEN/TPP-Sb-MMT-2

(V) General Limitations of the In-situ Polymerization Technique

Past literature has pointed in-situ polymerization as the preparation method that can potentially achieve the best dispersion of clay in the polymer matrix [61] as it involves the intercalation of monomers, which are smaller than the corresponding polymer. Furthermore, the functional groups of the organic cations which are used to modify clay can be tailor-made such that they are able to catalyze intralyer polymerization, or be tethered to the ends of growing polymer chains – both of which can greatly facilitate the delamination of clay in the polymer matrix. In this work however, the carefully engineered surface modification of clay is often altered as a result of degradation reactions which inevitably occurs during the long-time high-temperature exposures necessary for the polymerization reaction to take place. Consequently, the dispersion of clay in PEN achieved by the in-situ polymerization method is limited.

In addition, the severe discoloration and physical properties of the in-situ polymerized products suggest that organoclay degradation could also interfere with the polymerization process, causing the degradation of the PEN polymer, as well as changing its molecular weight and molecular weight distribution. As the in-situ polymerization method did not lead to impressive nanoscale dispersion of clay however, the degradation issue was not further studied.

The level of clay dispersion that can be realized by the in-situ polymerization technique in this work is also limited by the amount of shear force that can be achieved in the setup for in-situ polymerization. The TEM micrographs (Figure 3.16) indicate that individual layers in fact exist with multilayer stacks. This suggests that the mechanical mixing applied is insufficient to break up all the larger agglomerated

masses. The result is the general inhomogeneous distribution of clay in the in-situ polymerized material.

3.5.3 Melt Intercalation

Principles

The method of melt intercalation was explored in this work for the preparation of PEN/clay nanocomposites because it can potentially provide the greatest commercial viability. Furthermore, although melt compounding requires PEN to be heated up to similar high temperatures as in-situ polymerization, the residence time involved is much shorter, thus this preparation route may potentially bypass the problems of thermal degradation which are encountered during in-situ polymerization.

In the selection of a suitable clay modifier for the melt intercalation process, a new class of trialkylimidazolium-treated clays that was recently developed was considered, as previous work has demonstrated that they possess significantly greater thermal stability, compared to other organically-modified clays [33,34]. In particular, two types of trialkylimidazolium salt derivatives (Table 3.2) - 1,3-didecyl-2-methylimidazolium (IM2C10), which possesses two decyl chains and 1-hexadecyl-2,3-dimethylimidazolium (IMC16), which has only a s investigated.

To assess the ability of the various modified cl compounding conditions, isothermal TGA was perform temperature. Figure 3.17 displays the isothermal TGA cu organically-modified clays. Table 3.5 summarizes the ex observed in the modified clays under the simulated melt (The actual residence time of the material in the extruder

typically not more than 10 minutes, thus the isothermal TGA results only serve as a guide to compare the amount of thermal degradation that will occur in the various organoclays, and should not be used to determine the actual degradation that will occur in the organoclays during melt compounding.)

The isothermal TGA results indicate that the trialkylimidazolium-treated clays possess significantly greater thermal stability under the simulated melt compounding conditions compared to the ammonium-based CDA-MMT or the phosphonium-based TPP-MMT. They were thus used for the melt intercalation of PEN/clay hybrids. As a comparison, a PEN/clay hybrid based on unmodified Na-MMT was also prepared. (The complete list of PEN/clay hybrids that were prepared by the melt intercalation method was given in Table 3.4.)

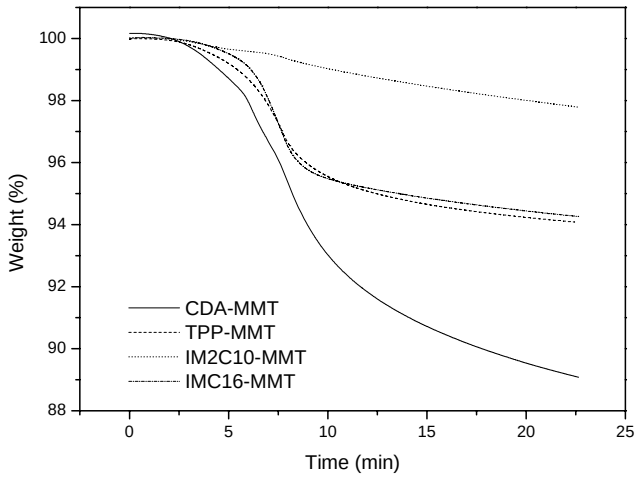

Figure 3.17 TGA curves of the organically modified clays. The clay samples were held isothermal at 295°C for 15 minutes. Time = 0 min corresponds to the end of the predrying step at 140°C before the sample was heated at 20°C/min to 295°C and held isothermal for 15 minutes.

Table 3.5 Extent of thermal degradation in the organically-treated clays, as evaluated by isothermal TGA at 295°C for 15 minutes.

Organoclay	Extent of thermal degradation (%)[a]
CDA-MMT	53.6
TPP-MMT	28.7
IM2C10-MMT	8.3
IMC16-MMT	22.4

[a] Evaluated by taking the total mass loss at the end of the heating process and dividing by the total organic content in the organoclays.

Discussion

(I) Effect of Clay Modification on Dispersion

Figures 3.18 and 3.19 display the XRD patterns of the two trialkylimidazolium-treated clays, and the corresponding PEN/clay hybrids respectively.

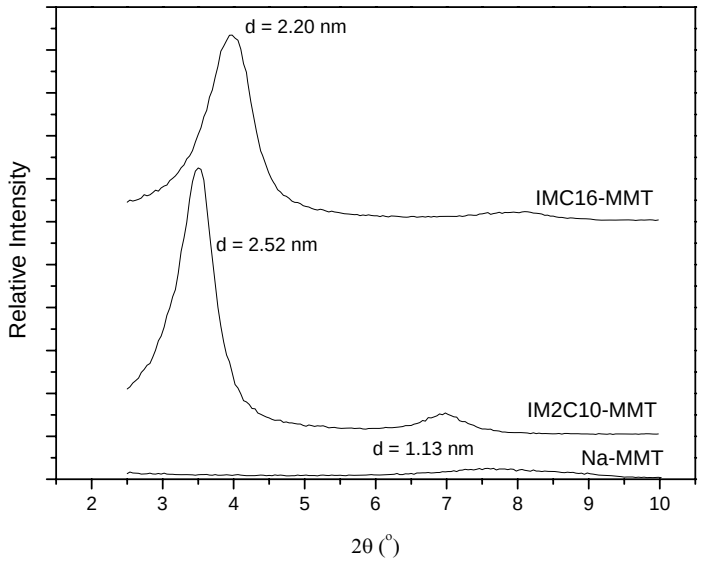

Figure 3.18 XRD patterns of clay before and after modification with the trialkylimidazolium ions.

POM and TEM provides additional information on the morphology of the PEN/clay hybrids. Figure 3.20 shows the clay dispersion in the PEN/clay hybrids, as observed under the POM. It is observed that large clay aggregates are still present in PEN/Na-MMT-2. Although the clay peak in the PEN/Na-MMT-2 hybrid is much broader and much lower in intensity compared to the other two organoclay hybrids, the presence of the large clay aggregates in PEN/Na-MMT-2 indicates that this is probably due to the high degree of disorder within the clay stacks in the untreated Na-MMT, rather than good dispersion. The presence of melt material between the clay aggregates in PEN/Na-MMT-2 further suggests that the shear force applied in the twin screw extruder during melt compounding is strong enough to break the large clay agglomerates into smaller tactoids, however, due to the hydrophilic nature of the Na-MMT surface, the clay will tend to reaggregate even after they have been successfully broken down. In contrast, most of the clay particles in PEN/IM2C10-MMT-2 and PEN/IMC16-MMT-2 have been effectively broken down into submicron- and nanometer-sized domains, which were almost invisible under the POM.

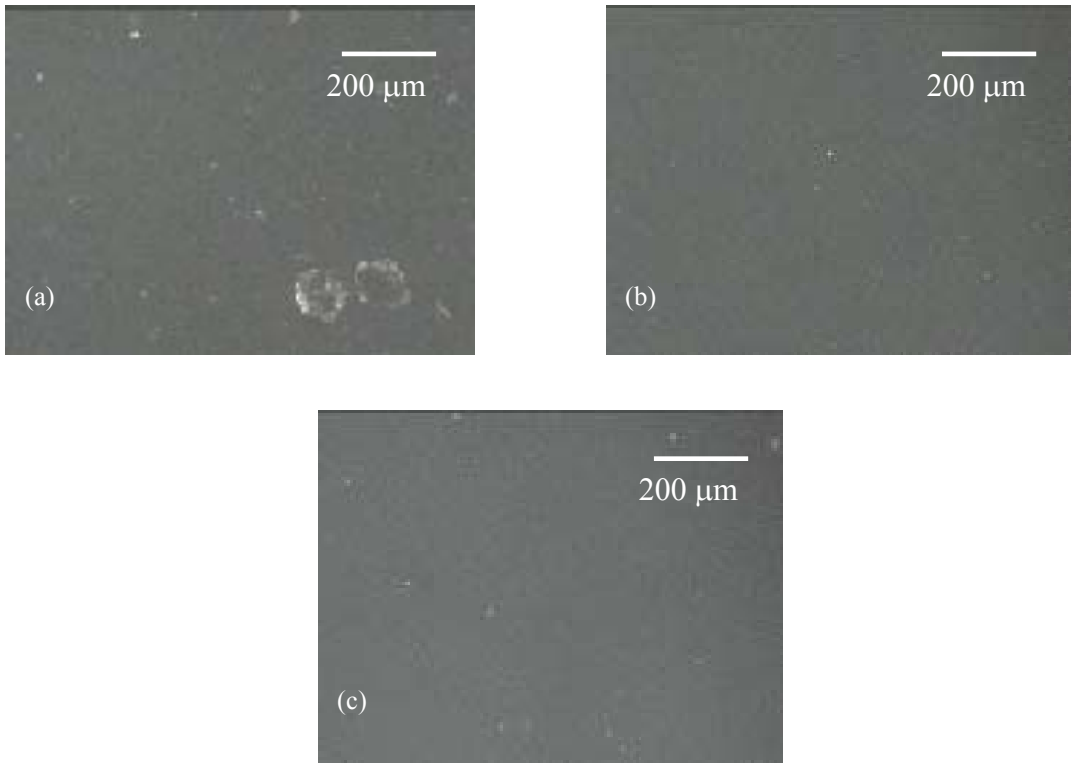

Figure 3.20 Images obtained with the POM under crossed polarizers (a) PEN/Na-MMT-2, (b) PEN/IM2C10-MMT-2 and (c) PEN/IMC16-MMT-2.

TEM images taken at a lower magnification (Figure 3.21) indicate that a homogeneous dispersion of clay has been achieved in both PEN/IM2C10-MMT-2 and PEN/IMC16-MMT-2. The average thickness of the clay stacks in PEN/IMC16-MMT-2 is however, smaller than those in PEN/IM2C10-MMT-2. TEM thus not only verifies the finding based on XRD, that a larger clay intergallery distance has been achieved in PEN/IMC16-MMT-2 due to the intercalation of PEN chains (Figure 3.22), it also provides direct evidence that the multilayer clay tactoids in PEN/IMC16-MMT-2 have been effectively broken down into thinner stacks, as a result of the better compatibility between PEN and IMC16-MMT (Figure 3.21).

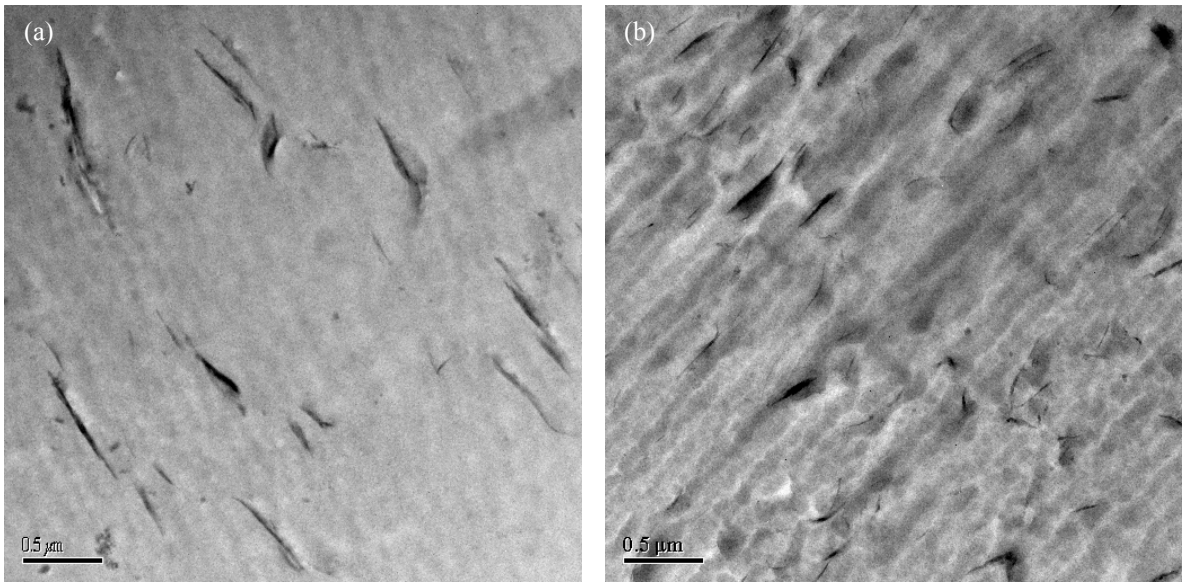

Figure 3.21 TEM micrographs of (a) PEN/IM2C10-MMT-2 and (b) PEN/IMC16-MMT-2 (Original magnification: 5000x).

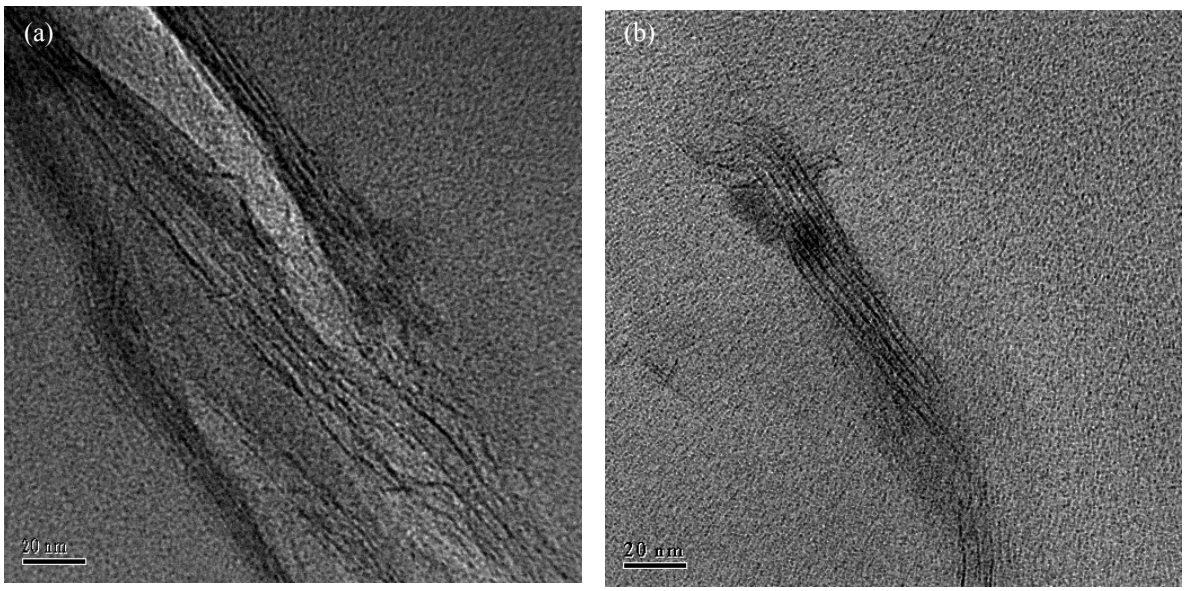

Figure 3.22 TEM micrographs of (a) PEN/IM2C10-MMT-2 and (b) PEN/IMC16-MMT-2 (Original magnification: 120 000x).

(II) Effect of Concentration and Second Compounding on Clay Dispersion

The effect of clay concentration and second compounding on the clay dispersion, which is important from both the processing and applications point of view, is further investigated in the PEN/IMC16-MMT system. A higher concentration (4 wt%) masterbatch was first prepared, the 4 wt% hybrid (PEN/IMC16-MMT-4) was then diluted with pure PEN and then melt compounded a second time to form a 2 wt% hybrid (PEN/IMC16-MMT-2B). Figure 3.23 displays the XRD patterns of PEN/IMC16-MMT-4 and PEN/IMC16-MMT-2B. The XRD profile of the 2 wt% PEN/IMC16-MMT-2 hybrid that was prepared by only one extrusion cycle was also shown as a reference.

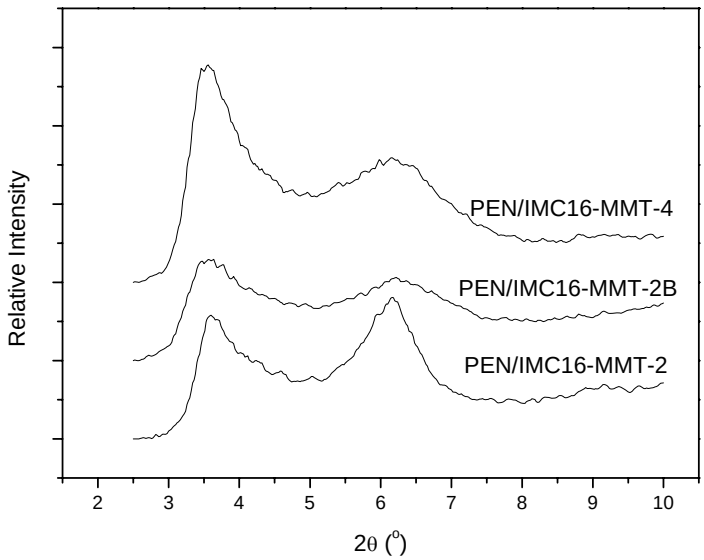

Figure 3.23 XRD patterns of the PEN/IMC16-MMT hybrids. The intensities of the clay peak have been scaled using the amorphous halo from the polymer as a reference.

Figures 3.24 and 3.25 further display the POM and TEM images obtained for PEN/IMC16-MMT-2B and PEN/IMC16-MMT-4.

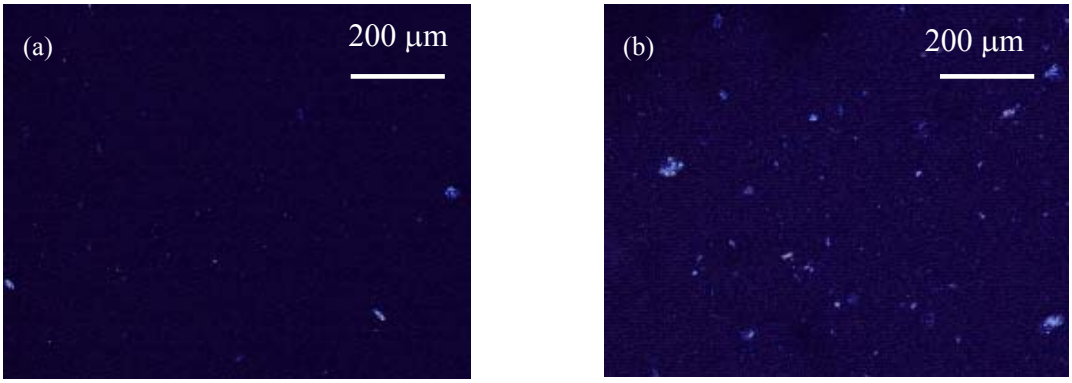

Figure 3.24 Images obtained with the POM under crossed polarizers (a) PEN/IMC16-MMT-2B and (b) PEN/IMC16-MMT-4.

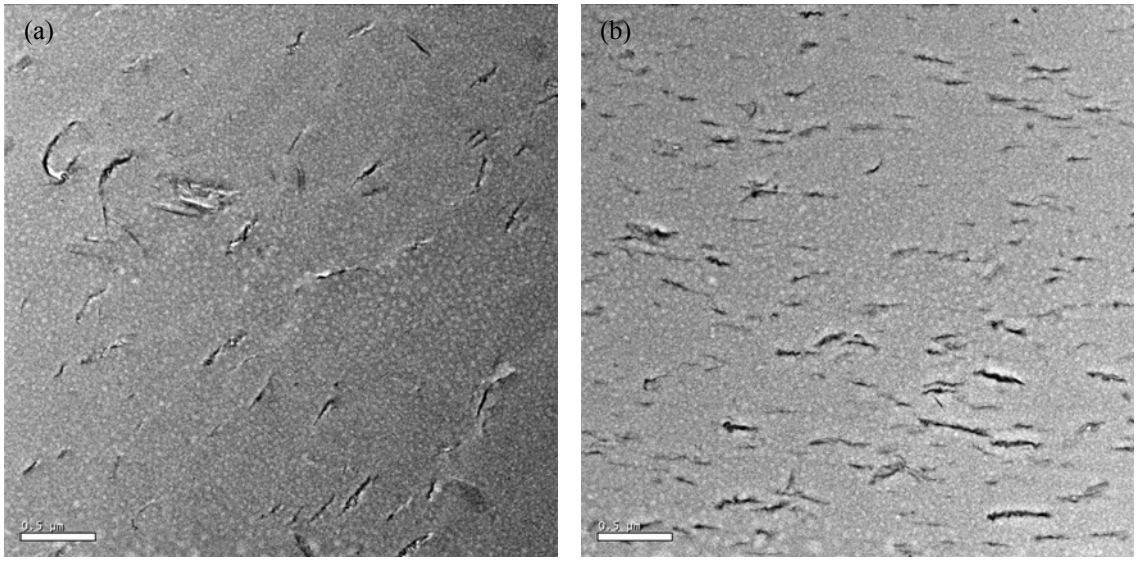

Figure 3.25 TEM micrographs of (a) PEN/IMC16-MMT-2B and (b) PEN/IMC16-MMT-4 (Original magnification: 5000x).

XRD indicates that the clay peak in PEN/IMC16-MMT-2B has a lower intensity, as well as a broader full width at half maximum (FWHM) compared to PEN/IMC16-MMT-2, which has the same clay content, but has only gone through a single extrusion cycle. This conclusion is verified by TEM observations (Figure 3.25(a)), which shows that the average size of the clay tactoids in PEN/IMC16-MMT-

2B is slightly smaller than that present in PEN/IMC16-MMT-2 (Figure 3.21(b)). The additional shear experienced during the second compounding cycle thus has some effect in further breaking apart the clay tactoids, although admittedly, the effect is not profound.

Compared to both 2 wt% hybrids, the 4 wt% hybrid (PEN/IMC16-MMT-4) exhibits a significantly poorer level of clay dispersion, as indicated by the higher intensity of the clay peak obtained in the XRD pattern, as well as the presence of thicker clay stacks in the TEM image. POM also reveals the presence of micron-sized agglomerates, which are absent in the 2 wt% hybrids. This result is in agreement to previous studies – generally, it becomes more difficult to disperse clay when it is present in higher concentrations [62,63], because the attractive interactions between adjacent clay platelets (both van der Waals' interactions and steric interactions due to the high aspect ratio of clay) becomes stronger.

(III) General Comments on the Melt Intercalation Method

The series of investigations performed in this section illustrates that the use of organoclays with sufficient thermal stability is of key importance in the preparation of polymer/clay nanocomposites. Adequate thermal stability is required to ensure that the carefully tailored organic surface will be retained during nanocomposite preparation, so that the compatibility with the polymer matrix can be maintained to allow the clay to delaminate in the polymer matrix. The melt intercalation approach has been able to achieve good nanoscale dispersion of the clays because of the less severe temperature excursions involved (as compared to the in-situ polymerization process), and the greater thermal stability of the trialkylimidazolium-modified clays used. In addition to thermal stability, the organically-treated clay must also possess

good compatibility with the polymer matrix, otherwise, it will not be able to intercalate into the gallery spaces of the organoclay during the melt compounding process to form a well-dispersed nanocomposite, as exemplified in this study by the case of PEN/IM2C10-MMT-2.

Furthermore, to take advantage of the carefully tailored compatibility, it is important to first ensure good homogeneity of the initial polymer/clay premix. In this work, the as-received PEN polymer is in the form of millimeter-sized pellets. To enhance the homogeneity of the polymer/clay mixture, the polymer was first ground into smaller sizes [58]. Figure 3.26 displays the POM image of a PEN/Na-MMT-2 hybrid, in which the polymer has not been ground into smaller sizes prior to the melt compounding step. The large numbers of micron-sized aggregates observed as compared to the hybrid shown in Figure 3.20(a) illustrates the importance of the polymer grinding step in achieving good homogeneity of the hybrids at the micron level.

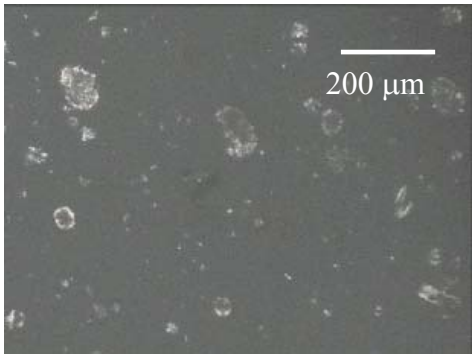

Figure 3.26 POM image of a PEN/Na-MMT-2 hybrid in which the polymer was not ground into smaller sizes before it was mixed with the clay for compounding.

If the conditions of thermal stability, good compatibility, as well as proper premixing are satisfied, the shear force applied in a twin-screw extruder is capable of

achieving a sufficient level of homogeneity in the resultant hybrid materials, at least at the submicron level. This is a major strength of the melt intercalation method over the in-situ polymerization route, because it is very difficult to achieve the same degree of physical mixing in the in-situ polymerization setup for PEN. Once the clay tactoids have been broken down into nanometer-sized domains however, it becomes increasingly more difficult to further break down the clay particles by the mere application of shear force. Consequently, the further enhancement in clay dispersion provided by a second compounding cycle is very limited.

3.6 Summary and Conclusions

The various preparation routes that have been investigated in the course of this work have helped to elucidate the factors that are critical to the effective dispersion of clay in PEN. It is found that modifier compatibility, organoclay stability, and proper mixing all play an important role in producing high levels of clay dispersion. Failure to consider any of these factors will typically result in poor dispersion of clay in the PEN matrix.

With respect to the two methods of preparation that have been explored, the TEM micrographs of the in-situ polymerized and melt intercalated hybrids reveal that the mechanisms of clay exfoliation in the two methods are in fact different. For in-situ polymerization, the diffusion of monomers and subsequent formation of polymers at the interlayer spaces are responsible for the peeling of the tactoids. Because of this mechanism of clay delamination, single layers of clay can co-exist side by side with multilayered clay stacks. On the other hand, for melt intercalation, it is the large stress transfer in the melt, as a result of the shearing profile applied, that breaks the micron-sized agglomerates into smaller tactoids (instead of peeling them into individual

sheets). For this reason, the size distribution of the clay tactoids in the melt-intercalated hybrids is much more homogeneous, although the tactoids are mostly of intermediate size.

This indicates that while melt intercalation has been established in this work as a production route that is capable of breaking the clay tactoids into smaller and more uniformly-sized stacks, in-situ polymerization still remains the method that exhibits the greatest potential of producing well exfoliated layers in the PEN matrix. Although the investigations performed in the course of this work have revealed several limitations of the in-situ polymerization technique as discussed in Section 3.5.2(V), these limitations are more the result of the shortcomings in the type of clay modification and the in-situ polymerization set-up used in this work, rather than problems inherent to the in-situ polymerization method. With the mixed intercalant system, the potential of the in-situ polymerization method to the preparation of well-dispersed hybrids has been demonstrated. With the use of more thermally stable organically-modified clays (for example, the trialkylimidazolium-treated clays) and a better in-situ polymerization set-up (which can achieve a higher shear force), the in-situ polymerization route still holds significant potential in the preparation of well-dispersed PEN/clay nanocomposites. For the further refinement of the in-situ polymerization technique therefore, the investigations performed in this work shall serve as a very useful reference by which future efforts can be based on.

Due to the better states of clay dispersion and homogeneity that have been achieved with the trialkylimidazolium-treated clay hybrids prepared via the melt intercalation route, this series of hybrids was selected for further systematic structural and property studies, as will be described in the following two chapters.

CHAPTER 4

Structure-Property Relationship in PEN/Clay Hybrids

4.1 Introduction

Having probed the clay dispersion that has been achieved in the PEN/clay hybrids, the actual performance of the hybrids is now examined. In particular, the dynamic mechanical properties and thermal stability of the materials are investigated to evaluate the effectiveness of nanoclay in improving these properties in PEN, which are important to its performance in real-life applications. Special emphasis has also been placed in understanding how the property changes in the hybrids are related to the dispersion and orientation of the clay phase, as well as the clay-induced modifications to the matrix crystalline morphology.

4.2 Dynamic Mechanical Behaviors

4.2.1 Introduction

One important reason for the great interest in polymer/clay nanocomposites is the exceptional material stiffness they provide at relatively low inorganic content. In spite of the superior reinforcing efficiency commonly observed in polymer/clay nanocomposites, the mechanisms responsible for their outstanding mechanical performance are not well understood. To fully exploit the potential of this class of nanocomposites, a more fundamental understanding of the correlation between their structures and properties need to be established.

Semicrystalline polymer/clay nanocomposites, in particular, exhibit a complex hierarchical morphology consisting of structural features organized at various length scales. Specifically, clay platelets of nanometer thickness, separated at a distance similar to their size, coexist with the crystalline lamellae of the polymer matrix. Further complications arise when the various components orient themselves under the effect of a shear field, which is commonly experienced in melt processing environments such as extrusion or injection molding [64]. Till now, it is not well understood how these different morphological features interact and influence the final properties exhibited by the polymer. In particular, it remains an issue of controversy whether the outstanding property enhancements observed in many semicrystalline polymer/clay nanocomposites arise mainly from the modifications in the polymer matrix structure caused by the presence of the dispersed clay phase, or can be explained by invoking conventional composite theories, where the reinforcement arise mainly from the high stiffness and high aspect ratio of the dispersed clay phase, while the contribution from the increased matrix modulus play a less important role [65].

In the determination of the structure-property relationship of PEN, the slow crystallizing characteristics of PEN [66] may in fact provide it with the unique advantage in that totally amorphous structures may be achieved easily during molding, and crystallinity can be introduced subsequently via an annealing treatment. In this way, the contributions of the modified matrix crystalline phase to the enhancement in properties may be better isolated and studied.

In this section, the thermomechanical properties of the hybrids are assessed by dynamic mechanical analysis. The effect of crystallization on the nanocomposite modulus is also evaluated by subjecting the initially amorphous as-molded specimens to an annealing treatment. The mechanical reinforcement achieved in the materials is

further correlated with the hierarchical structure they exhibit, to elucidate the underlying mechanisms by which the dispersed clay phase, as well as the modified polymer crystalline phase contribute to the mechanical reinforcement in the nanocomposites. Although the investigation was performed on PEN/clay nanocomposites, the structure-property relationship evaluated may also be extended to other semicrystalline polymer/clay nanocomposites, and serve as a useful reference by which their hierarchical structures may be predicted and controlled for optimal mechanical performance.

4.2.2 Experimental

(I) Dynamic Mechanical Analysis (DMA)

Dynamic mechanical analysis (DMA) was conducted with a TA Instruments DMA 2980 on specimens molded with a DACA Instruments Microinjector #5000 at a barrel temperature of 300^{o}C and a mold temperature of 45^{o}C. The specimens were cut out from the center of dog-boned shaped tensile bars, and have dimensions of 22.0 mm (length) x 4.0 mm (width) x 1.5 mm (thickness). Prior to testing, the sides of all specimens were carefully polished with fine sandpaper (grit 320 followed by grit 1200) to ensure that the dimension of the specimens were uniform throughout, down to the nearest 0.01 mm. This procedure has been especially undertaken, as small variations in the specimen dimensions have been found to be an important factor contributing to variations observed in DMA measurements [67].

3-point Bending Mode

The complex moduli of the as-molded samples were measured in the 3-point bending mode at a frequency of 1 Hz, a strain amplitude of 0.1% and with a preload force of

0.1 N. The support holder of the 3-point bending clamp has pressure points 15 mm apart. The specimens were heated at 3°C/min from room temperature to 130°C. A minimum of 3 specimens of each material were tested.

Tension Mode

To assess the effect of crystallization on the dynamic mechanical properties, the PEN and PEN/IMC16-MMT-2 samples were subjected to an annealing treatment at 240°C for 5 minutes. The complex moduli of both as-molded and annealed samples were measured in the tension mode at a frequency of 1 Hz, an amplitude of 5 μm and with a preload force of 0.03 N. A typical sample length of 15 mm was used. The samples were heated at 3°C/min from room temperature to 150°C (for as-molded samples) or 200°C (for annealed samples). A minimum of 3 specimens were tested for each set of materials.

(II) 2-Dimensional Wide-Angle X-Ray Diffraction

The x-ray diffraction patterns of the as-molded and annealed specimens were recorded in the reflection mode with a Bruker GADDS diffractometer equipped with a two-dimensional (2D), position-sensitive area detector using CuK_α radiation (λ = 0.154 nm) generated at 40 kV and 40 mA. The azimuthal average of the 2D diffraction patterns was determined with the GADDS software package to obtain intensity against 2θ plots. To assess the extent of clay orientation, the same software is used to determine the radial average of the 2D patterns from $2\theta = 2.5^o$ to 5.0^o, to obtain intensity versus azimuthal angle plots.

(III) Transmission Electron Microscopy (TEM)

To observe the effect of annealing on the distribution and orientation of clay in PEN/IMC16-MMT-2, ultrathin sections (~ 80 nm thick) were sectioned along the TD-ND plane (Figure 4.1) using a Leica Ultracut UCT Ultramicrotome. The sections were collected using 200 mesh carbon-coated copper grids, and examined using a JEOL 2010 TEM operating at an accelerating voltage of 200 kV.

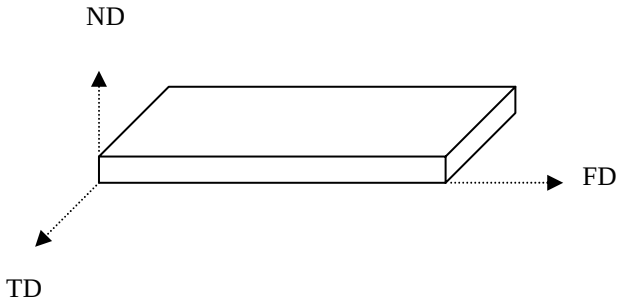

Figure 4.1 Nomenclature of the processing direction encountered in microinjection: the orthogonal axes labels represent the transverse direction (TD), flow direction (FD) and normal direction (ND).

(IV) Modulated Differential Scanning Calorimetry (MDSC)

MDSC measurements were performed on the annealed specimens on a TA Instruments MDSC 2920 under a nitrogen purge. The samples were heated at 3^{o}C/min to a temperature of 320^{o}C, with a modulation period of 60 seconds and a temperature amplitude of ± 0.477^{o}C. The percent crystallinity of the annealed samples was calculated by subtracting the reversing heat flow from the non-reversing heat flow, and diving by the heat of fusion for 100% crystalline PEN (170 J/g) [68]. The crystallinity values reported were based on the average of 3 independent measurements.

(V) Polymer Crystalline Morphological Studies

Thin polymer films for polarized optical microscopy (POM) and atomic force microscopy (AFM) were prepared by the following procedure: A thin sample piece was sandwiched between two glass coverslips, placed onto the hot stage (Linkham TMS 92) and melted at 300^{o}C to remove all residual crystallites. A gentle pressure was then applied to the upper glass to squeeze the melt into a very thin film before the upper glass coverslip was removed. The sample was then quenched to room temperature, and subsequently annealed at 240^{o}C for 15 minutes. After the annealing treatment, the sample was rapidly quenched again to room temperature.

To reveal the crystalline features more clearly, the samples were etched following the method of Shabana *et al* [69], by immersing them in a potassium permanganate solution at room temperature. The solution contained 10 mg of potassium permanganate per milliliter of a 10:4:3 vol:vol:vol mixture of concentrated sulfuric acid, orthophosphoric acid (85%) and water. After 40 minutes of sample immersion, the samples were recovered and placed in a cooled solution consisting of 3 parts concentrated sulfuric acid, 7 parts water and 10% hydrogen peroxide for 10 minutes, followed by several rinsing in deionized water.

POM was performed with a Nikon Eclipse E600 POL polarizing optical microscope under crossed polarizers. Tapping mode AFM images were obtained with a Dimension 3100 AFM (Digital Instruments) using Si tips. Both height and amplitude images were recorded simultaneously. All POM and AFM images were captured at room temperature.

4.2.3 Results and Discussion

In the following section, the dynamic mechanical behaviors of the hybrids will be discussed with respect to the effect of clay modification, second compounding, clay concentration and annealing treatment. The as-molded specimens were tested in the 3-point bending mode because it is the "purest" deformation mode, as clamping effects are effectively eliminated in this mode. For the annealed specimens however, the specimens were tested in the tension mode so that the modulus along the flow direction (and hence any possible effects of clay/crystallite orientation) can be determined.

The storage modulus (E') and glass transition temperature (T_g) values reported were evaluated based on the average of 3 independent measurements. Standard deviations for E' were typically less than 5% of the values reported.

4.2.3.1 Effect of Clay Modification

Figures 4.2 shows representative plots for the temperature dependence of the storage modulus (E') and loss modulus (E") for as-molded samples of PEN and its hybrids.

E' is the part of the modulus that is in phase with the applied stress. The actual stiffness of a polymer is thus strongly dependent on its E' value. The E' of the various systems are compared at 35^{o}C and 80^{o}C and the results are listed in Table 4.1. The effectiveness of clay as a reinforcement for the PEN matrix is elucidated by taking the ratio of the storage modulus of the hybrid (E'_h) to that of the neat PEN (E'_m). The glass transition temperatures (T_g) of the materials, as determined from the peak in the E" versus temperature curves are also listed in Table 4.1.

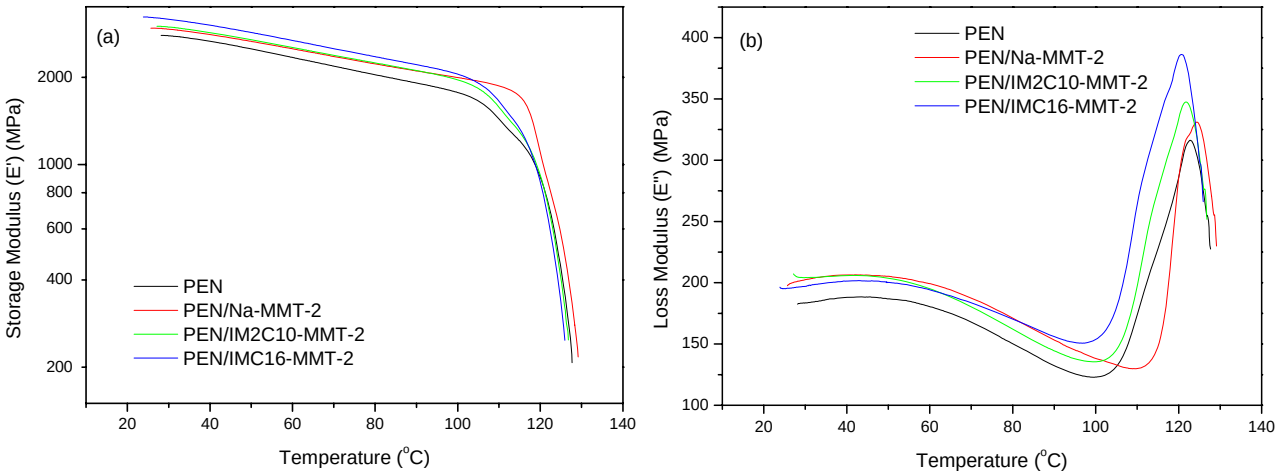

Figure 4.2 (a) Storage modulus (E') and (b) loss modulus (E") as a function of temperature for as-molded samples of PEN and its hybrids.

Table 4.1 DMA data of as-molded samples of PEN and its hybrids in the 3-point bending mode[a].

System	E' at 35°C (MPa)	E'_h / E'_m (35°C)	E' at 80°C (MPa)	E'_h / E'_m (80°C)	T_g (°C)
PEN	2763 ± 26	-	2045 ± 15	-	123
PEN/Na-MMT-2	2839 ± 50	1.03	2189 ± 50	1.07	124
PEN/IM2C10-MMT-2	2932 ± 14	1.06	2241 ± 20	1.10	122
PEN/IMC16-MMT-2	3160 ± 39	1.14	2343 ± 10	1.15	121

[a] Errors given represent one standard deviation from the mean.

X-ray diffraction analysis (Figure 4.3) indicates that the specimens are almost amorphous after molding. The reinforcement effect observed in the hybrids is thus mainly due to the dispersed clay phase only.

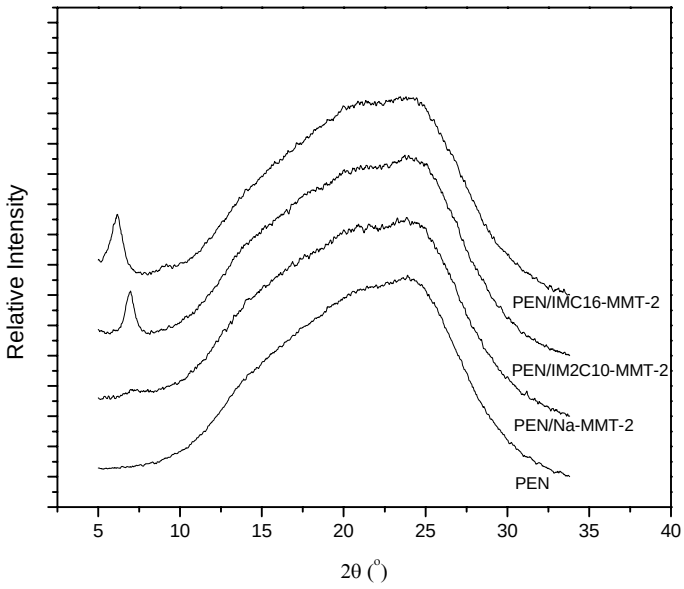

Figure 4.3 X-ray diffraction patterns of as-molded samples of PEN and its hybrids. The specimens were oriented such that the incident beam is reflected off the TD-FD plane.

Table 4.1 indicates that the intercalated nanocomposite, PEN/IMC16-MMT-2 exhibits significantly greater reinforcement effects compared to the two less well-dispersed hybrids, PEN/Na-MMT-2 and PEN/IM2C10-MMT-2. The intercalation of polymer into the IMC16-MMT interlayer galleries results in an increase in the active surface area and aspect ratio of the filler within the matrix. The increase in the degree of mechanical reinforcement with better clay dispersion results from an increase in the aspect ratio of the dispersed clay phase, as the reinforcement efficiency of inorganic fillers is strongly related to their aspect ratios [70]. The moduli at 80°C further indicates that the presence of clay helps to maintain the stiffness of PEN at a higher level even at elevated temperatures, which is an important property required for the PEN/clay nanocomposites for high-temperature applications.

In addition, it was found that the presence of clay has no significant impact on the T_g of the hybrids.

4.2.3.2 Effect of Second Compounding and Clay Concentration

The dynamic mechanical properties of PEN/IMC16-MMT-2B and PEN/IMC16-MMT-4 were also examined to evaluate the effect of second compounding and clay concentration on the storage modulus.

Figures 4.4 displays the variation of E' and E" with temperature for as-molded specimens of this series of hybrids. The important data obtained from the DMA curves are summarized in Table 4.2.

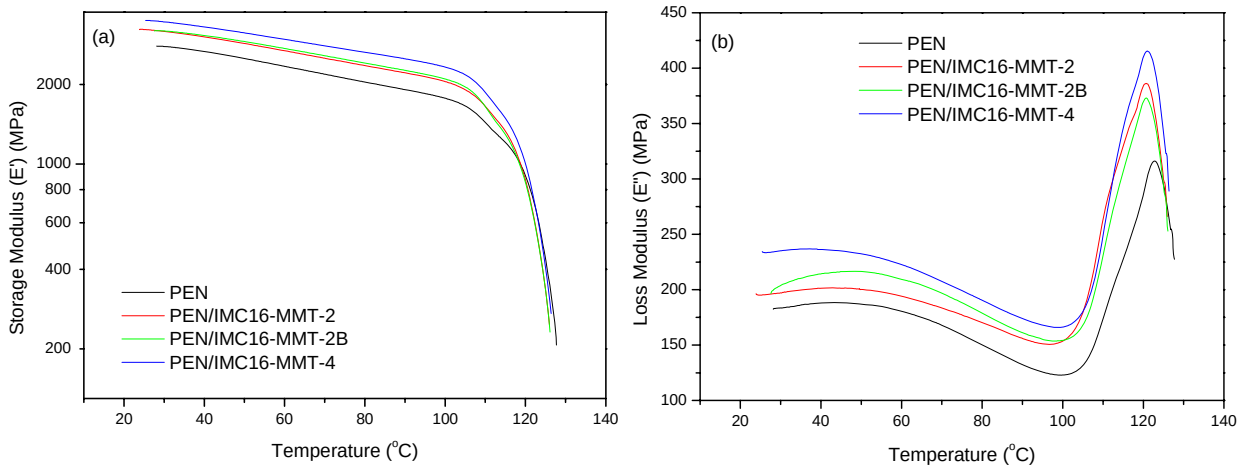

Figure 4.4 (a) Storage modulus (E') and (b) loss modulus (E") as a function of temperature for as-molded samples of PEN/IMC16-MMT-2B and PEN/IMC16-MMT-4. The curves for PEN and PEN/IMC16-MMT-2 are also presented as a reference.

Table 4.2 DMA data of as-molded samples of PEN/IMC16-MMT-2B and PEN/IMC16-MMT-4 in the 3-point bending mode. The data for pure PEN and PEN/IMC16-MMT-2 are also shown for comparison[a].

System	E' at 35°C (MPa)	E'_h/E'_m (35°C)	E' at 80°C (MPa)	E'_h/E'_m (80°C)	T_g (°C)
PEN	2763 ± 26	-	2045 ± 15	-	123
PEN/IMC16-MMT-2	3160 ± 39	1.14	2343 ± 10	1.15	121
PEN/IMC16-MMT-2B	3154 ± 52	1.14	2375 ± 25	1.16	120
PEN/IMC16-MMT-4	3393 ± 51	1.23	2555 ± 36	1.25	121

[a] Errors given represent one standard deviation from the mean.

From Table 4.2, it is observed that a similar extent of reinforcement is achieved in PEN/IMC16-MMT-2B as PEN/IMC16-MMT-2. Matayabas and Turner have previously suggested that the presence of organoclay can severely degrade the molecular weight of polyesters during melt extrusion [71]. The additional round of extrusion probably induces additional degradation in the PEN matrix, which offsets, to some degree, the additional reinforcement that should have been brought about by an improvement in the clay dispersion in PEN/IMC16-MMT-2B [72].

Furthermore, it is observed that at 4 wt% clay loading, the efficiency of PEN reinforcement by the clay declines. The smaller increase in the storage modulus with a further addition of clay may be attributed to the presence of micron-sized agglomerates in PEN/IMC16-MMT-4 which reduces the reinforcing efficiency of the dispersed clay phase.

4.2.3.3 Effect of Annealing Treatment

Figures 4.5 displays the typical variation of E' and E" with temperature for as-molded and annealed specimens of pure PEN and PEN/IMC16-MMT-2 in the tension mode. The values for E' at 35°C, 80°C and 160°C (for the annealed samples), as well as the T_g of the materials are summarized in Table 4.3.

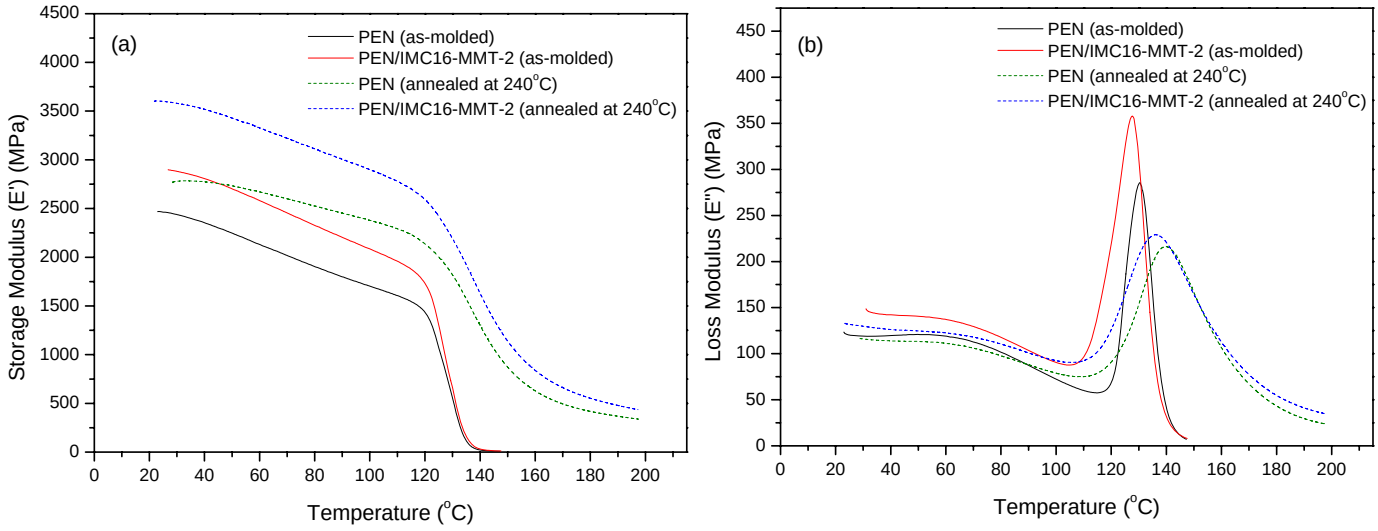

Figure 4.5 (a) Storage modulus (E') and (b) loss modulus as a function of temperature for as-molded (solid lines) and annealed (dashed lines) samples of PEN and PEN/IMC16-MMT-2 in the tension mode.

Table 4.3 DMA data for as-molded and annealed samples of PEN and PEN/IMC16-MMT-2 in the tension mode[a].

Thermal History	As-molded		Annealed	
System	PEN	PEN/IMC16-MMT-2	PEN	PEN/IMC16-MMT-2
E' at 35°C (MPa)	2393 ± 55	2843 ± 23	2833 ± 147	3530 ± 23
$E'_h/ E'_{m\,(35°C)}$	1.19		1.25	
E' at 80°C (MPa)	1919 ± 19	2310 ± 15	2456 ± 100	3098 ± 13
$E'_h/ E'_{m\,(80°C)}$	1.20		1.26	
E' at 160°C (MPa)	-	-	624 ± 12	819 ± 19
$E'_h/ E'_{m\,(160°C)}$	-	-	1.31	
Tg (°C)	131	129	138	137

[a] Errors given represent one standard deviation from the mean.

(I) Modulus Enhancement below the Glass Transition Temperature

From Table 4.3, we observe that as-molded PEN/IMC16-MMT-2 exhibits a 19% increase in E' compared to neat PEN at 35°C. After annealing treatment, the reinforcement effect observed in PEN/IMC16-MMT-2 is further enhanced, as the annealed samples of PEN/IMC16-MMT-2 exhibits a 25% improvement in modulus at 35°C over the neat PEN samples that have been subjected to the same annealing treatment.

Structural Explanations for Enhanced E' Improvement below T_g after Annealing

To evaluate the possible factors that could have contributed to the enhanced reinforcement after annealing, the hierarchical structures of the nanocomposite before and after annealing treatment were examined.

Interfacial Interactions

Previous studies have indicated that when there is a strong interfacial bond formed between the polymer matrix and the filler, the interfacial interactions may suppress the mobility of the polymer segments at the interphase, and give rise to an increase in the T_g or a second transition above the glass transition [73,74]. In this case however, it is observed that there is no significant difference in the T_g between the neat PEN and PEN/IMC16-MMT-2 in both the as-molded and annealed specimens. This suggests that the interfacial interactions between PEN and the IMC16-MMT particles have not been significantly strengthened as a result of the annealing process. The additional modulus enhancement observed in PEN/IMC16-MMT-2 after annealing treatment is therefore unlikely to be due to an alteration of the interfacial interactions between the PEN polymer and the clay.

Clay Orientation and Distribution

Figure 4.6 shows the geometry of the x-ray diffractometer which is used to determine the orientation of clay in the molded specimens in this work. The 2D x-ray diffraction patterns of the specimens are captured by a 2D detector. When a crystal plane is oriented parallel to the sample surface, its reflection will appear at the equator of the 2D x-ray diffraction pattern. The converse is not true however – when a crystal plane is perpendicular to the sample surface, its reflection is usually not observed at the meridian of the x-ray diffraction pattern (or at least for the case when the crystal plane is *perfectly* oriented perpendicular to the sample surface). This is due to the curvature of the Ewald sphere, which results in a loss of information in the vicinity of the reciprocal Z-axis [75].

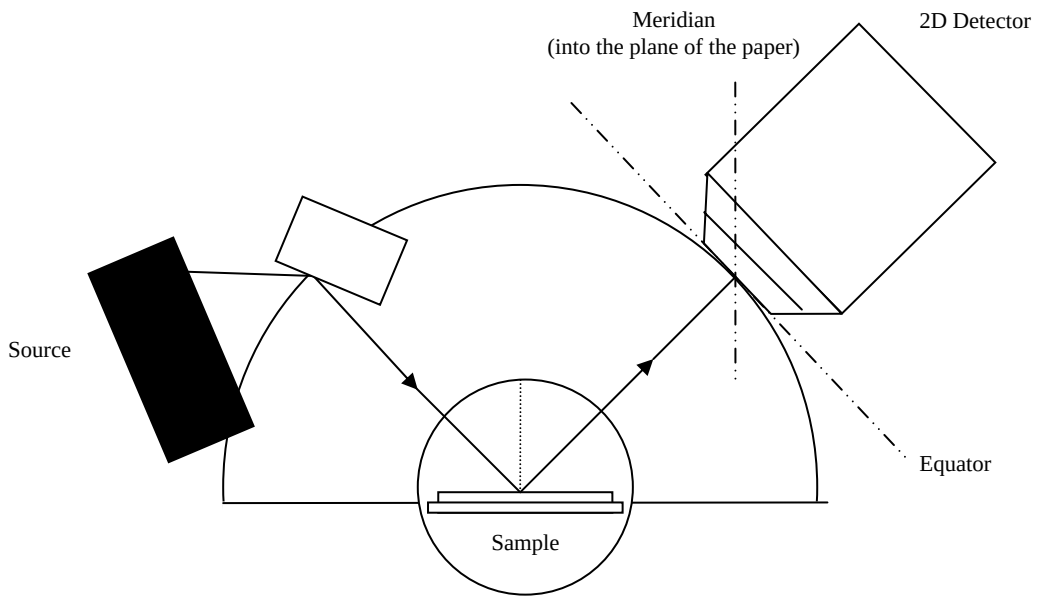

Figure 4.6 Geometry of the 2D x-ray diffractometer used to determine the clay orientation in the molded specimens.

Figure 4.7 displays the 2D x-ray diffraction patterns and the corresponding azimuthal plots of an as-molded specimen of PEN/IMC16-MMT-2 before the annealing treatment. When the x-ray beam is incident on the TD-FD and FD-ND planes, a strong streak is observed along the equatorial direction in the 2D x-ray diffraction pattern (as indicated by the black arrow). On the other hand, when the x-ray beam is incident on the TD-ND plane, no clay diffraction peaks are observed in the equatorial direction. This indicates that the clay sheets in the as-molded specimens tend to align such that their basal planes are parallel to the injection direction as a result of the shear field experienced during the microinjection process (Figure 4.8). The presence of meridional clay reflections (as indicated by the white arrows) when the x-ray beam is incident on the TD-ND plane is due to a slight tilting of the clay basal planes with respect to the normal of the sample surface.

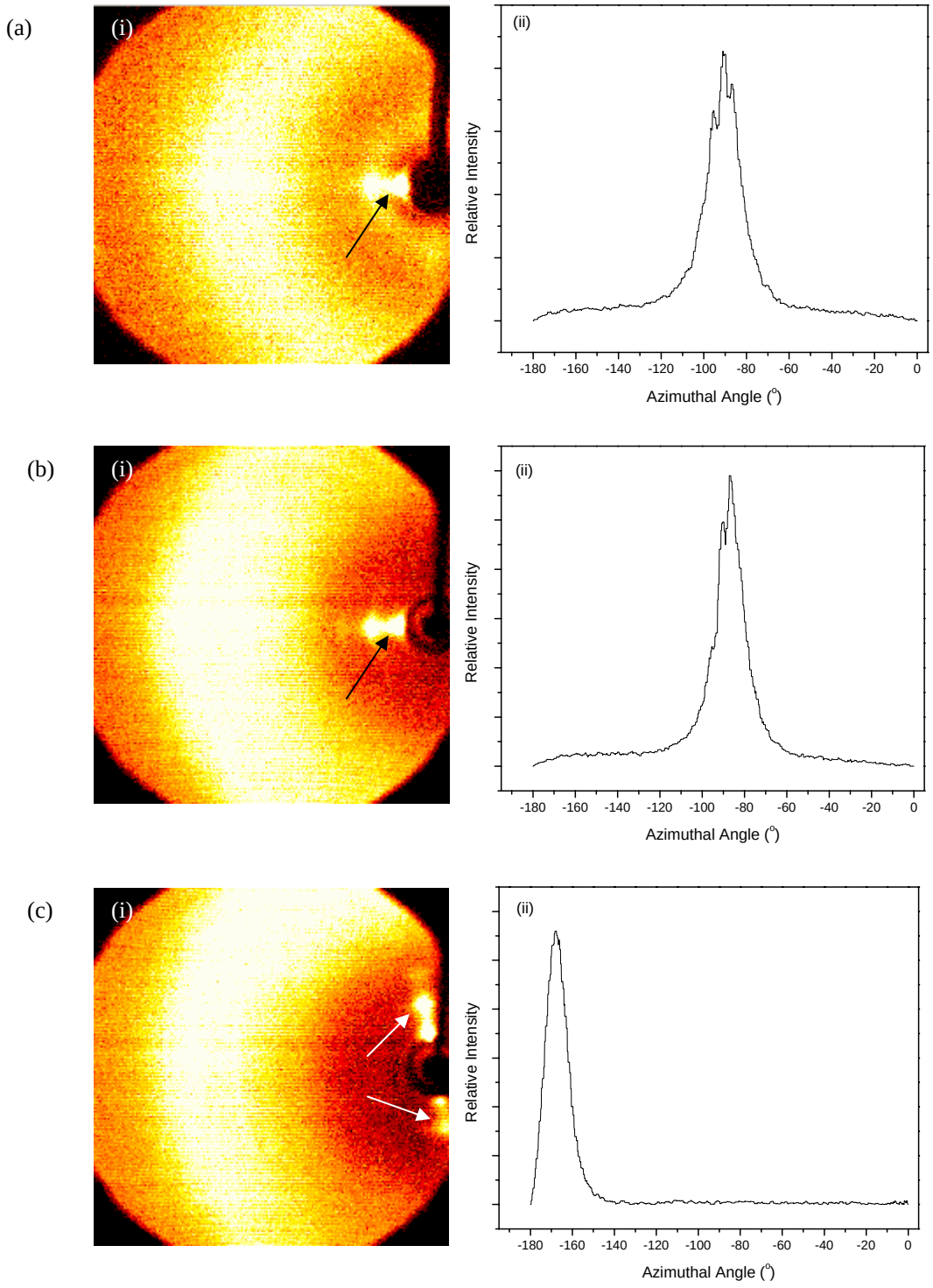

Figure 4.7 (i) 2D x-ray diffraction patterns and (ii) the corresponding azimuthal plots from 2.5° to 5.0° of an as-molded specimen of PEN/IMC16-MMT-2 when the x-ray beam is incident on the (a) TD-FD, (b) FD-ND and (c) TD-ND plane. The sharpness of the azimuthal peak reflects the extent of orientation of the normal of the clay (001) basal plane.

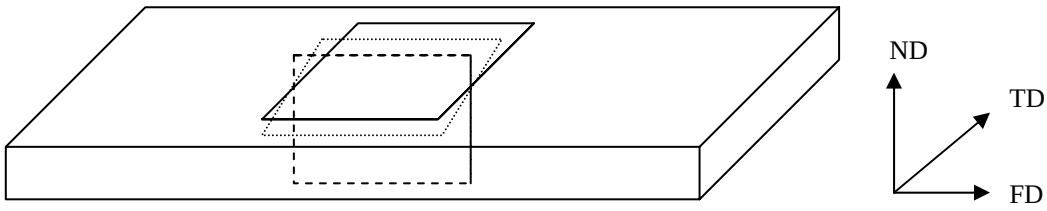

Figure 4.8 Preferential orientation of clay sheets in an as-molded specimen of PEN/IMC16-MMT-2, as deduced from 2D x-ray diffraction. The clay sheets tend to align with their basal planes preferentially oriented parallel to the flow direction.

After the annealing process, the azimuthal plots obtained when the x-ray beam is incident on the TD-FD and FD-ND planes are slightly broader (Figure 4.9(a) and (b)). This indicates that some of the clay sheets are slightly rotated about the transverse or normal directions, which cause their basal planes to be no longer parallel to the flow direction (Figure 4.10). The absence of any clay reflections at the equator when the x-ray beam is incident on the TD-ND plane further provides evidence that the relaxation of the clay orientation during annealing is only very slight as none of the clay sheets in the annealed specimen are aligned normal to the flow direction. Probably, the relaxation of the clay sheets to a plane normal to the flow direction is hindered to some extent because of the nature of the attractive interactions between the anisotropic clay platelets and the restrictions imposed by the polymer chains (which tend to be aligned along the flow direction during molding).

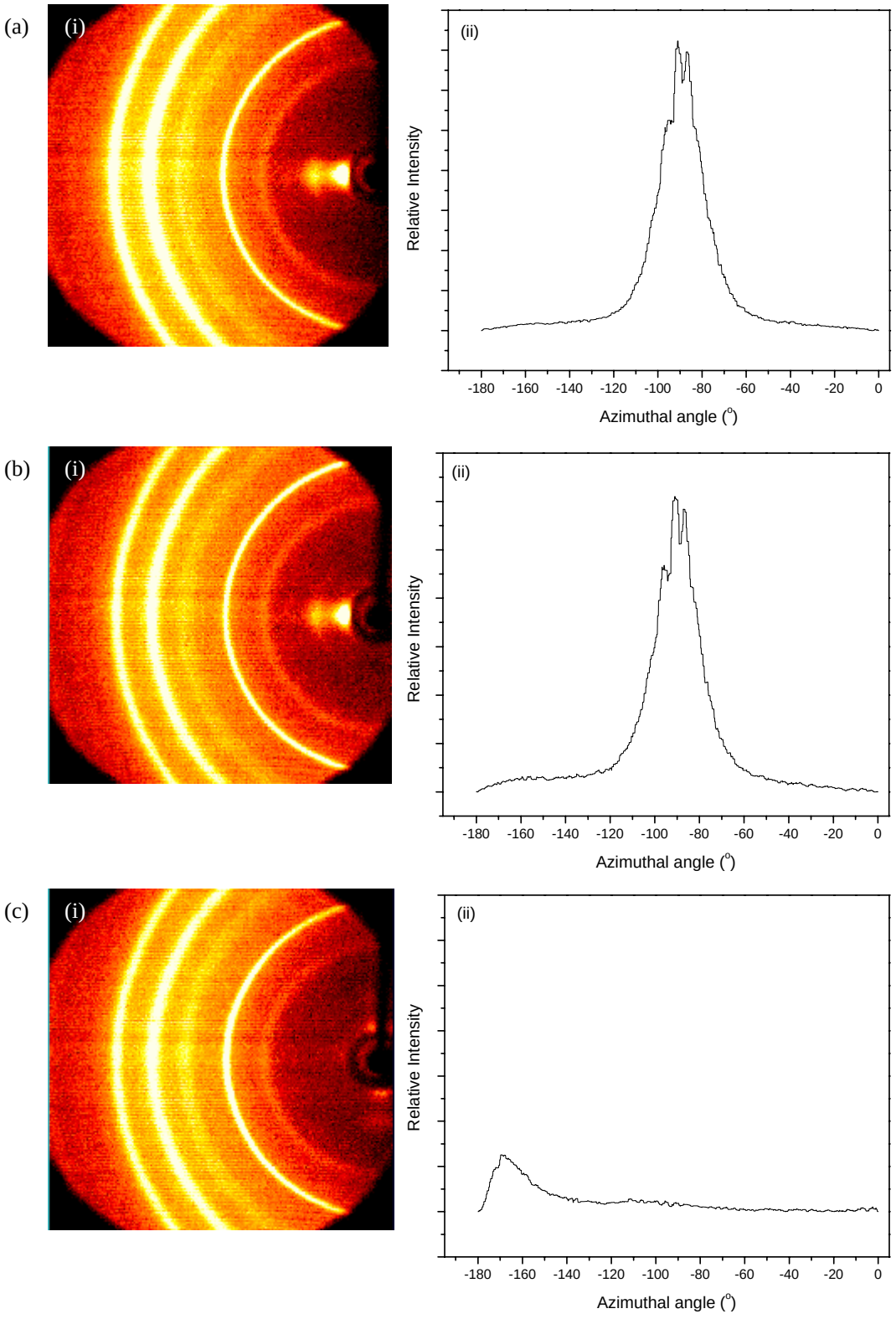

Figure 4.9 (i) 2D x-ray diffraction patterns and (ii) the corresponding azimuthal plots from 2.5° to 5.0° of an annealed specimen of PEN/IMC16-MMT-2 when the x-ray beam is incident on the (a) TD-FD, (b) FD-ND and (c) TD-ND plane.

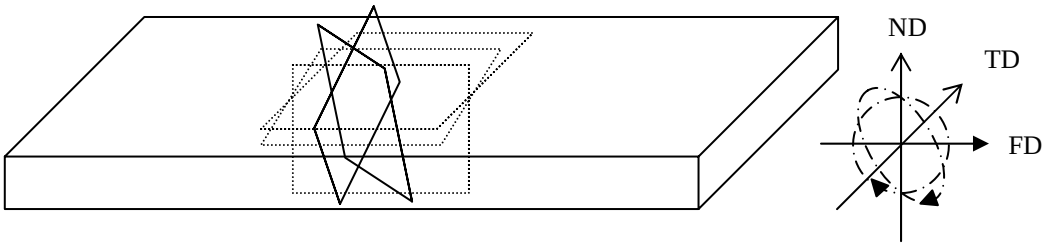

Figure 4.10 Arrangement of the clay sheets in PEN/IMC16-MMT-2 after annealing. Some of the clay sheets are rotated along the TD or ND axes, which cause their basal planes to be no longer parallel to the FD (as exemplified by the clay sheets with solid borders).

Figure 4.9(c) also shows that very weak clay reflections are observed at the meridional positions when the x-ray beam is incident on the TD-ND plane. In comparison to the x-ray diffraction pattern in the as-molded specimen, these reflections exhibit a significant loss of intensity. This is probably attributed to a reduction in the degree of the orientation of the clay basal planes and the curvature of the Ewald sphere close to the reciprocal Z-axis.

The orientation of the clay platelets in the annealed specimens is corroborated by TEM observations of ultrathin films that were sectioned from the TD-ND plane (Figure 4.11(b)), in which majority of the clay platelets appear edge-on. TEM also verifies that the clay platelets remain homogeneously distributed after the annealing treatment, thus precluding any possibility of additional reinforcement due to the preferred segregation of clay during the annealing treatment, as has been previously suggested by Maiti *et al* [76].

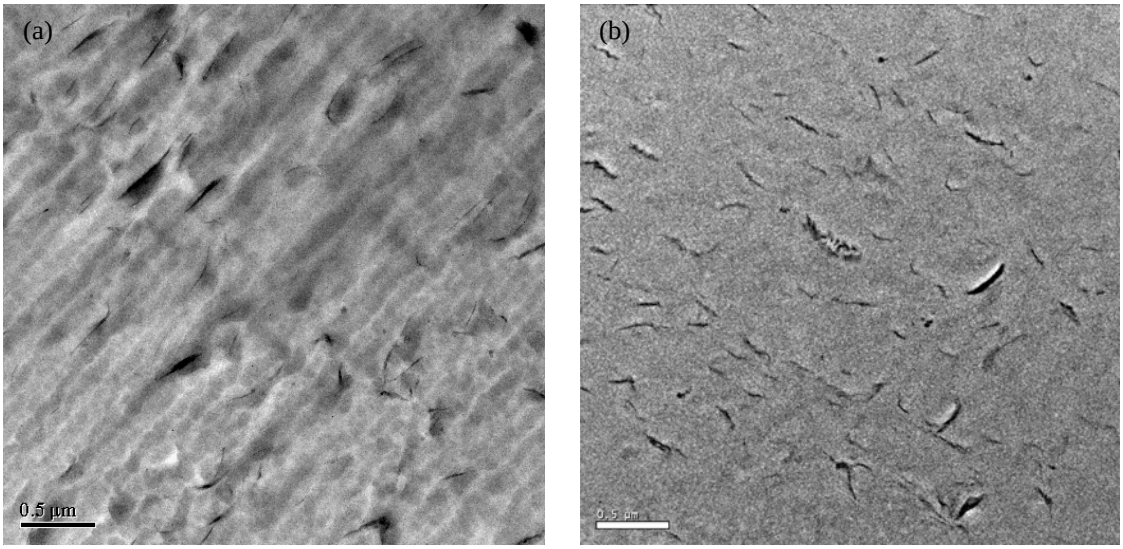

Figure 4.11 Typical transmission electron micrographs of PEN/IMC16-MMT-2 (a) before and (b) after annealing at 240^{o}C. The TEM sections are obtained from the TD-ND plane.

Although the clay orientation is partially relaxed after annealing treatment, the relaxation of the clay orientation would cause a reduction of E', instead of the additional E' improvement which is observed after annealing. Eliminating the possible contributions that could arise from the polymer-clay interfacial interactions or the relaxation of the clay orientation, the additional reinforcement observed in the nanocomposite after the annealing treatment should therefore originate from the modifications to the polymer crystalline phase that is induced by the presence of the dispersed clay phase.

Degree of Crystallinity and Crystal Structure

To ascertain the effect of the nanoclay on the PEN crystalline phase, MDSC was first carried out to elucidate the degree of crystallinity as well as the melting point of the annealed samples. The data obtained (Table 4.4) indicated no significant difference in either the final melting temperature or the overall degree of crystallinity, χ_c, in

PEN/IMC16-MMT-2 with respect to pure PEN. X-ray diffraction analysis (Figure 4.12) of the annealed samples further shows that both materials crystallize in the α-crystal form. The results suggest that the greater mechanical enhancement observed in PEN/IMC16-MMT-2 after the annealing treatment is not due to a difference in the crystallinity levels or crystal forms developed.

Table 4.4 MDSC data for annealed samples of PEN and PEN/IMC16-MMT-2[a].

System	ΔH_f (J/g)	χ_c (%)	T_m (°C)
PEN	49.5 ± 1.3	29.1	270
PEN/IMC16-MMT-2	48.9 ± 1.2	28.8	270

[a] Errors given represent one standard deviation from the mean.

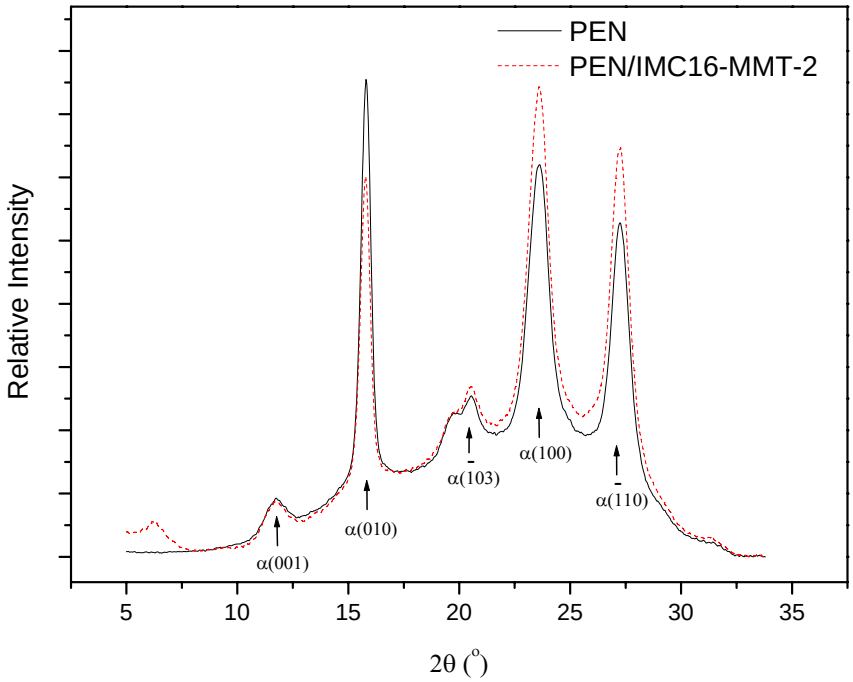

Figure 4.12 X-ray diffraction profiles of PEN and PEN/IMC16-MMT-2 after annealing at 240°C. The samples are oriented such that the x-ray beam is incident parallel to the TD-FD plane. The intensities of the profiles have been normalized using the halo from the amorphous phase as a reference.

Crystalline Morphology

The crystalline morphology of the hybrid was observed under the POM and AFM to understand how the presence of clay can affect the mesoscopic arrangement of the PEN crystallites during annealing.

Figure 4.13 shows the typical POM images of PEN and PEN/IMC16-MMT-2 after complete crystallization. Gaps present at the interspherulitic regions are due to the depletion of polymer as it diffuses toward the growing crystals. These regions are essentially free of polymer at the end of the crystallization process [77]. The optical micrographs show that PEN/IMC16-MMT-2 crystallizes in a less regular spherulitic superstructure compared to pure PEN. Furthermore, the boundaries between the spherulites were indistinct in PEN/IMC16-MMT-2, in contrast to the well-defined edges observed in the pristine polymer.

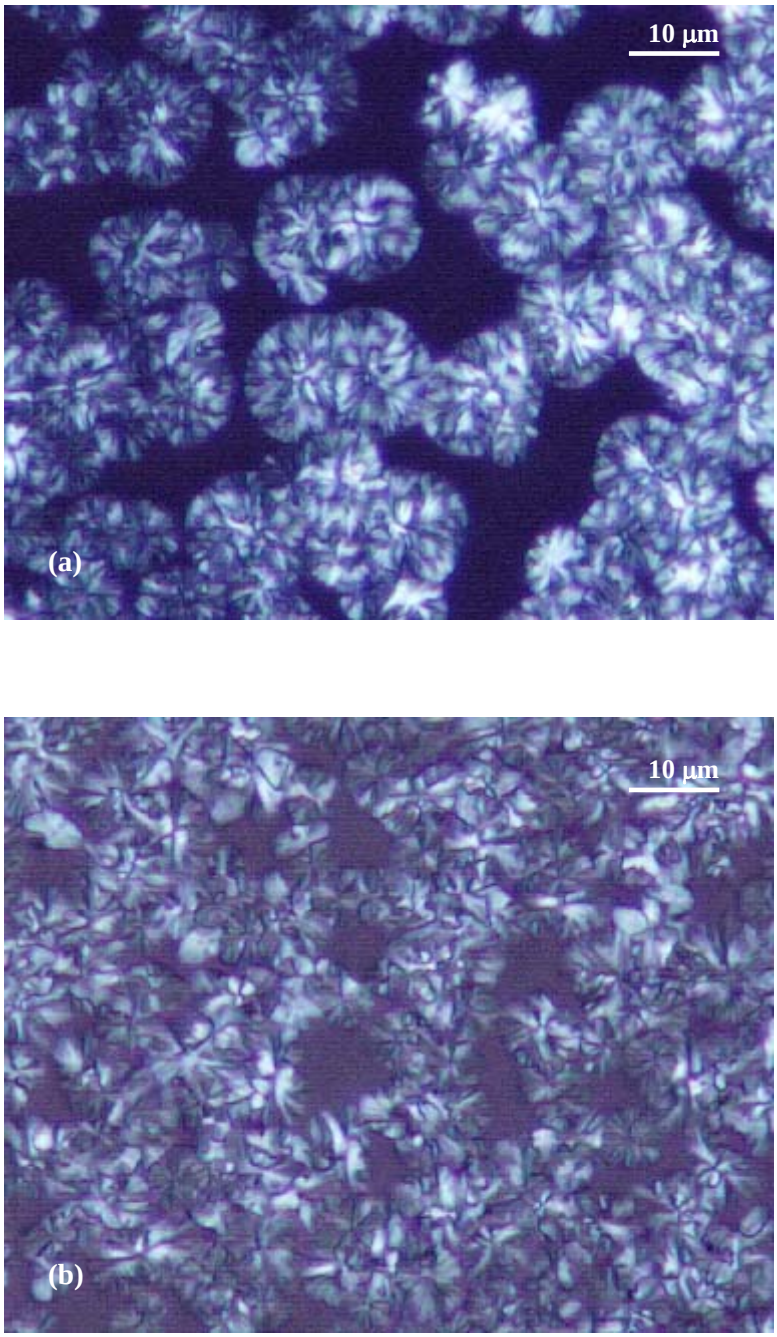

Figure 4.13 Polarized light optical micrographs of (a) pure PEN and (b) PEN/IMC16-MMT-2 thin films, cold crystallized at 240^{o}C.

To reveal the spherulitic features in greater detail, the surface morphology of PEN and PEN/IMC16-MMT-2 was further examined under the AFM. Before annealing, the etched surfaces of amorphous PEN and PEN/IMC16-MMT-2 appear smooth and featureless (Figure 4.14).

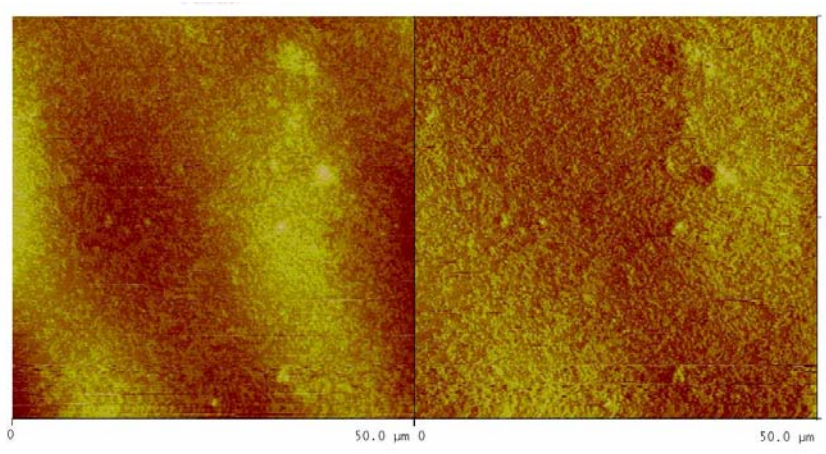

Figure 4.14 AFM height and amplitude images of quenched PEN/IMC16-MMT-2.

After annealing and etching, it was observed that semicrystalline PEN and PEN/IMC16-MMT-2 exhibit distinctly different surface morphologies. Figure 4.15(a) shows the surface morphology of pure PEN after annealing and etching. A typical spherulitic structure and distinct boundaries between the spherulites can be observed. The micrograph for PEN/IMC16-MMT-2 (Figure 4.15(b)(i)) on the other hand, indicates that the lamellae do not have a spherical superstructure when viewed from the surface. The higher magnification image in Figure 4.15(b)(ii) further reveals that although the lamellar texture is radial in a smaller region, the arrangement of the lamellae in adjacent lamellar collections can be almost perpendicular to each other, which implies that the boundaries observed may not be caused by impingement.

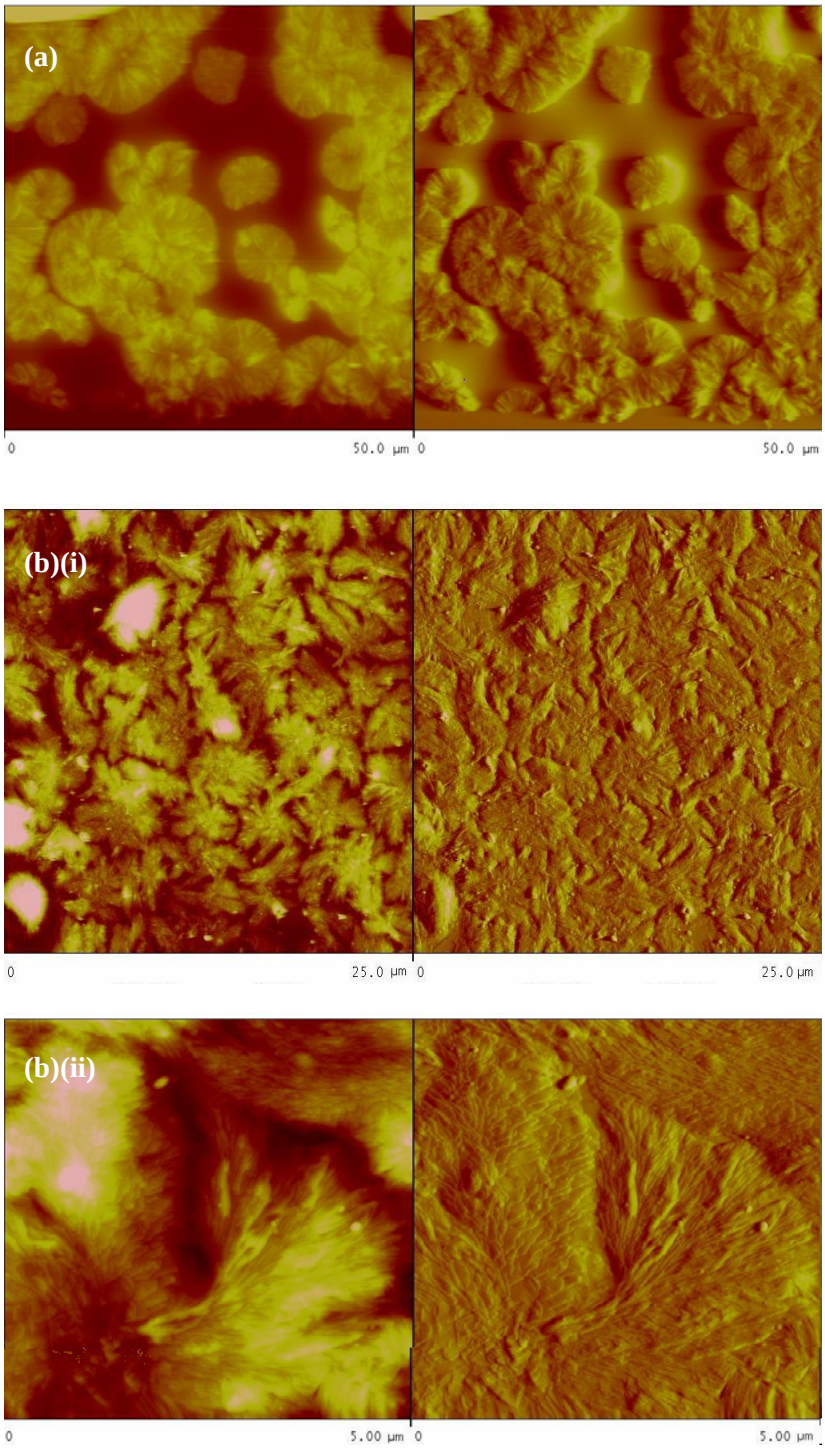

Figure 4.15 AFM height and amplitude images of (a) pure PEN and (b) PEN/IMC16-MMT-2 cold crystallized at 240^{o}C.

The POM and AFM observations thus provide evidence that in the presence of the high-aspect-ratio clay platelets which are distributed at an interparticle distance much smaller than the size of the spherulites, the crystalline morphology of PEN can be significantly altered. The unique crystalline morphology exhibited by the nanocomposite, in which the arrangement of the lamellae in adjacent lamellar collections can be almost perpendicular to each other, further suggests that the high-aspect-ratio clay alters the development of the mesostructure in PEN by arresting lamellae growth when the crystallite growth front collides with its basal plane (Figure 4.16(b)): When growing primary lamellae of the PEN crystallites encounter a clay platelet with its basal plane oriented roughly perpendicular to the growth front, the large surface area presented by the clay basal plane may block the crystallization front and prevent the crystallite from extending outwards in that direction. An amorphous space is thus created around the clay particle where the crystallite growth is disrupted (Figure 4.16(b)(i)). The effect is especially pronounced if the clay is situated relatively close to the nucleating center. These amorphous regions may then be filled by secondary lamellae branched out from the primary lamellae of the same spherulite in the nearby regions (Figure 4.16(b)(ii)), or lamellae developed from other nearby nucleating centers (Figure 4.16(b)(iii)). In this way, adjacent lamellar collections which are oriented almost perpendicular to one another are created in the PEN/clay nanocomposite (as observed in Figure 4.15(b)(ii)).

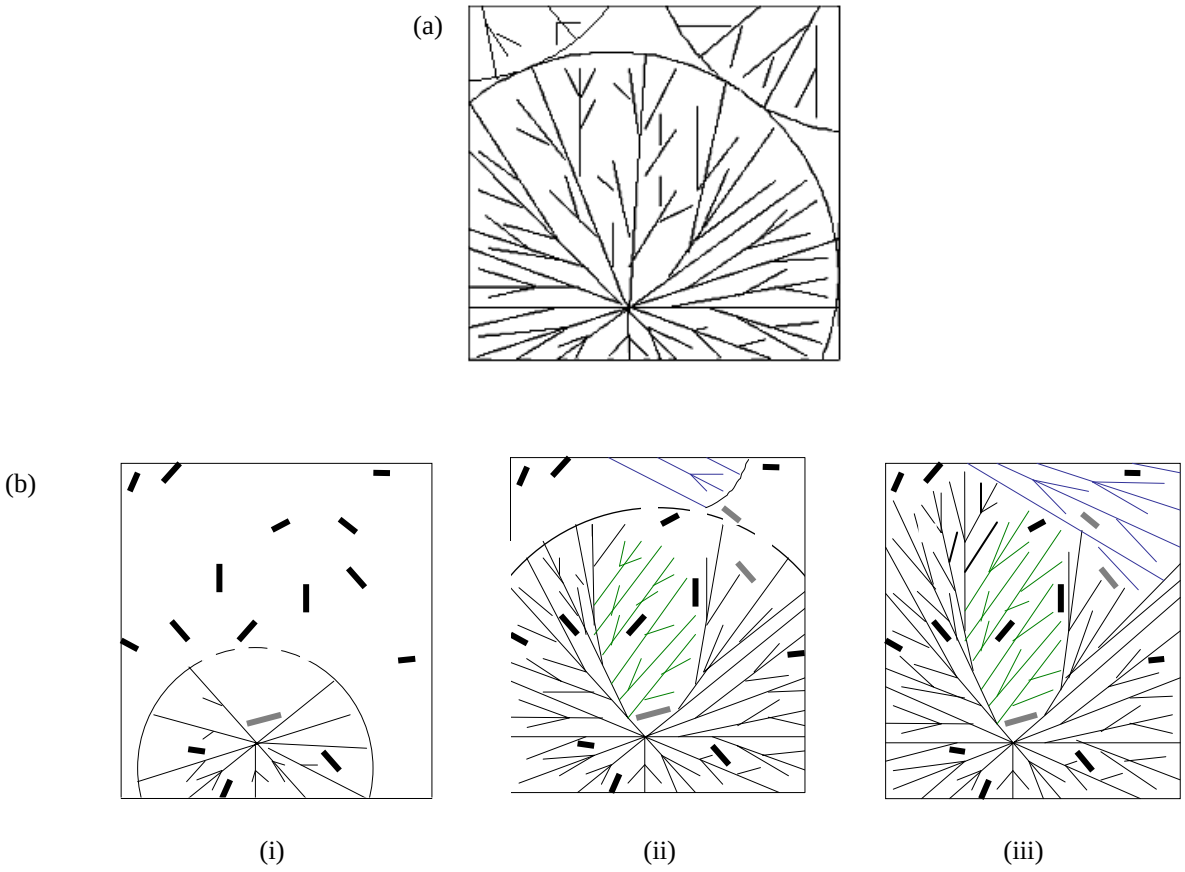

Figure 4.16 Schematic diagrams showing the crystalline morphologies developed: (a) in pristine PEN, crystallites grow radially outwards to form spherulites. Primary lamellae grow first to provide a skeleton for the spherulite. Secondary lamellae grow behind the main growth front, and fill in the spaces between the primary lamellae. Growth is stopped when the spherulites impinge with one another; (b) (i) in PEN/IMC16-MMT-2, the growth of the primary lamellae is disrupted by clay platelets located close to the nucleus. The amorphous spaces (which is indicated by the dashed arc) are subsequently filled in by (ii) secondary lamellae branched out from the primary lamellae of the same spherulite (colored green), or (iii) lamellae developed from other nearby nucleating centers (colored blue). (The clay platelets which are oriented such that they disrupt lamellae growth are colored grey for clarity).

Lamellar Orientation Induced by Orientation of Clay

In Figure 4.15, the crystalline morphology of the nanocomposite is visualized from thin films in which the clay particles are not expected to possess any preferred orientation. 2D x-ray diffraction and TEM observations have however indicated that the clay platelets tend to align with their basal planes oriented parallel to the injection direction in the molded specimens (Figure 4.10), even after annealing treatment.

As the growth of a lamella can be arrested by the basal planes of clay, the clay layers will tend to present greater perturbance to the development of lamellae when their growth fronts are oriented roughly perpendicular to the clay basal planes. Due to the preferred alignment of the clay basal planes along the injection direction in the molded specimens, the crystalline lamellae in the nanocomposite will be forced to develop such that they are also roughly parallel to the clay basal planes (that is, along the injection direction), because it is in this direction that their growth will be the least obstructed by the clay.

Part of the additional reinforcement in the annealed nanocomposite may thus arise as a result of this preferred alignment of the high-aspect-ratio PEN crystalline lamellae along the direction of the applied stress, which is induced by the oriented clay phase.

Orientation Correlation of PEN Crystallites with Dispersed Clay Phase

Examination of the x-ray diffraction profile of the annealed specimens also reveals that the relative intensities of the various α-crystal peaks in PEN/IMC16-MMT-2 are different from those of the neat PEN. In particular, it is observed that the intensity of the peak due to the $(\bar{1}10)$ plane in PEN/IMC16-MMT-2 is significantly enhanced with respect to that of the same peak in neat PEN. The orientation of the naphthalene ring

of PEN lies very close to the $(\bar{1}10)$ plane ($(\bar{3}20)$ is the actual plane of the naphthalene ring) [78]. This suggests that the oriented clay phase can also enhance the alignment of the PEN naphthalene rings along the basal plane of clay. This probably arises as a result of the better affinity of the PEN naphthalene rings for the clay sheets, similar to what has been observed for the phenyl rings in poly(styrene) [79].The preferential alignment of the crystallites of the polymer matrix under the influence of the dispersed clay phase has also been reported for nylon-6/clay nanocomposites, in which the γ-(020) hydrogen-bonded planes have been found to orient parallel to the interface with the MMT inclusions [80,81] The preferred orientation of the PEN naphthalene rings along the stress direction could also have contributed to the additional reinforcement observed in the nanocomposite after annealing.

(II) Modulus Enhancement above the Glass Transition Temperature

The temperature dependence of E' in the annealed specimens (Figure 4.5(a)) also indicates that the reinforcing efficiency of IMC16-MMT increases when the materials are heated beyond their glass transition temperatures. Table 4.3 shows that at 35°C, the modulus increase by 25%, when heated to 160°C, (beyond the glass transition temperature), the modulus increment rises to 31%. The additional enhancement in modulus observed above the glass transition temperature is attributed to the softening of the amorphous part of the PEN matrix - the larger difference in modulus between the clay and the matrix enhances the efficiency of load transfer from the matrix to the filler particles [82,83].

4.3 Thermal Stability

4.3.1 Experimental

The thermal stability of the materials was determined by its weight loss behavior during thermogravimetric analysis (TGA). TGA was performed on a TA Instruments Hi-Res TGA 2950 Thermogravimetric Analyzer from 25^{o}C to 800^{o}C at a heating rate of 10^{o}C/min and under an air flow rate of 50 cc/min.

4.3.2 Results and Discussion

Figures 4.17 and 4.18 show the weight loss behaviors of PEN and the hybrids, the temperature at which 5% weight fraction loss is observed, T_d, and the peak derivative weight loss temperature (as given by the first maximum in the derivative weight loss (DTG) curve), T_{max} are summarized in Table 4.5.

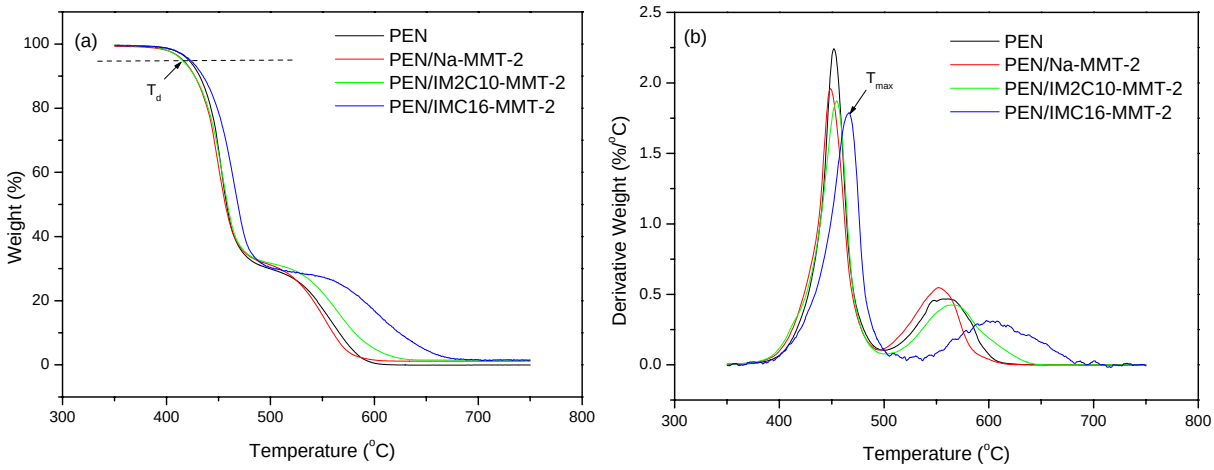

Figure 4.17 (a) TGA and (b) DTG curves of PEN and PEN/clay hybrids.

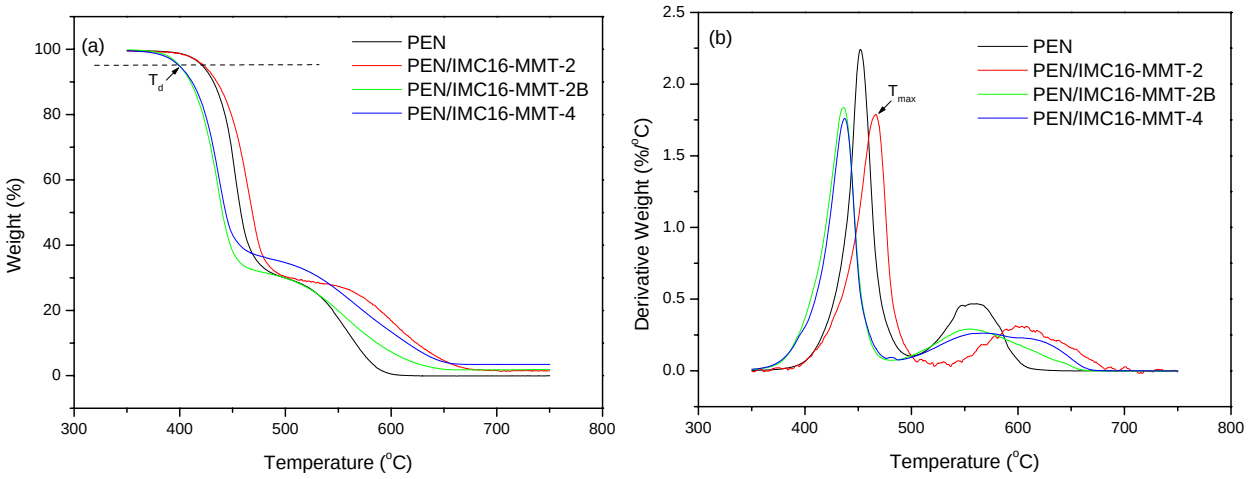

Figure 4.18 (a) TGA and (b) DTG curves for the PEN/IMC16-MMT series of hybrids. The curves for PEN are also shown as a reference.

Table 4.5 5% weight fraction loss (T_d) and peak derivative weight loss temperatures (T_{max}) of PEN and its hybrids.

System	T_d (°C)	T_{max} (°C)
PEN	421	452
PEN/Na-MMT-2	416	448
PEN/IM2C10-MMT-2	415	455
PEN/IMC16-MMT-2	423	467
PEN/IMC16-MMT-2B	400	437
PEN/IMC16-MMT-4	399	437

For the PEN/clay hybrids that contain 2 wt% clay and which have gone through a single extrusion step, it was observed that the addition of clay did not significantly increase the T_d in PEN. This observation is unlike many other reported nanocomposite systems, in which the thermal stabilities of polymers have often been enhanced with the incorporation of clay because the clay particles can act as a

superior insulator and mass transport barrier to volatile decomposition products [3]. A possible reason is that the clay layers also possess catalytic sites, such as adsorbed water and hydroxyl groups, which may accelerate the decomposition of polyesters [32,84]. The two effects work antagonistically to each other, which explain why the T_d of PEN remains relatively unchanged after the addition of clay. PEN/IMC16-MMT-2 however, exhibits a peak derivative weight loss temperature that is more than 10^{o}C higher than PEN and the other two less well-dispersed hybrids. This suggests that the presence of well-dispersed clay layers in the PEN matrix may still exert a positive effect on the thermal stability of PEN.

For the PEN/IMC16-MMT-2B hybrid that has been subjected to two rounds of extrusion cycle however, it was observed that there was a reduction in both the T_d and T_{max}. Although there is a slight improvement in the clay dispersion in PEN/IMC16-MMT-2B, the second extrusion cycle also induces additional reduction in molecular weight in the polymer matrix, which negates the effect of a better clay dispersion and results in the poorer thermal stability in the PEN/IMC16-MMT-2B hybrid.

A lower T_d and T_{max} is also observed for the PEN/IMC16-MMT-4 hybrid. The presence of a higher content of clay at a poorer overall level of dispersion probably intensifies the catalytic effect of clay on the degradation of the PEN matrix, while increasing the insulating and barrier effect of clay to a lesser extent - this gives rise to the poorer thermal stability in the 4 wt% hybrid.

4.4 Summary and Conclusions

The effect of clay dispersion on the dynamic mechanical and thermal properties of the PEN/clay nanocomposites was assessed. Similar to previous studies, it was found that the ability of the clay particles in enhancing the modulus and thermal stability in PEN

is invariably related to its level of dispersion within the PEN matrix. The most well-dispersed PEN/clay hybrid, PEN/IMC16-MMT-2 exhibits the most significant enhancements in both its modulus and thermal stability.

In addition, the contribution of the modified matrix crystalline phase to the modulus enhancement in the nanocomposite was evaluated by subjecting the largely amorphous as-molded specimens to an annealing treatment. The greater modulus enhancement observed in the nanocomposite after crystallization (with respect to the neat PEN that has been subjected to the same annealing treatment) was rationalized on the basis of the structural and morphological changes exhibited by the PEN crystalline phase in the presence of the nanoclay particles. AFM observations provide evidence that the development of the PEN spherulites may be disrupted by the high-aspect-ratio clay platelets. It was thus postulated that the preferred orientation of the clay platelets could force the analogous alignment of the polymer crystalline lamellae along the flow direction where the growth of the lamellae is the least restricted by the dispersed clay phase. X-ray diffraction also reveals that the PEN naphthalene rings tend to preferentially align parallel to the clay basal planes, a phenomenon which could also have contributed to additional reinforcement in the crystallized nanocomposite. The study performed in this chapter thus illustrates how structural synergism can be achieved between the oriented clay phase and the polymer crystalline phase and how this can be exploited to achieve additional reinforcement in the nanocomposite.

CHAPTER 5

Polymorphism Behavior of PEN/Clay Hybrids

5.1 Introduction

In the previous chapter, it was demonstrated how the modified crystalline phase in the PEN/clay nanocomposite can contribute to additional reinforcement in the material. The enhanced stiffening observed in the hybrid after annealing treatment was attributed to the modified crystalline morphology, and the alignment of the PEN lamellae/crystallites, which is induced by the oriented clay phase.

In addition to the morphology and orientation of the crystalline phase, other aspects of the matrix crystalline structure can also have a tremendous impact on the final properties exhibited by the nanocomposites. In particular, clay-induced polymorphism has often been cited as an important factor contributing to the unique combination of properties exhibited by polymer/clay nanocomposites. Previous studies have, for instance, reported on the simultaneous dramatic improvement in both stiffness and toughness in nylon-6 and polyvinylidene fluoride (PVDF)/clay nanocomposites, which is at least partially contributed by the formation of a different crystal phase [1,2]. It is thus important, especially from a design standpoint, to understand what factors give rise to the preferred formation of a particular polymorphic form in the matrix polymer in the presence of nanoclays, and how this can impact the physical and mechanical properties exhibited by the nanocomposites.

PEN is known to crystallize in two crystalline forms. The α-crystal form is obtained when amorphous PEN is annealed in the solid state, while the β-crystal

phase is formed when PEN is crystallized directly from the melt at higher temperatures [85]. An understanding of the type of crystalline phase that the PEN/clay hybrids form under different processing conditions is an important aspect by which their properties can be predicted and controlled. In addition, the ease with which the different crystalline forms of PEN can be controlled by varying its thermal treatment makes it a potentially useful system by which the underlying mechanisms responsible for clay-induced polymorphism may be elucidated. A more fundamental understanding of how clay can influence the type of crystal phase formed in the matrix polymer will enable the structures of semicrystalline polymer/clay nanocomposites to be better engineered to suit specific applications.

In this chapter, the polymorphism behaviors of the PEN/clay hybrids were examined. In particular, the effects of the nature of the clay surface as well as the crystallization conditions, on the type of crystalline phase developed were investigated. The focus of this work is on elucidating the underlying basis by which clays alter the type of crystalline phase formed in PEN. The impact of the clay-induced polymorphism on nanocomposite properties, though an important area of investigation, will not be pursued in this work.

5.2 Crystalline Forms Observed in PEN

PEN can be crystallized into two crystal modifications, α and β, depending on the thermal treatment [78,85-89]. Table 5.1 lists the crystallographic data, as well as other important properties of the α- and β-forms of PEN.

In the α-polymorph of PEN, the polymer chains exist in an extended all-trans conformation, in which the attached ester groups adopt the trans arrangement across the naphthalene rings, while in the β-polymorph, the polymer chains are not

completely extended but tend to adopt a more sinusoidal conformation because the ester groups on alternating naphthalene rings are attached in the trans and cis arrangements (Figure 5.1) [85,87]. The β-phase is believed to be more thermodynamically stable, while the α-phase is more kinetically favored [78]; this has been found to be true for both pure PEN and PEN/clay nanocomposites [90].

Table 5.1 Crystallographic and miscellaneous data for the α- and β-forms of PEN.

Property	α [86]	β [88]
Crystal structure	Triclinic	Triclinic
Lattice constants	a = 6.51 Å b = 5.75 Å c = 13.2 Å α = 81.3° β = 144° γ= 100°	a = 9.26 Å b = 15.59 Å c = 12.73 Å α = 121.6° β = 95.6° γ= 122.5°
Crystallographic reflections	(010): 2θ = 15.6° (100): 2θ = 23.3° $(\bar{1}10)$: 2θ = 27.0°	$(\bar{1}\bar{1}1)$: 2θ = 16.4° (020): 2θ = 18.6° $(2\,\bar{4}\,2)$: 2θ = 25.5°
No. of chains per unit cell	1	4
Density (g/cm^3)	1.407	1.439

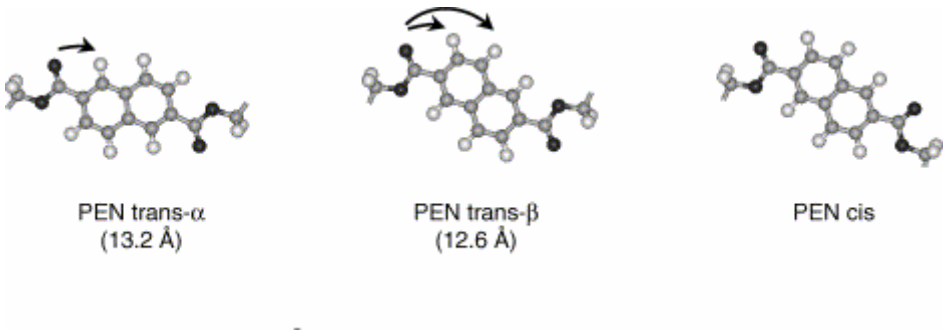

Figure 5.1 Conformations of aromatic rings in PEN [87].

5.3 Effect of Clay on Polymorphism in Polymer/Clay Nanocomposites – Previous Studies

Clay-induced polymorphism is a widely reported phenomenon in polymer/clay nanocomposites. In this section, the findings and mechanisms proposed for the modification of crystal phase in some polymer/clay nanocomposite systems will be reviewed to provide a background against which the effect of clay on the crystal structure of the PEN system can be better understood.

The review focuses mainly on nylon-6/clay nancocomposites, since the most extensive studies have been performed for this nanocomposite system, but the polymorphic behaviors of other polymer/clay nanocomposites will also be addressed at appropriate points to complement the discussion.

Nylon-6 exhibits two crystalline forms - α and γ. The α-crystalline form is more thermodynamically stable [91] and is normally obtained in the usual melt crystallization of nylon-6. The presence of clay has however been found to promote the formation of the γ-crystalline form instead [1,91-98].

Solid-state ^{15}N NMR studies performed by Mathias and co-workers [91] have indicated that in-situ polymerized nylon-6/clay nanocomposites tend to form only the γ-crystal phase under an annealing treatment that would only give rise to the α-crystal phase in pure nylon-6. It was suggested that the parallel arrangement of the nylon-6 chains tightly bound to the clay surface tends to inhibit the formation of hydrogen-bonded sheets between anti-parallel chains of the α-form - the γ-form is thus generated by default.

Studies by VanderHart *et al* [92] on in-situ polymerized and melt blended nylon-6/clay nanocomposites however indicated that the γ-crystal form is formed in both blended and in-situ polymerized samples. Covalent attachment of the nylon to

the clay surface is thus not the main factor that gives rise to the preferred formation of the γ-phase. Furthermore, it was found that the γ-crystallites tend to reside near the polymer/clay interface. Parallel DSC studies performed by the authors indicated that crystal nucleation in the nanocomposites takes place at a significantly higher temperature compared to the pure polymer; the dominance of the γ-phase is thus in part related to the fact that γ-phase growth from the clay surface obtains a head start on any growth of the α-phase originating in regions away from the clay surface.

Studies by Lincoln and co-workers [93,94] arrived at similar conclusions, that is, the γ-phase is formed preferentially in the proximity of the clay layers, while the α-phase exists away from the polymer-clay interphase region. Furthermore, the proximity of the clay surface, irrespective whether the chains are ionically tethered (for in-situ polymerized samples) or weakly bonded (for melt compounded samples), will force the amide groups out of the plane formed by the chains. Such changes in chain conformation limit the formation of H-bonded sheets, and thus stabilize a dominant γ-phase. The relative fractions of α- and γ-phases obtained is however, dependent on the interfacial interactions between the clay and the polymer. Strong polymer-clay interactions tend to increase the width of the interfacial regime, where formation of the equilibrium α-crystallite form is hindered.

Wu *et al* [95] proposed a slightly different explanation for the preferred formation of the γ-phase in nylon-6 nanocomposites. Based on FTIR study of hydrogen bonding in the nanocomposites, the authors found that clay layers weaken the hydrogen bonding in both the α- and γ- phases. It was thus conceived that the clay layers primarily acts by limiting molecular mobility and the extent of hydrogen bonding. The favored conformations during crystallization then end up having the amide groups outside the plane and the γ-phase is obtained.

Isothermal crystallization studies further indicate that the isothermal crystallization rates in the nucleation-controlled regime are significantly faster for the nanocomposites than for the pristine nylon-6 [96]. This result provides evidence that clay indeed acts as nucleating centers for γ-phase crystallization.

Taken in sum, the common theme that runs through these studies is the possible effects that clay can exert on the chain conformations and chain mobility of nylon-6, so that the γ-phase is preferentially nucleated at the vicinity of the clay layers.

The possible role played by clay-induced biasing of chain conformations in altering the polymorphic behavior of the polymer matrix is also highlighted in the crystallization studies of syndiotactic polystyrene (s-PS)/clay nanocomposites [99]. In the study, it was proposed that the presence of clay helps to overcome the transition energy barrier from a TTGG to a TTTT chain conformation. The TTTT chain conformation is necessary for the initial molecular reorder to form crystals, in this way, clay acts as a nucleus for the formation of the β-crystal phase, which is usually less kinetically favored than the α-crystal form in neat s-PS.

Maiti *et al* also proposed the possibility of clay acting as a template for the epitaxial crystallization of γ-nylon [50]. Due to its ability to form hydrogen-bonded sheets, a pseudohexagonal packing can result when the clay layers and nylon forms hydrogen bonding with each other. This mechanism is supported by the elevated-temperature wide-angle x-ray scattering observations of Nair and Ramesh [98], where an unusually large crystal size normal to the γ(100) plane was detected during the initial crystallization of the nylon-6/clay nanocomposite from the melt state. Epitaxial nucleation was also suggested by Shah *et al* in explaining the polymorphic behavior of polyvinylidene fluoride (PVDF) [2]. The preferential formation of the β-phase was

rationalized on the basis of the matching of the crystal lattice of the nanoclay with that of the PVDF β-phase.

5.4 Experimental

(I) Materials

The series of studies detailed in this chapter was performed on the melt-intercalated PEN/clay hybrids which contain 2 wt% of MMT, and have been through only 1 melt compounding cycle (Table 3.4). To clarify the possible roles played by the intercalated surfactants in influencing the polymorphism of the hybrids, a PEN/IMC16 blend containing the same amount of 1-hexadecyl-2,3-dimethylimidazolium (IMC16) surfactant (ca. 0.8 wt%) has also been prepared using the same method as described in Section 3.3.3(II). The amount of IMC16 surfactant that has been incorporated into IMC16-MMT was evaluated by thermogravimetric analysis (TGA) of IMC16-MMT in air, as described in Section 3.4.1(I).

(II) Melt Crystallization of Samples

As PEN and its hybrids have been found to crystallize only in the α-crystal phase when annealed from the glassy state [85], only samples subjected to melt crystallization are presented in this study on the polymorphism behavior of PEN and its hybrids. Dried pellets of PEN and PEN/clay hybrids were melted at 290^{o}C for 5 minutes in a convection oven to completely remove their thermal history. The melted samples were then immediately transferred to an oil bath set at 180^{o}C, 190^{o}C or 200^{o}C, allowed to crystallize for 15 minutes (for crystallization at 180^{o}C and 190^{o}C) or 30 minutes (for crystallization at 200^{o}C), before they were air-cooled to ambient temperatures. To eliminate effects due to preferred orientation of the crystallites, all

the materials were ground into a fine powder using a Fritsch Pulverisette 14 and an 80-μm sieve for the x-ray diffraction experiments.

(III) X-ray Diffraction (XRD)

Room-temperature x-ray diffraction was performed with a Shimadzu x-ray diffractometer in a Bragg-Brentano θ-2θ geometry with CuK_α radiation (λ = 0.154 nm) generated at 30 kV and 30 mA. The samples were scanned at 0.25^o/min from 2.5^o to 40.0^o.

Deconvolution of the superposed crystalline and amorphous peaks in the x-ray diffraction pattern was performed using the profile fitting program XFIT. Profile fitting was carried out at a 2θ range of 8.0^o to 40.0^o to cover all the intense crystalline and amorphous peaks observed in PEN. Peak fitting was performed by holding the peak locations in 2θ constant, while allowing the peak heights and widths to vary. Before the auto-fit program was executed, the widths of each peak were adjusted manually if necessary to provide a reasonable starting point for the curve fitting algorithm to begin. Each peak was modeled by a Pseudo-Voigt profile function. Figure 5.2 shows an example of how the crystalline and amorphous scattering components were deconvoluted using the peak fitting software.

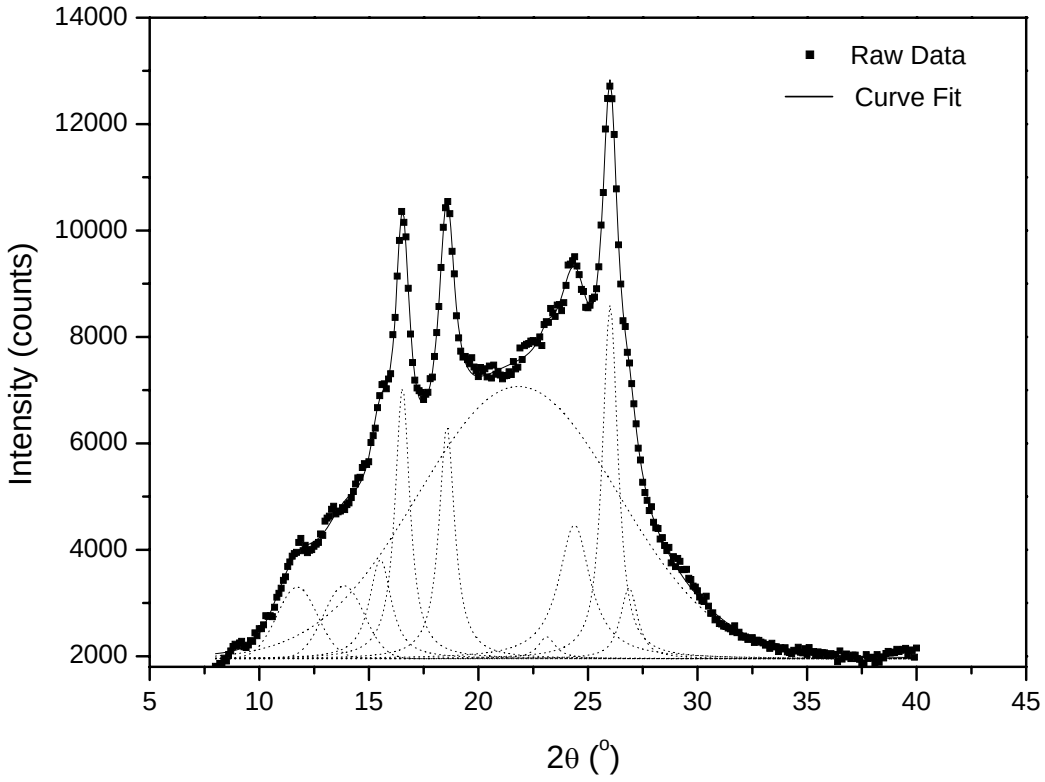

Figure 5.2 An x-ray diffraction pattern (PEN/IM2C10-MMT-2 melt crystallized at 200°C) and the profile fitting technique used to deconvolute the peaks from the amorphous and crystalline phases. The curve fit is given by the sum of the components shown by the dashed lines. Linear background was removed prior to deconvolution.

High-temperature x-ray diffraction patterns were recorded with a Bruker GADDS x-ray diffractometer equipped with a two-dimensional, position-sensitive area detector using CuK_α radiation generated at 40 kV and 40 mA. The samples, in the form of powder, were packed into glass capillaries (Hampton Research, HR6-194) before they were placed into the temperature chamber of the x-ray diffractometer. The glass capillary is specially manufactured for x-ray diffraction experiments, and it does not exhibit any peak in the range of $2\theta = 2.5^o - 10.0^o$. The samples were heated at a rate of 20°C/min to 300°C, allowed to melt for 3 minutes, before they were cooled at

20^{o}C/min to the desired melt crystallization temperature. A data acquisition time of 200 seconds was employed and the x-ray diffraction patterns were collected while the sample was held isothermal at the desired melt crystallization temperature, until no further changes in the diffraction patterns were observed. The two-dimensional scattering patterns were integrated radially to obtain intensity against 2θ plots using the GADDS software package.

(IV) Fourier Transform Infrared Spectroscopy (FTIR)

FTIR spectra were collected with a Perkin Elmer AutoImage FTIR Microscope equipped with a mercury cadmium telluride detector. For the in-situ monitoring of the melt crystallization process, thin polymer films on gold-coated glass coverslips were used. The samples were placed on top of the FTIR 600 Linkam hotstage and melted at 280^{o}C for 3 minutes before they were cooled at a rate of 50^{o}C/min to the desired melt crystallization temperatures. FTIR spectra were collected during the melt crystallization process in the reflection mode with a mean collection time of 45 seconds per spectrum. The spectra were obtained by coadding 32 scans.

For IMC16 and IMC16-MMT, the spectra were collected in the transmission mode at a resolution of 2 cm^{-1}, from KBr pellets placed on top of the FTIR 600 Linkam hotstage. The clay was heated using the same temperature profile as that used for the melt crystallization process and the respective IR spectra were collected at various temperature points of the melt crystallization process by averaging 32 scans.

(V) Differential Scanning Calorimetry (DSC)

The dynamic crystallization exotherms of the materials were measured using a TA Instruments MDSC 2920. The sample was first heated to 300^{o}C and held for 5

minutes to remove its thermal history. It was then cooled at a controlled rate of 5^{o}C/min to 25^{o}C. All experiments were performed under a nitrogen purge.

(VI) Thermogravimetric Analysis (TGA)

The degradation behaviors of IMC16-MMT during melt compounding and melt crystallization were examined by using a TA Instruments TGA 2050 Thermogravimetric Analyzer. The clays were first subjected to a predrying step at 140°C for 1 hour to remove physiabsorbed water and gases. To simulate the melt compounding process, the clay was heated at 10°C/min to 290°C and held for 5 minutes. The clay residues were then collected and subjected to a second heating cycle simulating the melt crystallization process: the clays were reheated at 20^{o}C/min to 300°C and kept isothermal for 3 minutes, before it was cooled at a rate of 20°C/min to 180°C or 200°C and held at that temperature for 30 minutes. All the TGA procedures were carried out under an air atmosphere.

5.5 Results and Discussion

(I) Polymorphism Behaviors of PEN and the Hybrids

Figures 5.3 to 5.5 display the x-ray diffraction (XRD) patterns of PEN and PEN/clay hybrids that were melt crystallized at 200^{o}C, 190^{o}C and 180^{o}C respectively. The crystal phase and diffraction plane from which each crystalline reflection comes from are indicated. As a comparison, the XRD patterns of the PEN/IMC16 blend that were melt crystallized at 200°C and 180°C are also shown in Figure 5.6. Similar to previous studies, the formation of the β-phase is favored at higher melt crystallization temperatures. This trend is observed for both PEN and its hybrids.

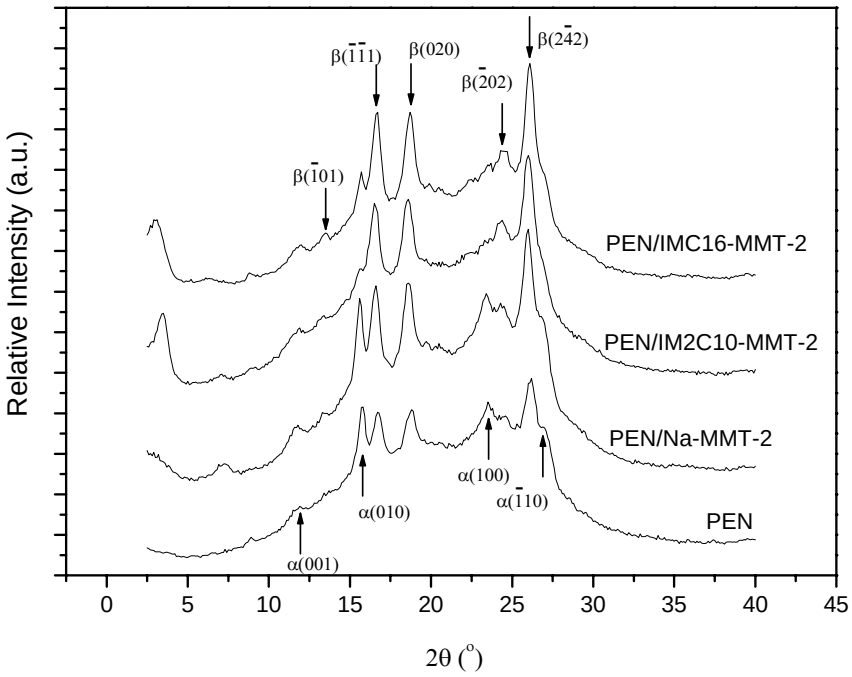

Figure 5.3 X-ray diffraction patterns of PEN and PEN/clay hybrids melt crystallized at 200°C.

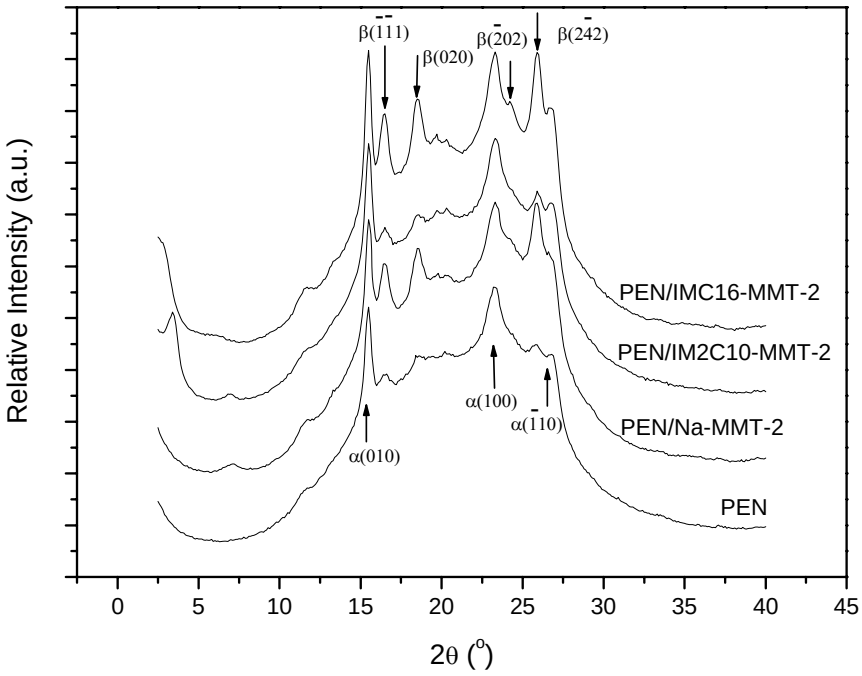

Figure 5.4 X-ray diffraction patterns of PEN and PEN/clay hybrids melt crystallized at 190°C.

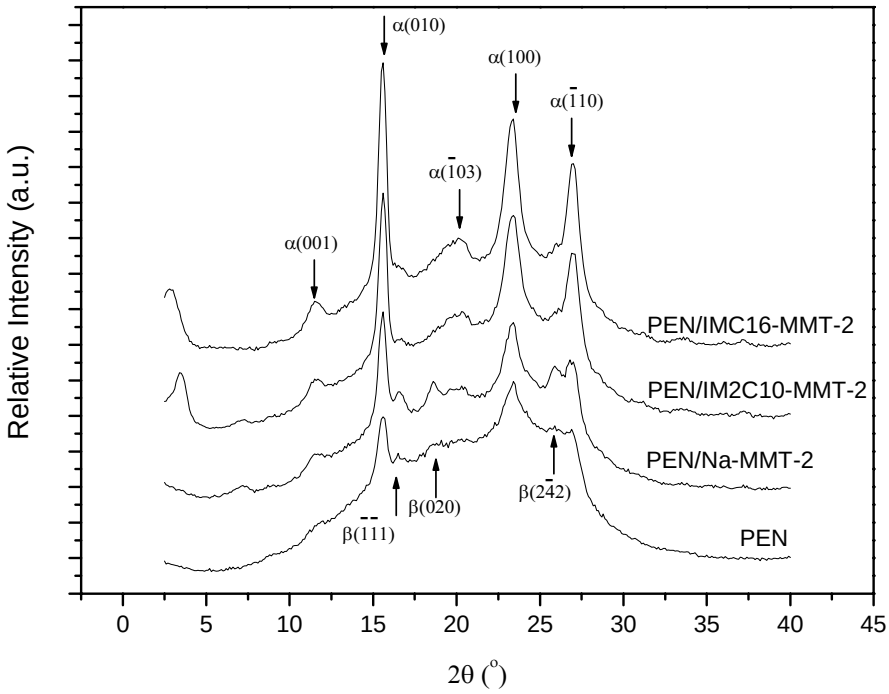

Figure 5.5 X-ray diffraction patterns of PEN and PEN/clay hybrids melt crystallized at 180°C.

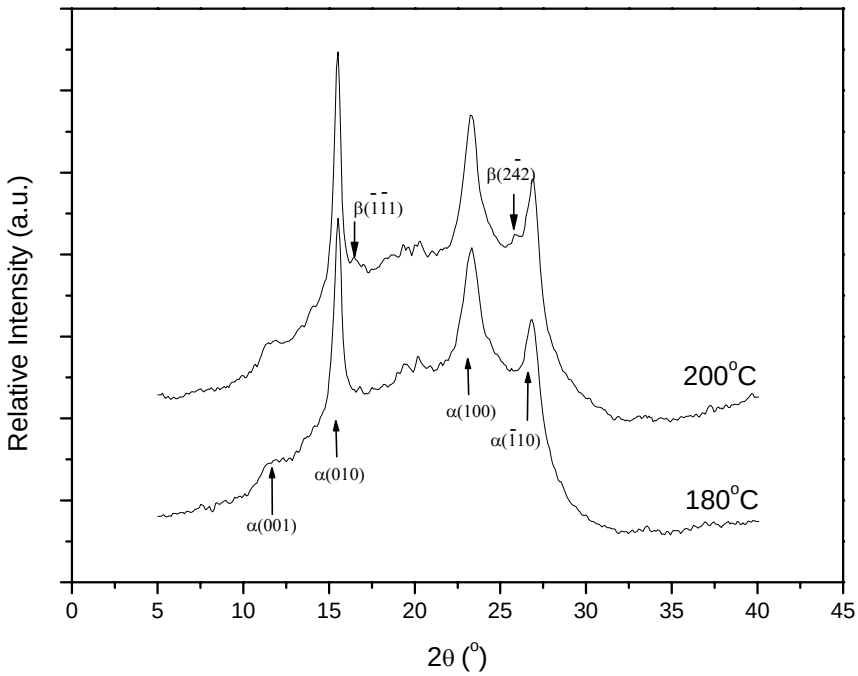

Figure 5.6 X-ray diffraction patterns of PEN/IMC16 melt crystallized at 200°C and 180°C.

An index, K_β, is used as a measure of the relative amount of β-crystalline form present:

$$K_\beta = \frac{A_{\beta(\bar{1}\bar{1}1)} + A_{\beta(020)} + A_{\beta(2\bar{4}2)}}{A_{\alpha(010)} + A_{\alpha(100)} + A_{\alpha(\bar{1}10)} + A_{\beta(\bar{1}\bar{1}1)} + A_{\beta(020)} + A_{\beta(2\bar{4}2)}} \times 100\%$$

where A refers to the integrated intensity associated with the crystal peak of interest. Table 5.2 summarizes the calculated K_β values of PEN and the hybrids melt-crystallized at the 3 temperatures. The standard error estimated for the values of K_β, based on 3 independent measurements and fitting procedures, is on the order of ±1% of the mean K_β. The variation of the K_β index with melt crystallization temperature is also illustrated in Figure 5.7.

Table 5.2 K_β values for PEN and PEN hybrids melt crystallized at various temperatures.

Melt Crystallization Temperature (^oC)	Sample	K_β (%)
200	PEN	56
	PEN/Na-MMT-2	66
	PEN/IM2C10-MMT-2	78
	PEN/IMC16-MMT-2	70
	PEN/IMC16	15
190	PEN	37
	PEN/Na-MMT-2	46
	PEN/IM2C10-MMT-2	39
	PEN/IMC16-MMT-2	46
180	PEN	30
	PEN/Na-MMT-2	42
	PEN/IM2C10-MMT-2	0
	PEN/IMC16-MMT-2	0
	PEN/IMC16	0

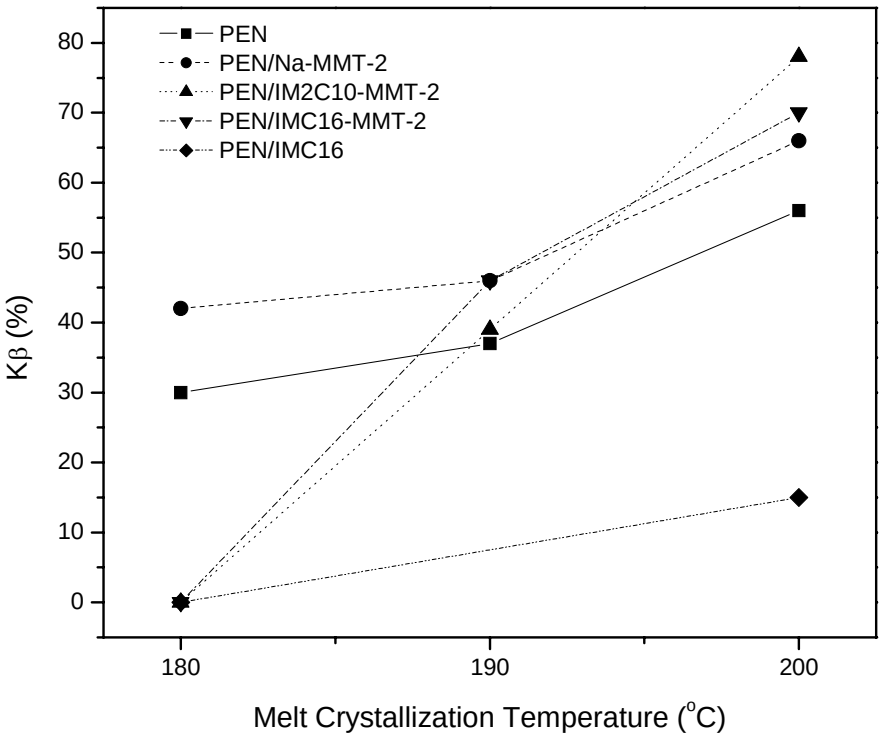

Figure 5.7 Variation of the K_β index with melt crystallization temperatures for PEN and its hybrids.

The results presented above indicate that pristine Na-MMT tends to promote the formation of the β-phase in PEN at all melt crystallization temperatures. On the other hand, the effect of the organoclays on the polymorphism behavior of PEN is found to vary with the crystallization temperature. At 200°C, the presence of the organoclay tends to promote the formation of the β-crystal phase in PEN. In particular, IM2C10-MMT possesses a stronger promoting effect on the β-phase than IMC16-MMT as evidenced by the higher K_β value of PEN/IM2C10-MMT-2. The β-phase enhancement effect of the organoclays however diminishes with reducing melt crystallization temperatures, and at 180°C, the two PEN/organoclay hybrids is found

to preferentially form the α-crystalline form instead, even though a small amount of β-crystals is still observed in pure PEN. Interestingly, the presence of the IMC16 surfactant alone in the PEN/IMC16 blend is found to enhance the formation of the α-crystal phase instead.

The polymorphism behaviors of the materials were corroborated by FTIR spectroscopy. Figure 5.8 shows representative spectra of PEN and the hybrids at the quiescent melt state and after complete crystallization at 200^{o}C and 180^{o}C. The band frequencies that are highly sensitive to the structural changes that occur during crystallization are labeled and their assignments provided in Table 5.3 [85,100].

Table 5.3 Band assignments of PEN in the amorphous, α and β crystalline phases[a].

IR Frequencies (cm^{-1})			Assignments
amorphous	α cystalline	β crystalline	
1477 m	1477 m		CH_2 bending (trans)
1452 m			CH_2 bending (gauche)
	1004 m		C-O stretching (trans)
964 m		974 sh	C-O stretching (gauche)
931 sh 916 s	931 s	917 s	O=C-O out-of-plane bending
822 m			CH_2 rocking (amorphous)
	838 m, 811 m	832 m	CH_2 rocking (crystalline)

[a] Abbreviations: s = strong, m = medium, sh = shoulder

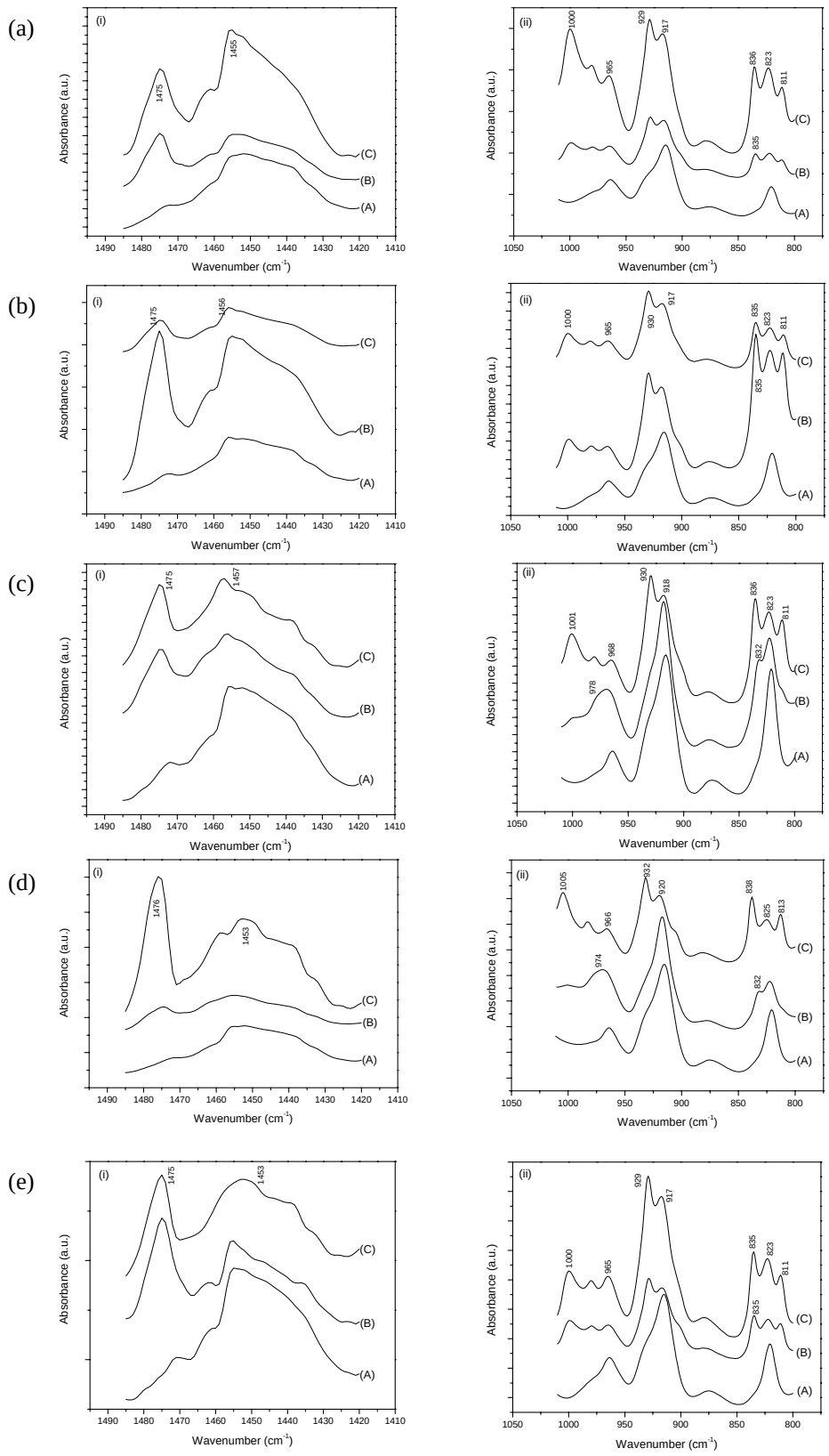

Figure 5.8 FTIR spectra of (a) PEN; (b) PEN/Na-MMT-2; (c) PEN/IM2C10-MMT-2; (d) PEN/IMC16-MMT-2 and (e) PEN/IMC16 in the (A) melt state and after melt crystallization at (B) 200°C and (C) 180°C: (i) 1485 – 1420 cm^{-1}; (ii) 1010 – 800 cm^{-1}.

It is observed that as the polymer passes from the melt state to the crystal phase, new absorption bands appear in the IR spectrum, or splitting occurs in the bands present in the spectra of the melt. These changes arise because of the changes in conformations and/or intermolecular interactions of the polymer chains as they pack into the ordered crystal phase. In addition, the relative intensities of the α-phase related bands at 1477, 1004, 931 and 811 cm^{-1}, together with the position of the crystal band at ~832-838 cm^{-1}, confirms the x-ray diffraction results presented earlier, that is, under melt crystallization at 200^{o}C, the β-phase is enhanced in PEN/organoclay hybrids, but at 180^{o}C, the α-phase is enhanced instead.

(II) In-situ Crystallization Behaviors of PEN and the Hybrids

To elucidate the underlying mechanisms for the unusual temperature-dependent polymorphism behavior exhibited by the PEN/organoclay hybrids, the crystallization process of the hybrids was monitored in-situ by high-temperature FTIR spectroscopy and x-ray diffraction. (As similar trends were observed in the two organoclay hybrids, only the crystallization behavior of PEN/IMC16-MMT-2 was investigated in detail in the subsequent sections, however, the crystallization behavior of PEN/IM2C10-MMT-2 is expected to follow a similar trend.)

High-temperature FTIR spectroscopy was used to probe the conformational changes of the PEN chains during the course of crystallization. To monitor the conformational changes, the evolution of the crystalline- and amorphous-dependent bands in the region of 850 - 800 cm^{-1} was plotted as a function of time during melt crystallization at 200°C and 180°C (Figure 5.9). In this frequency range, the band associated with the CH_2 rocking mode is split into two (for the β-crystal form) or three (for the α-crystal form) bands. The additional bands are at around 832 cm^{-1} (for

the β-crystal form), and 838/811 cm^{-1} (for the α-crystal form). Because the bands at 832 and 838 cm^{-1} are located very close to each other, only one band is observed in the FTIR spectra, even if the sample contains a mixture of α and β crystal forms, however, the relative proportions of each phase can still be deduced from the position of this band. To qualitatively compare the conformational changes in the polymer backbone over the course of crystallization, the normalized peak heights of the crystalline-sensitive band at ~832 - 838 cm^{-1} are plotted as a function of crystallization time (Figure 5.10).

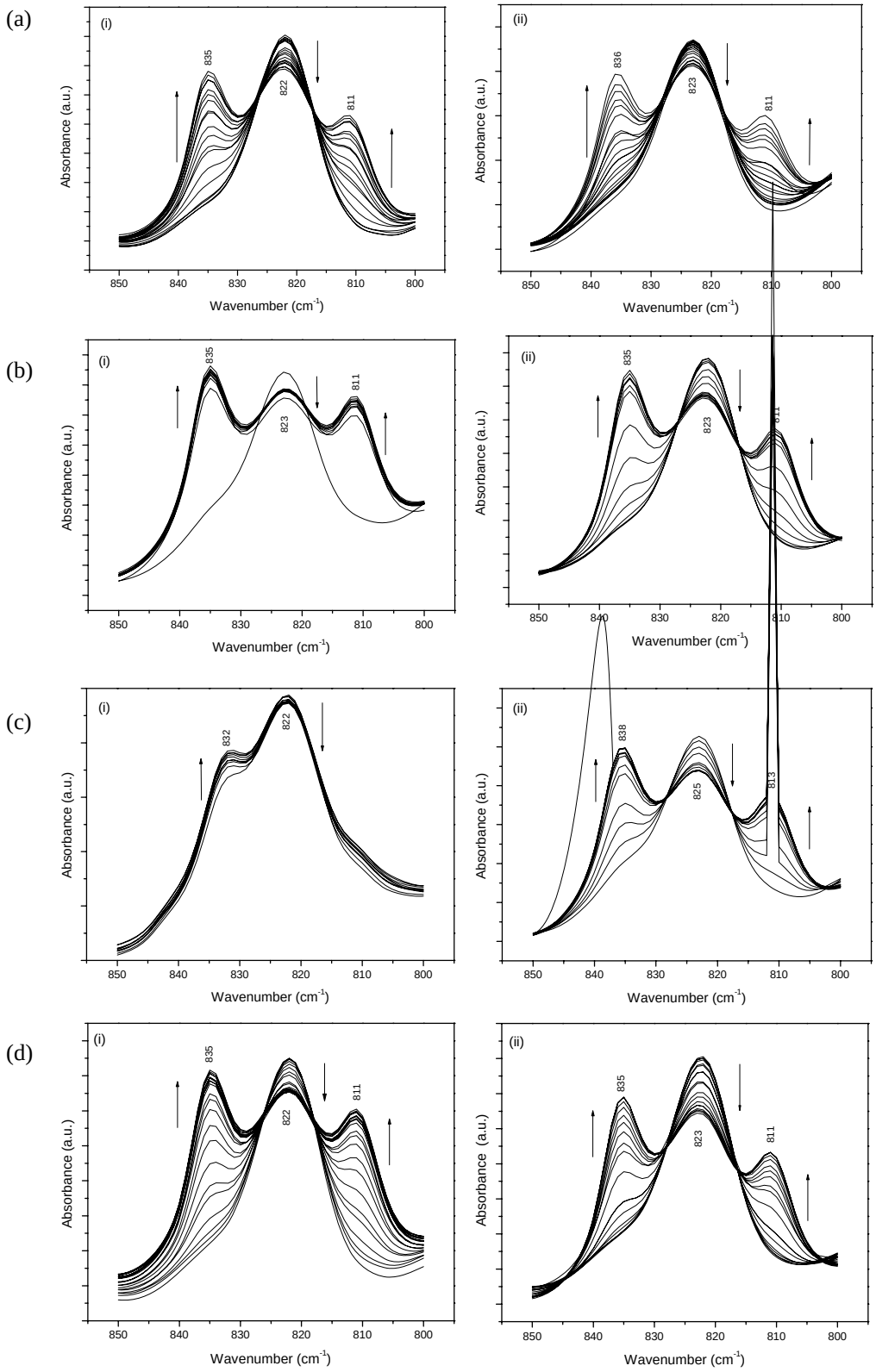

Figure 5.9 Time-resolved spectra of (a) PEN; (b) PEN/Na-MMT-2; (c) PEN/IMC16-MMT-2 and (d) PEN/IMC16 in the range of 850 - 800 cm^{-1} during melt crystallization at (i) 200^{o}C and (ii) 180^{o}C. The spectra were arranged with a 90 seconds interval.

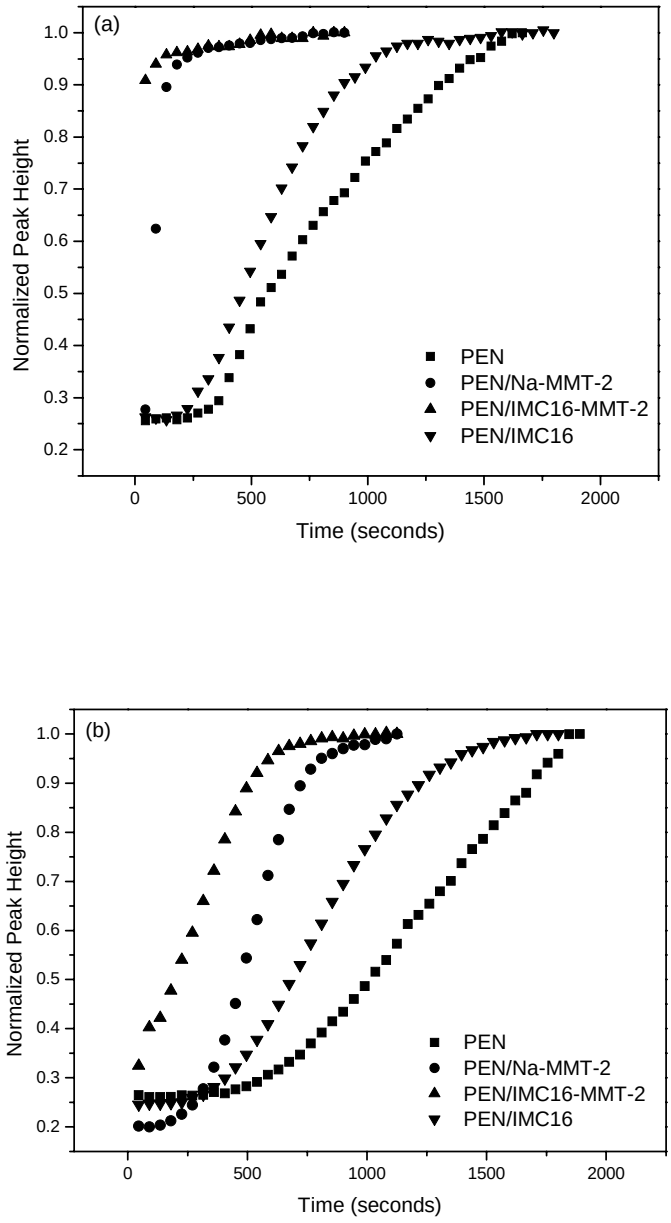

Figure 5.10 Normalized peak heights of the crystalline-sensitive band at ~ 832-838 cm^{-1} as a function of crystallization time at (a) 200^{o}C and (b) 180^{o}C.

To directly monitor the development of the two polymorphic forms during crystallization, the melt crystallization of PEN and the hybrids was also followed in-situ by high-temperature XRD. The development of the x-ray diffractograms with time during the initial 2000 seconds of the melt crystallization is displayed in Figure

5.11. The curves at t = 0 second correspond to the scans obtained whilst the samples were cooling from ~240°C to the desired crystallization temperature. Due to the limited cooling rate (20°C/min) that can be achieved by the high-temperature setup in the x-ray diffractometer, the materials tend to crystallize substantially before they reach 180°C so that the initial stages of melt crystallization at 180°C could not be captured properly. The x-ray data at 180°C are thus not reported here.

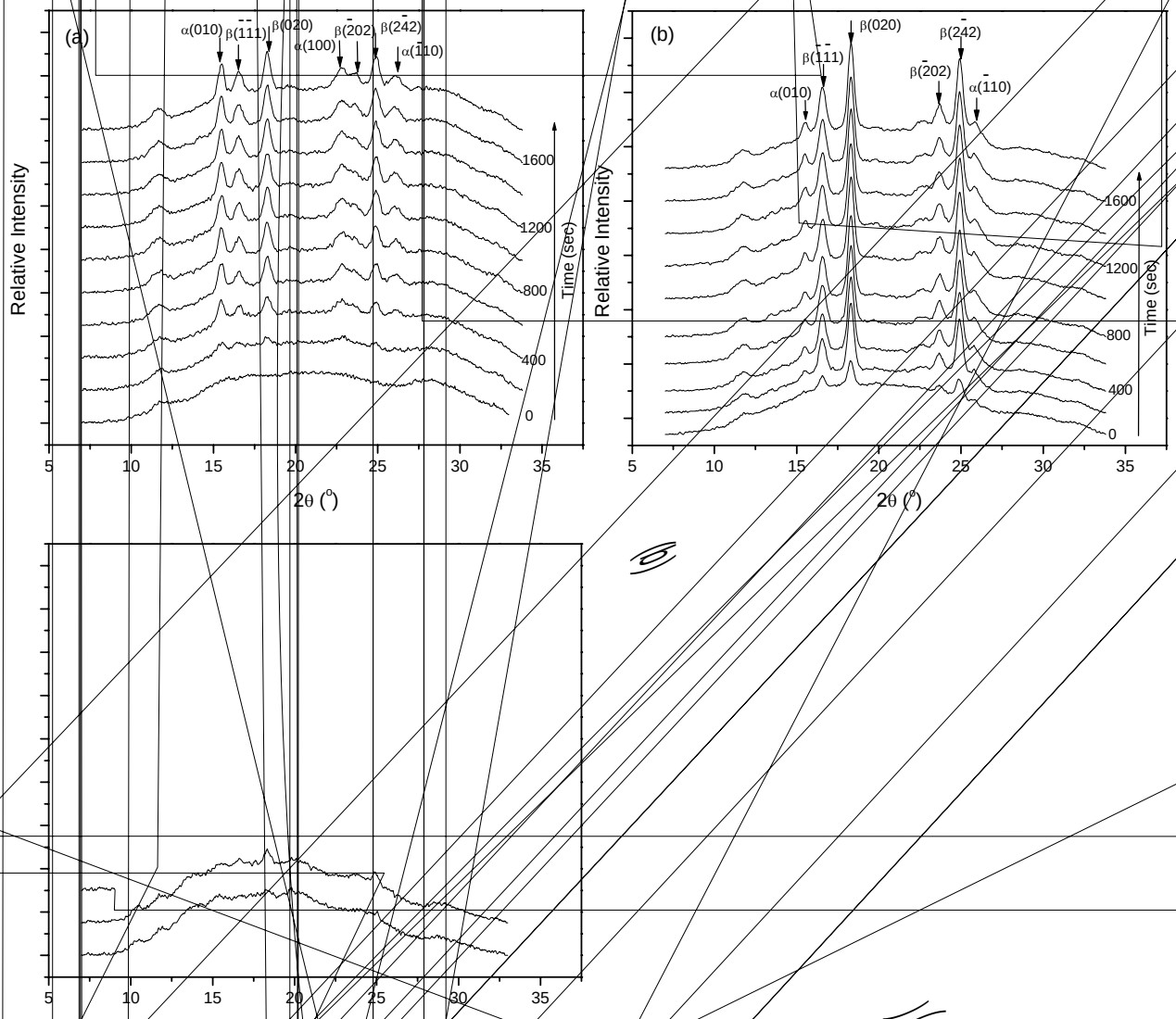

Figure 5.11 X-ray diffractograms of (a) PEN; (b) PEN/Na-MMT-2; (c) PEN/IMC16-MMT-2 and (d) PEN/IMC16 obtained during melt crystallization at 200°C.

The development of the α- and β-crystalline forms with time is followed by monitoring the intensities of the (010) and (020) peaks of the α- and β-phase respectively (Figure 5.12). The relative amounts of α- and β-phase formed at a particular time t is measured by an index, χ (t) where:

$$\chi_\alpha(t) = \frac{I_{\alpha(010)}(t)}{I_{\alpha(010)}(\infty) + I_{\beta(020)}(\infty)}$$

$$\chi_\beta(t) = \frac{I_{\beta(020)}(t)}{I_{\alpha(010)}(\infty) + I_{\beta(020)}(\infty)}$$

$I(t)$ refers to the intensity of the respective peaks at time t, after subtraction of the amorphous background and $I(\infty)$ refers to the final intensity of the peak after crystallization has reached completion.

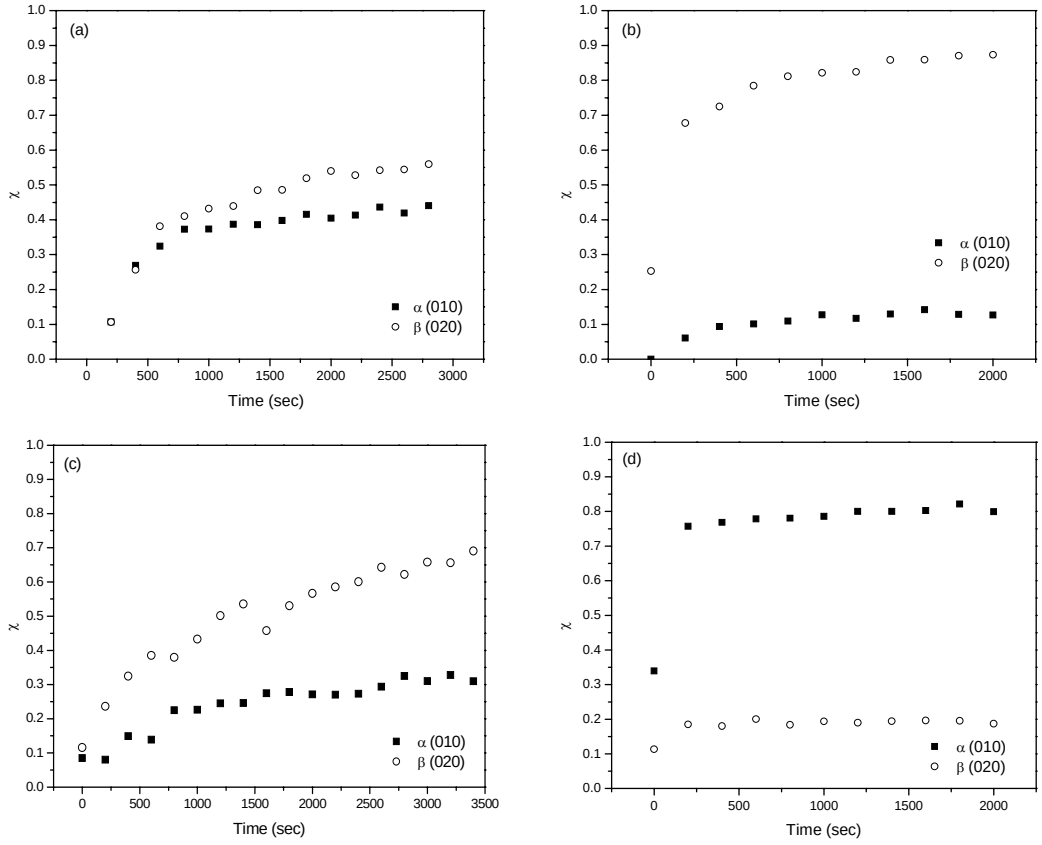

Figure 5.12 Development of the α- and β-crystallinities with time for (a) PEN; (b) PEN/Na-MMT-2; (c) PEN/IMC16-MMT-2 and (d) PEN/IMC16 melt crystallized at 200°C.

In the following sections, the in-situ crystallization behaviors of each system will be examined towards providing insights into the origin of the polymorphic differences between the various systems.

PEN/IMC16

At the melt compounding temperature, the surfactant IMC16 exists in the liquid state (Figure 5.13), and is able to mix with PEN at the molecular level. PEN/IMC16 is therefore a miscible blend, or better called plasticized PEN, as a reduction in T_g has been observed in the blend (Table 5.4).

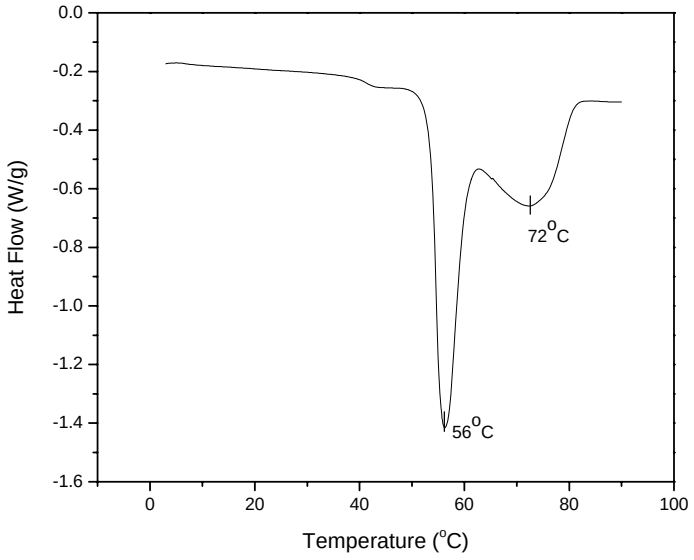

Figure 5.13 DSC thermogram of 1-hexadecyl-2,3-dimethylimidazolium (IMC16) chloride. The presence of two melting peaks can be attributed to the fusion of two crystalline phases possessing different degrees of stability [101].

Table 5.4 Glass transition temperatures (T_g) of PEN and its hybrids, as determined by DSC in the second heating run at 5°C/min.

System	PEN	PEN/Na-MMT-2	PEN/IMC16-MMT-2	PEN/IMC16
Glass Transition Temperature (T_g) (°C)	122	121	123	111

High-temperature XRD confirms that the α-crystalline phase is preferentially formed in PEN/IMC16 during melt crystallization at 200°C. In addition, the XRD results reveal that PEN/IMC16 exhibits the highest initial crystallinity at t = 0 seconds (Figures 5.11 and 5.12). In-situ FTIR also shows that the system exhibits more rapid conformational changes with respect to pure PEN at the two melt crystallization temperatures (Figure 5.10). The faster crystallization rate in PEN/IMC16 observed from in-situ XRD and FTIR is consistent with the higher hot crystallization temperature observed from DSC cooling experiments (Table 5.5). The faster overall crystallization rates observed in PEN/IMC16 can be attributed to the plasticizing effect caused by the dispersion of the IMC16 molecules in the PEN matrix at the molecular level. The plasticizing effect did not change the thermodynamics of the system however (the β phase is still enhanced at higher temperatures and hence remains as the more thermodynamically stable phase); rather, it has altered the kinetics of the system such that the α-phase now grows much faster than the β-phase in comparison to pure PEN (Figure 5.12(a) and (d)). This is because the α-phase is the kinetically favored phase with a smaller free energy of activation for a chain crossing the phase boundary to the crystals [78]. The increase in chain mobility would therefore increase the crystallization rate of the α-phase to a greater extent than for the

β-phase. The addition of IMC16 thus gives rise to an α-enhancement effect in the PEN matrix.

Table 5.5 Hot crystallization temperatures of PEN and its hybrids, under dynamic cooling at 5°C/min.

System	PEN	PEN/Na-MMT-2	PEN/IMC16-MMT-2	PEN/IMC16
Hot Crystallization Temperature (°C)	224	232	217	235

PEN/Na-MMT-2

The crystallization behavior of PEN/Na-MMT-2 reveals that pristine Na-MMT exerts a heterogeneous nucleating effect on PEN, with the β-crystal phase being preferentially nucleated at both crystallization temperatures. This is evidenced by the rapid conformational changes PEN/Na-MMT-2 displayed in real-time FTIR spectroscopy (Figure 5.10), as well as the fast initial crystallization rates exhibited by PEN/Na-MMT-2 in high-temperature XRD (Figure 5.12(b)) and its higher hot crystallization temperature observed from dynamic cooling DSC measurements (Table 5.5). It is worth noting that heterogeneous nucleation-induced β-phase enhancement in PEN has also been observed with other types of nucleating agents [102]. The effect is believed to be related to the surface geometry of the nucleating agent, although further studies are required to provide experimental evidence for this claim.

PEN/IMC16-MMT-2

Figure 5.10 shows that the intensity of the crystalline-sensitive band increases most rapidly in PEN/IMC16-MMT-2. This indicates that the presence of IMC16-MMT in

the polymer matrix can induce rapid conformational changes in the PEN chains as they pack into the ordered crystal phase. In addition, the polymer chain conformations that are induced by the presence of IMC16-MMT tend to vary with temperature. At 200^{o}C, the favored chain conformations are closer to that of the β-crystal form (as indicated by the band position at 832 cm^{-1} in Figure 5.9(c)(i)); at 180^{o}C however, the α-crystal conformations are favored instead (as suggested by the band position at 838 cm^{-1} in Figure 5.9(c)(ii)).

High-temperature XRD confirms that the formation of the β-crystalline phase is favored during melt crystallization at 200°C. In contrast to the case of PEN/Na-MMT-2 or PEN/IMC16 however, the rapid conformational changes observed in real-time FTIR spectroscopy are not accompanied by a corresponding appearance of Bragg peaks in the XRD diagrams, as no significant peaks are observed in the x-ray diffractograms during the very initial stage of the crystallization process (at t = 0 second). The slower overall rate at which crystals develop in PEN/IMC16-MMT-2 is also supported by its lower hot crystallization temperature during dynamic cooling on the DSC. The apparent different observations obtained with in-situ FTIR spectroscopy, and XRD/DSC measurements can be rationalized by understanding that the "crystallinity" detectable by the three techniques is in fact different. FTIR measures the concentration of the "crystalline isomer", which could be a short-range order or intramolecular phenomenon. In contrast, XRD measures intermolecular order as a result of chain packing, while DSC measures crystallinity based on the "meltable" portion of the polymer – both methods thus require order to be present on a longer range. Although short-range order is a necessary condition for long-range order to be present, it is also possible for short-range order to exist without any long-range order [103]. The results thus indicate that although local skeletal conformational

changes are induced much earlier in PEN/IMC16-MMT-2, the development of long-range order is somehow hindered on the organically modified clay surface in comparison to the untreated clay surface. A similar paradoxical result has also been reported on an exfoliated poly(L-lactic acid)/clay nanocomposite [104], in which intrachain interactions corresponding to PLLA 10_3 helix formation have been found to occur earlier than interchain interactions. The nanocomposite exhibits a slower nucleation rate, as interchain interactions are the dominant factor for the creation of stable nuclei from the highly entangled melt.

As the initial conformational changes observed in PEN/IMC16-MMT-2 are not accompanied by the formation of three-dimensional order, they in fact indicate the ordering present in the PEN chains during the *induction period* of crystallization. The abrupt change in the concentration of α and β "crystalline conformers" between 200°C and 180°C thus reflects a change in the equilibrium nuclei distribution for the two phases. To investigate the origins of this phenomenon, the thermally-induced structural changes of IMC16-MMT and their influences on clay surface and polymer/clay interface were further examined.

(III) Effect of Melt Crystallization Temperature on Surfactant Conformation in IMC16-MMT

To understand how the structure of IMC16-MMT changes with temperature, high-temperature FTIR was employed to probe the molecular conformation of IMC16 surfactant molecules at the various melt crystallization temperatures [105].

Figure 5.14 shows the high wavenumber CH stretching region of IMC16-MMT at various temperatures of the melt crystallization process. The band at ~2920 cm^{-1} arises from the CH_2 asymmetric, υ_{as} (CH_2) stretch. In general, the band width

and position of υ_{as} (CH_2) are sensitive to the trans/gauche conformer ratio, as well as the packing density of methylene chains. A broadening and shift of this band to a higher frequency signify that the intercalated methylene chains change from a more ordered structure with more trans conformations to a more disordered structure with more gauche conformations [106]. The frequencies of the IMC16-MMT υ_{as} (CH_2) band at the various temperatures are summarized in Table 5.6. The significantly higher wavenumber of υ_{as} (CH_2) at temperatures ≥ 180°C (relative to that at 25°C) is due to the occurrence of a melting-like order-disorder transition at ~48°C (Figure 5.15), which drastically increases the gauche conformer ratio in the intercalated surfactant molecules [107]. As this transition occurs at a temperature way below the melt crystallization temperatures however, it is not expected to affect the melt crystallization behavior of PEN in any way.

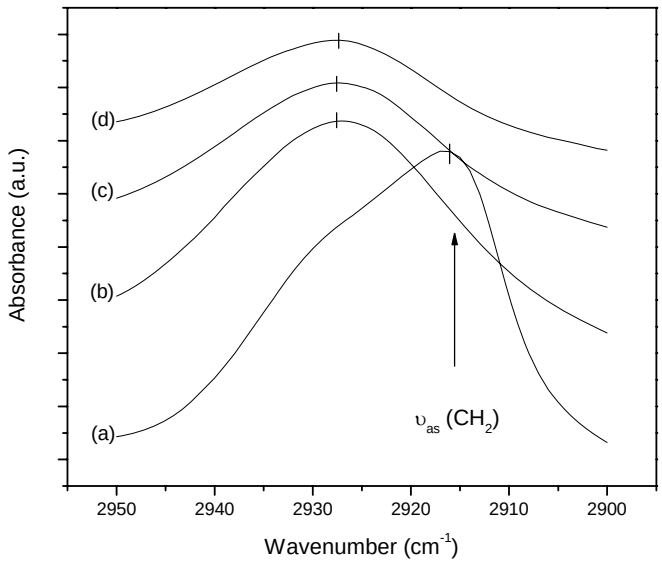

Figure 5.14 Representative FTIR spectra of IMC16-MMT in the region 2950 - 2900 cm^{-1} acquired at (a) 25°C; (b) 280°C and subsequent cooling to (c) 200°C and (d) 180°C. The approximate peak positions of the υ_{as} (CH_2) band, as determined by the Perkin Elmer Spectrum software are indicated.

Table 5.6 Wavenumber of υ_{as} (CH_2) in IMC16-MMT and IMC16 at various temperature points of the melt crystallization process. (Errors given represent one standard deviation from the mean, based on 3 independent measurements.)

Temperature (^oC)	υ_{as} (cm^{-1})	
	IMC16-MMT	IMC16
25^oC	2916.3 ± 0.3	2915.4 ± 0.2
180^oC	2927.5 ± 0.4	2925.4 ± 0.2
200^oC	2927.6 ± 0.3	2925.1 ± 0.2
280°C	2927.3 ± 0.2	-

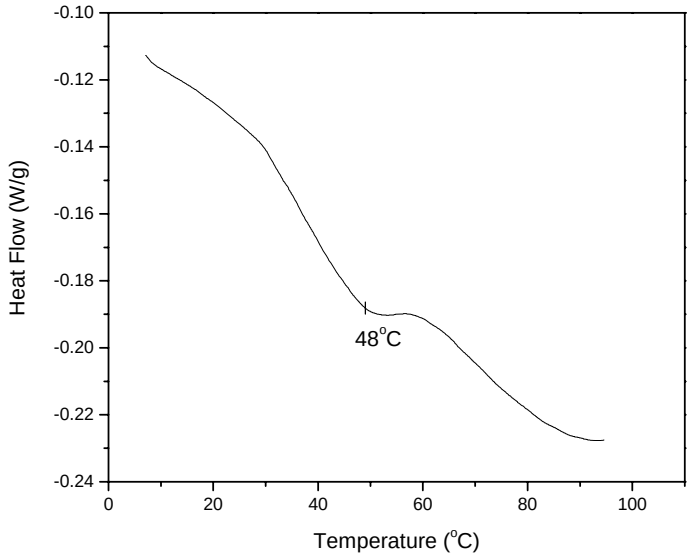

Figure 5.15 DSC thermogram for IMC16-MMT during heating at 5°C/min.

Table 5.6 shows that there exists no significant difference in the conformations of the surfactant molecules in IMC16-MMT at 200°C and 180°C. To ascertain whether the minimal conformational change experienced by the surfactant molecules at these two temperatures is due to their restricted conformational freedom, as a result

of their confinement within the clay galleries (before the galleries are expanded by the intercalation of the polymer chains), the FTIR spectra of the IMC16 salt were also acquired at 200°C and 180°C, and listed in Table 5.6. From Table 5.6, it is observed that even without the geometric constraining effect of the clay layers, the IMC16 chains still undergo very little conformational changes between 200°C and 180°C. This indicates that the conformational changes of PEN chains observed in PEN/IMC16-MMT-2 between the two melt crystallization temperatures were not induced by the conformational changes experienced by the surfactant chains, as has been previously suspected [108].

(IV) Thermal Degradation Behaviors of IMC16-MMT

To examine the weight loss behaviors of IMC16-MMT under the melt compounding and melt crystallization conditions, TGA was performed, simulating the temperature profiles of these two processes (Figure 5.16). Table 5.7 summarizes the extent of degradation that was observed in IMC16-MMT under the simulated melt compounding and melt crystallization conditions.

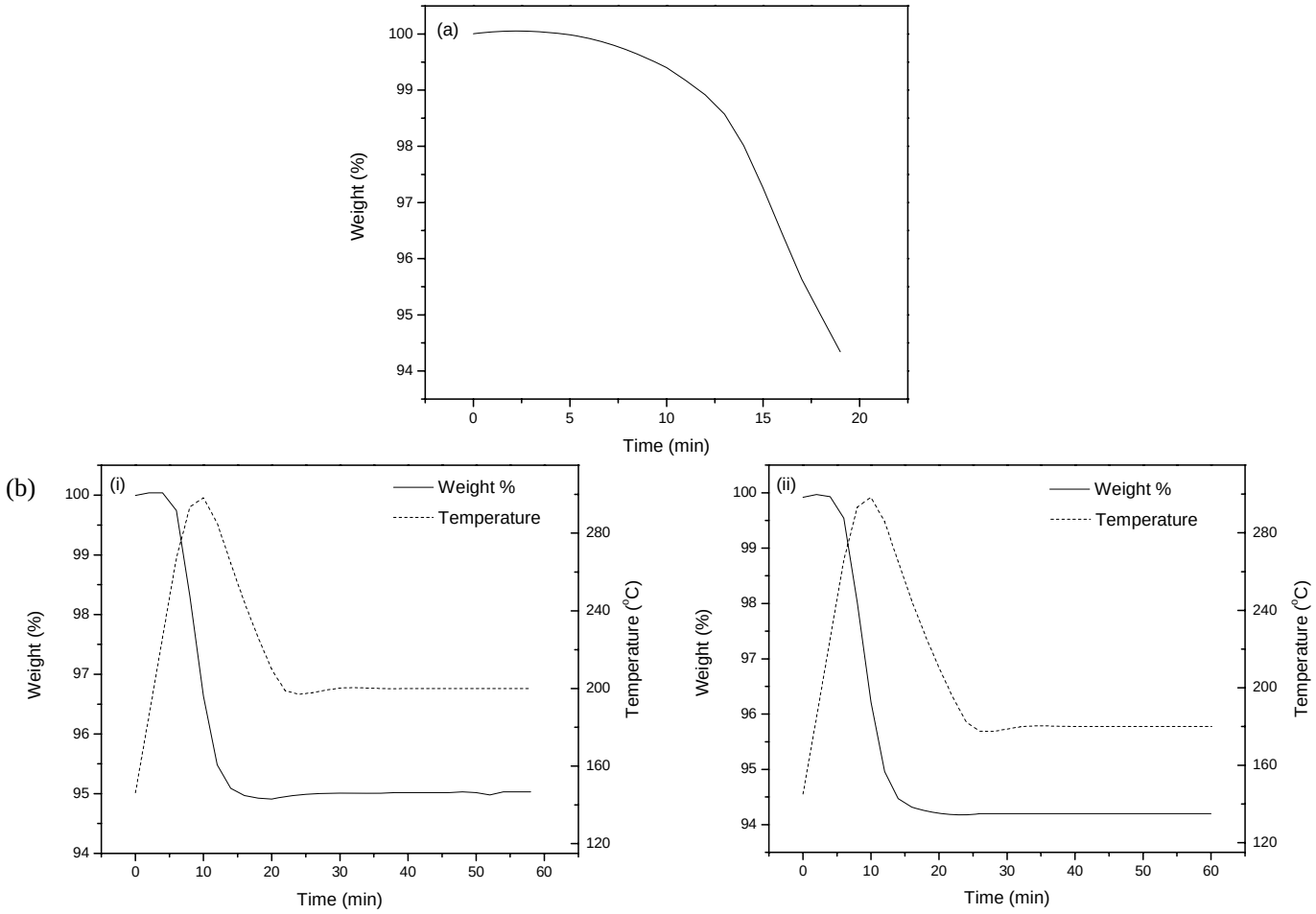

Figure 5.16 TGA profiles of IMC16-MMT under the simulated conditions of (a) melt compounding and (b) melt crystallization at (i) 200°C and (ii) 180°C. Time = 0 min corresponds to the end of the predrying step at 140°C.

Table 5.7 Extent of thermal degradation in IMC16-MMT during the simulated melt compounding and melt crystallization conditions, as evaluated by TGA.

Condition		Weight Loss (%)[a]
Melt compounding		5.9
Melt crystallization	200°C	4.7
	180°C	4.6

[a] The amount of degradation is expressed in terms of the % weight loss in the original IMC16-MMT. All values stated are the average obtained from 3 independent measurements.

From Table 5.7, it is observed that significant degradation has occurred in IMC16-MMT, both during melt compounding and melt crystallization. There is however, no significant difference in the extent of degradation between melt crystallization at 200^{o}C and 180^{o}C. In fact, the degradation that occurs during melt crystallization takes place during the melting process, and no further degradation occurs during the crystallization process at 200^{o}C or 180^{o}C (Figure 5.16(b)). The finding thus rules out the possibility that the abrupt change in the concentration of α and β "crystalline conformers" formed between 200°C and 180°C is due to a *difference* in the degradation behavior of IMC16-MMT at these two temperatures.

(V) Role of the Clay Surface Modification

As discussed earlier, although short-range molecular ordering is induced very quickly during the induction period in PEN/IMC16-MMT-2, the development of long-range order is somehow hindered - this implies that the formation of stable nuclei is more difficult at the PEN/IMC16-MMT interface than at the PEN/Na-MMT interface. The hindered formation of stable nuclei is likely to be the major cause for the large change in equilibrium nuclei distribution for the two phases between 200° and 180°C, as this effect may tend to have a more pronounced influence on the thermodynamically less stable α-phase. At 200°C, the nearly absence of the 811 cm^{-1} band at the initial stage of crystallization (Figure 5.9(c)(i)) indicates that most "crystalline conformers" of the less stable α-phase are unable to develop into stable nuclei of a critical size at the PEN/IMC16-MMT interface, so that its concentration remains extremely low. At 180°C on the other hand, both types of nuclei could reach their critical size, diffusion thus becomes the controlling factor, and so the kinetically favored α-phase becomes dominant.

The above discussion opens up an important question as to what constrains the formation of stable nuclei at the PEN/IMC16-MMT interface. One hypothesis is that the crystals are initiated from polymer chains which are intercalated in clay galleries of nanometer thicknesses [109]. To clarify the possible role that the intercalated polymer chains may play in the nucleation of the PEN crystallites, a comparison can be made between the morphologies and polymorphism behaviors exhibited by PEN/IMC16-MMT-2 and PEN/IM2C10-MMT-2. As discussed in Section 3.5.3(I), surfactant IM2C10 is less compatible with PEN than IMC16; it is thus unable to provide sufficient driving force for PEN to diffuse into the intergallery spaces and so the clay basal spacing in PEN/IM2C10-MMT-2 remained relatively unchanged after melt compounding with PEN. The K_β of PEN/IM2C10-MMT-2 is however, even more sensitive to the crystallization temperature (it changes from 78% at 200°C to ~ 0% at 180°C). This indicates that the hindered formation of stable nuclei at the PEN/IMC16-MMT-2 interface does not originate from the constrained polymer chains which are intercalated between the clay layers. The hindrance to the formation of stable nuclei should thus come from the unique nature of the polymer/organoclay interface.

In polymer/clay nanocomposites, the cationic surfactants typically reside at (1) the *intergallery* spaces (intercalated) or (2) are ionically bound on the *surface* of the clay layers. Based on the results presented above however, it is found that significant degradation and/or desorption of the surfactants has occurred during both melt compounding and melt crystallization. As a result, significant amounts of small molecular products from the degradation of the surfactants may also be found in (3) the *bulk* of the polymer matrix (mainly from the surfactants that degrade during the melt compounding process) and (4) at *close vicinity* to the clay surface (mainly from

the surfactants that degrade during melt crystallization). The concentration of the small molecules (either the surfactants or their degradation products) in the bulk of PEN/IMC16-MMT-2 might be much lower than that found in the bulk of the PEN/IMC16 blend, however, their concentration at the polymer/clay interfacial regions could be fairly significant.

The effect of the intercalated surfactant molecules (1) on the polymorphism behavior of PEN may be ignored, while the small molecules in the bulk (3) may lead to a plasticizing effect in the bulk of the PEN matrix. On the other hand, the combination of the small molecules located at (2) and (4) may give rise to a unique interface, which is different from the interface formed by the untreated Na-MMT surface and the unplasticized melt. Firstly, on the organically modified clay surface, although the nucleation is still “heterogeneous” in nature, the thermodynamics of the system is different (the formation of stable nuclei is hindered). Secondly, with a highly plasticized interfacial region, the kinetics of the system is different (the difference between the crystallization rates of the two phases is larger). The combination of the heterogeneous nucleating and plasticizing effects causes the interface to be more sensitive to temperature changes than the interface formed by Na-MMT and the unplasticized melt. At a melt crystallization temperature of 200^{o}C, the heterogeneous nucleating effect is dominant, but the α-phase nuclei are largely unstable at the interface due to the flexible nature of the surfactant. This is supported by the fact that increasing the flexibility of the surfactant, for example, in the case of PEN/IM2C10-MMT-2, results in an increase in K_{β} at 200°C. At 180^{o}C on the other hand, both types of nuclei are stable, and so the plasticizing effect becomes dominant. The kinetically favored α-crystal phase thus preferentially forms at both the interface and the bulk.

5.6 Summary and Conclusions

In this chapter, the effect of the melt crystallization temperature on the polymorphic behavior of the PEN/clay nanocomposites was evaluated. It was found that pristine Na-MMT enhances the formation of the β-crystal phase, over the more common α-crystal form, at all melt crystallization temperatures. For the PEN/organoclay hybrids however, the polymorphism behavior was found to vary with the crystallization temperature, with the β-crystal form being enhanced at higher temperatures, but the α-crystal phase being more favored instead at lower temperatures. This is also the first time that such a temperature-dependent polymorphism behavior has been observed in polymer/clay nanocomposites.

In-situ FTIR spectroscopy and XRD was employed to elucidate the underlying mechanisms for the unusual temperature-dependent polymorphism behaviors exhibited by the PEN/organoclay nanocomposites. Real-time FTIR spectroscopy of PEN/IMC16-MMT-2 reveals an abrupt change in the concentration of α and β "crystalline conformers" at the initial stage of crystallization with crystallization temperature. The development of short-range order occurs prior to the development of three-dimensional order, which implies that the formation of stable nuclei is hindered at the PEN and IMC16-MMT interface. In addition, surfactant degradation also caused the interface between PEN and IMC16-MMT to be highly plasticized, which could increase the crystallization rate of the kinetically-favored α-phase more, in comparison to the β-phase. It is this combination of the hindered heterogeneous nucleating and plasticizing effects which cause the PEN/organoclay interface to be more sensitive to temperature: at 200^{o}C, the heterogeneous nucleation effect is dominant, which cause the β-phase to be favored; at 180^{o}C, stable nuclei of both

crystal phases are able to form, diffusion thus becomes the controlling factor, and the kinetically favored α-phase is preferentially formed instead.

The findings of this work thus provide new insights on the role that the clay surface modification can play in affecting the type of crystal structure developed in the matrix polymer, which may not only be relevant for the PEN system, but may also be applicable to other semicrystalline polymer/clay nanocomposites exhibiting different polymorphic forms as well.

CHAPTER 6

Summary and Conclusions

In this work, a novel system of polymer/clay nanocomposites based on poly(ethylene naphthalate) (PEN) was developed. The properties of the nanocomposites were examined and correlated with their structures. In addition, the polymorphism behavior of the nanocomposites was studied and the underlying mechanism governing the type of crystal phase formed in the nanocomposites was investigated. In this chapter, the major findings of this work, as well as the important contributions that this work has made in the field of polymer/clay nanocomposites will be reviewed.

6.1 Preparation of PEN/Clay Nanocomposites

Two routes for the preparation of PEN/clay nanocomposites, namely in-situ polymerization and melt intercalation, have been explored. Through the investigation of these two routes of preparation, the critical factors that affect the dispersion of clay in the PEN matrix were evaluated.

In-situ polymerization, traditionally viewed as the preparation route that would achieve the best clay dispersion, was found to provide only limited clay dispersion in this case due to the high temperature and long-time exposure required for the polymerization of PEN, which often results in degradation of the organically-modified clay. Nevertheless, the potential of this method in peeling the clay tactoids into individual sheets was demonstrated with the use of a mixed intercalant system, in

which the clay was modified with a combination of catalytic ions and organic surfactants.

For the melt intercalation method, it was found that the shear force applied via a twin-screw extruder is able to break the micron-sized clay agglomerates into submicron- or even smaller-sized clay tactoids. The success of this method is also contingent on the initial homogeneity of the starting materials, the thermal stability of the organoclay, as well as the compatibility of the modifier with the PEN matrix. When all the above conditions have been fulfilled, effective dispersion of the clay in the PEN matrix, at both the nano- as well as the micron-scale can be achieved. Specifically, the use of a newly developed 1-hexadecyl-2,3-dimethylimidazolium-modified clay, which possesses considerably greater thermal stability than the traditional alkylammonium clays, has resulted in a nanocomposite possessing an intercalated structure. This is also one of the first reported PEN/clay nanocomposite systems.

6.2 Structure-Property Relationship in PEN/Clay Nanocomposites

The dynamic mechanical behaviors and thermal stability of the PEN/clay hybrids were examined. The results indicate that the property enhancements exhibited by the hybrids are related to the level of clay dispersion (at both the nano- and micron-scale) in the PEN matrix.

Comparison of the modulus enhancements exhibited by the largely amorphous as-molded and annealed specimens also reveals that the nanocomposite displays a greater modulus enhancement with respect to the neat PEN after both materials were allowed to crystallize. The result indicates that the mechanical reinforcement in the PEN/clay nanocomposite can arise not only from the high modulus and high aspect

ratio of the dispersed clay phase, but may also contain an important contribution from the clay-induced modifications to the PEN crystalline phase. In particular, the additional reinforcement observed in the nanocomposite after crystallization was attributed to the preferred alignment of the high-aspect-ratio polymer lamellae (along with the clay sheets) in the injection direction, and the orientation correlation that exists between the clay platelets and the PEN naphthalene rings.

6.3 Polymorphism Behavior of PEN/Clay Nanocomposites

The crystal forms developed in the PEN/clay nanocomposites under melt crystallization at different temperatures were investigated. Unmodified Na-MMT was found to exert a heterogeneous nucleating effect on PEN, enhancing the formation of the β-phase, while the organoclays exhibit a strong temperature-dependent polymorphic behavior, with the β-phase being more favored at higher temperatures, but the α-crystal being preferentially formed at lower temperatures.

Real-time FTIR spectroscopy of PEN/IMC16-MMT-2 reveals an abrupt change in the concentration of α and β "crystalline conformers" at the initial stage of crystallization with crystallization temperature. In addition, the formation of stable nuclei at the PEN and IMC16-MMT interface was found to be hindered, as evidenced by the development of three-dimensional order long after the existence of short-range order. The occurrence of significant surfactant degradation during melt compounding and melt crystallization could also cause the interface between PEN and IMC16-MMT to be highly plasticized, which could increase the crystallization rate of the kinetically-favored α-phase to a greater extent than for the β-phase.

It was postulated that the strong temperature dependence of the polymorphism behavior of the PEN/organoclay hybrids arises due to this combination of the

hindered heterogeneous nucleating and plasticizing effects: at 200^{o}C, the hindered heterogeneous nucleation effect is dominant, which cause the β-phase to be favored; at 180^{o}C, stable nuclei of both crystal phases are able to form, the plasticizing effect thus becomes dominant and the kinetically favored α-phase is preferentially formed instead.

CHAPTER 7

Recommendations for Future Research

The investigations performed in this work have established a foundation from which future work in the development of PEN/clay nanocomposites, or other semi-rigid polyester/clay nanocomposite systems can build upon. At the same time, the study has revealed some interesting aspects of the PEN/clay nanocomposite system which are worth further exploration. The major directions which future efforts can be focused on are discussed below.

7.1 Preparation of PEN/Clay Nanocomposites

Although limited success has been attained in this work with the in-situ polymerization technique, the potential of this strategy in dispersing clay at the single-layer level has been demonstrated with the mixed intercalant clay system. Further efforts can be based on a similar clay modification procedure, but with the use of a more thermally stable organic modifier (a promising candidate is the trialkylimidazolium salt derivatives that have been employed for the melt intercalation route in this work), as well as an improved polymerization set-up (which is able to provide a higher shear force to break up the clay agglomerates at the micron level).

For the melt intercalation route, the dispersion and homogeneity of the nanocomposites can be further optimized by systematically studying the effects of the various processing conditions (such as the processing temperatures, screw speeds,

residence times, and screw geometries) on the morphologies exhibited by the resulting nanocomposites.

7.2 Characterization of Nanocomposite Properties

In this work, the effects of nanoclay on the dynamic mechanical behaviors and thermal stability of PEN have been investigated. In addition to the above properties, the determination of the other properties of the nanocomposites [such as their tensile properties (for example, Young's modulus, ultimate strengths and elongation at break), barrier properties, toughness and optical transparency] is also necessary in order to have a better assessment of their performance in their potential applications.

7.3 Effect of β-phase Formation on Properties

In this work, the addition of clay has been found to enhance the formation of the β-crystal phase in PEN over the more common α-crystal form under certain conditions. The effect of β-phase formation on the properties of the PEN/clay nanocomposites has not been studied however, but it is expected that the β-crystal form, which possesses a different molecular conformation and a higher density than the α-phase will exhibit different properties (stiffness, toughness, barrier properties etc). In this respect, the conditions for preferential β-phase formation, as documented in this thesis, shall serve as a useful process guideline for this aspect of the structure-property studies of PEN/clay nanocomposites.

7.4 Impact of Crystallite Orientation on Modulus

In Chapter 4, the additional modulus enhancement observed in PEN/IMC16-MMT-2 after annealing has been attributed to the preferred alignment of the polymer lamellae along the flow direction. Since this phenomenon implies extensive anisotropy of the modulus, the transverse modulus of the specimens (i.e. the modulus perpendicular to the flow direction) can be measured to confirm this phenomenon.

7.5 TEM Observations of Polymer Crystalline Morphology

AFM studies performed in the course of this work have provided significant insights on the subspherulitic features that developed in PEN under the influence of nanoclay. The AFM technique is limited to thin films however, while it is also of interest to visualize the mesoscopic arrangement of the crystallites in the bulk samples. In this context, the direct observation of the lamellar morphology of the PEN/clay nanocomposites by TEM offers much interest. Selective staining of the amorphous phase can be achieved by ruthenium tetraoxide to obtain a contrast between the crystalline polymer lamellae and the amorphous regions [110]. The lamellar scale contrast will allow the direct visualization of the lamellar organization in the nanocomposites, as well as provide information about the orientation of the polymer lamellae with respect to the clay platelets. The ability to observe the crystalline organization in the PEN matrix formed in the presence of nanoclay at the high resolution offered by TEM will yield additional insights on the correlation between the mesoscale arrangement in the nanocomposites and its mechanical behavior.

7.6 SAXS Analysis of Nanocomposite Hierarchical Structure

In this work, the information on the hierarchical organization of the PEN/clay hybrids is primarily derived from AFM observations and 2-dimensional x-ray diffraction. To obtain a more complete understanding of the morphological organization in the nanocomposites, small-angle x-ray scattering (SAXS) is necessary to determine the orientation of the clay layers and PEN crystallites. From SAXS, structural information on the lamellar organization of the PEN crystallites (specifically, the long spacing, lamellar crystal thickness and the amorphous layer thickness) may also be determined. With this information, the effect of the spatial arrangement of the clay layers on the PEN lamellar superstructure can be better ascertained.

REFERENCES

1. Y. Kojima, A. Usuki, M. Kawasumi, A. Okada, Y. Fukushima, T. Kurauchi, O. Kamigaito, Mechanical properties of nylon 6-clay hybrid, Journal of Materials Science, 8 (1993) 1185-1189.

2. D. Shah, P. Maiti, E. Gunn, D.F. Schmidt, D.D. Jiang, C.A. Batt, E.P. Giannelis, Dramatic enhancements in toughness of polyvinylidene fluoride nanocomposites via nanoclay-directed crystal structure and morphology, Advanced Materials, 16 (2004) 1173-1177.

3. S.S. Ray, M. Okamoto, Polymer/layered silicate nanocomposites: a review from preparation to processing, Progress in Polymer Science, 28 (2003) 1539-1641.

4. M. Alexandre, P. Dubois, Polymer-layered silicate nanocomposites: preparation, properties and uses of a new class of materials, Materials Science and Engineering, 28 (2000) 1-63.

5. J. Jager, J.A. Juijn, C.J.M. Van den Heuvel, R.A. Huijts, Poly(ethylene-2,6-naphthalenedicarboxylate) fiber for industrial applications, Journal of Applied Polymer Science, 57 (1995) 1429-1440.

6. E.P. Giannelis, R. Krishnamoorti, E. Manias, Polymer-silica nanocomposites: model systems for confined polymers and polymer brushes, Advances in Polymer Science, 138 (1999) 108-147.

7. M. Kato, A. Usuki, Polymer-clay nanocomposites, Polymer-Clay Nanocomposites, John Wiley and Sons (2000) 97-109.

8. R. Levy, C.W. Francis, Interlayer adsorption of polyvinylpyrrolidone on montmorillonite, Journal of Colloid Interface Science, 50 (1975) 442-450.

9. C. M. Koo, H.T. Ham, M.H. Choi, S.O. Kim, I.J. Chung, Characteristics of polyvinylpyrrolidone-layered silicate nanocomposites prepared by attrition ball milling, Polymer, 44 (2003) 681-689.

10. Z. Shen, G.P. Simon and Y. Cheng, Comparison of solution intercalation and melt intercalation of polymer-clay nanocomposites, Polymer, 43 (2002) 4251-4260.

11. N. Ogata, S. Kawakage, T. Ogihara, Poly(vinyl alcohol)-clay and poly(ethylene oxide)-clay blend prepared using water as a solvent, Journal of Applied Polymer Science, 66 (1997) 573-581.

12. D.J. Greenland, Adsorption of polyvinylalcohols by montmorillonite, Journal of Colloid Science, 18 (1963) 647-664.

13. J. Billingham, C. Breen, J. Yarwood, Adsorption of polyamine, polyacrylic acid and polyethylene glycol on montmorillonite: an in-situ study using ATR-FTIR, Vibrational Spectroscopy, 14 (1997) 19-34.

14. N. Ogata, G. Jimenez, H. Kawai, T. Ogihara, Structure and thermal/mechanical properties of poly(L-lactide)-clay blend, Journal of Polymer Science Part B: Polymer Physics, 35 (1997) 389-396.

15. G. Jimenez, N. Ogata, H. Kawai, T. Ogihara, Structure and thermal/mechanical properties of poly(ε-caprolactone)-clay blend, Journal of Applied Polymer Science, 64 (1997) 2211-2220.

16. H.G. Jeon, H.T. Jung, S.W. Lee, S.D. Hudson, Morphology of polymer silicate nanocomposites: high-density polyethylene and a nitrile, Polymer Bulletin, 41 (1998) 107-113.

17. A. Usuki, Y. Kojima, M. Kawasumi, Y. Fukushima, T. Kurauchi, O. Kamigaito, Synthesis of nylon 6-clay hybrid, Journal of Materials Research, 8 (1993) 1179-1184.

18. T. Lan, P.D. Kaviratna, T.J. Pinnavaia, Mechanism of clay tactoid exfoliation in epoxy-clay nanocomposites, Chemistry of Materials, 7 (1995) 2144-2150.

19. T.Y. Tsai, C.H. Li, C.H. Chang, W.H. Cheng, C.L. Hwang, R.J. Wu, Preparation of exfoliated polyester/clay nanocomposites, Advanced Materials, 17 (2005) 1769-1773.

20. Y. Imai, S. Nishimura, E. Abe, H. Tateyama, A. Abiko, A. Yamaguchi, T. Aoyama, H. Taguchi, High-modulus poly(ethylene terephthalate)/expandable fluorine mica nanocomposites with a novel reactive compatibilizer, Chemistry of Materials, 14 (2002) 477-479.

21. J. Ma, Z. Yu, Q. Zhang, X. Xie, Y. Ma, I. Luck, A novel method for preparation of disorderly exfoliated epoxy/clay nanocomposite, Chemistry of Materials, 16 (2004) 757-759.

22. M.W. Weimer, H. Chen, E.P. Giannelis, D.Y. Sogah, Direct synthesis of dispersed nanocomposites by in-situ living free radical polymerization using a silicate-anchored initiator, Journal of the American Chemical Society, 121 (1999) 1615-1616.

23. J.S. Bergman, H. Chen, E.P. Giannelis, M.G. Thomas, G.W. Coates, Synthesis and characterization of polyolefin-silicate nanocomposites: a catalyst intercalation and in situ polymerization approach, Chemical Communications, (1999) 2179-2180.

24. R.A. Vaia, E.P. Giannelis, Lattice model of polymer melt intercalation in organically-modified layered silicates, Macromolecules, 30 (1997) 7990-7999.

25. R.A. Vaia, E.P. Giannelis, Polymer melt intercalation in organically-modified layered silicates: model predictions and experiment, Macromolecules, 30 (1997) 8000-8009.

26. T.D. Fornes, P.J. Yoon, H. Keskkula, D.R. Paul, Nylon 6 nanocomposites: the effect of matrix molecular weight, Polymer, 42 (2001) 9929-9940.

27. T.D. Fornes, D.L. Hunter, D.R. Paul, Nylon-6 nanocomposites from alkylammonium-modified clay: the role of alkyl tails on exfoliation, Macromolecules, 37 (2004) 1793-1798.

28. T.D. Fornes, P.J. Yoon, D.L. Hunter, H. Keskkula, D.R. Paul, Effect of organoclay structure on nylon 6 nanocomposite morphology and properties, Polymer, 43 (2002) 5915-5933.

29. S. Hotta, D.R. Paul, Nanocomposites formed linear low density polyethylene and organoclays, Polymer, 45 (2004) 7639-7654.

30. M. Kawasumi, N. Hasegawa, M. Kato, A. Usuki, A. Okada, Preparation and mechanical properties of polypropylene-clay hybrids, Macromolecules, 30 (1997) 6333-6338.

31. B.J. Chisholm, R.B. Moore, G. Barber, F. Khouri, A. Hempstead, M. Larsen, E. Olson, J. Kelley, G. Balch, J. Caraher, Nanocomposites derived from sulfonated poly(butylene terephthalate), Macromolecules, 35 (2002) 5508-5516.

32. W. Xie, Z. Gao, W. Pan, D. Hunter, A. Singh, R. Vaia, Thermal degradation chemistry of alkyl quaternary ammonium montmorillonite, Chemistry of Materials, 13 (2001) 2979-2990.

33. C.H. Davis, L.J. Mathias, J.W. Gilman, D.A. Schiraldi, J.R. Shields, P. Trulove, T.E. Sutto, H.C. Delong, Effects of melt-processing conditions on the quality of poly(ethylene terephthalate) montmorillonite clay nanocomposites, Journal of Polymer Science Part B: Polymer Physics, 40 (2002) 2661-2666.

34. J.W. Gilman, W.H. Awad, R.D. Davis, J. Shields, R.H. Harris, C. Davis, A.B. Morgan, T.E. Sutto, J. Callahan, P.C. Trulove, H.C. DeLong, Polymer/layered silicate nanocomposites from thermally stable trialkylimidazolium-treated montmorillonite, Chemistry of Materials, 14 (2002) 3776-3785.

35. D.F. Schmidt, F. Clement, E.P. Giannelis, On the origins of silicate dispersion in polysiloxane/layered-silicate nanocomposites, Advanced Functional Materials, 16 (2006) 417-425.

36. J.I. Weon, H.J. Sue, Effects of clay orientation and aspect ratio on mechanical behavior of nylon-6 nanocomposite, Polymer, 46 (2005) 6325-6334.

37. J. H. Chang, D.K. Park, Nanocomposites of poly(ethylene terephthalate-co-ethylene naphthalate) with organoclay, Journal of Polymer Science Part B: Polymer Physics, 39 (2001) 2581-2588.

38. J.H. Chang, D.K. Park, Various organoclays-based nanocomposites of poly(ethylene terephthalate-co-ethylene naphthalate), Polymer Bulletin, 47 (2001) 191-197.

39. T.M. Wu, C.Y. Liu, Poly(ethylene 2,6-naphthalate)/layered silicate nanocomposites: fabrication, crystallization behavior and properties, Polymer, 46 (2005) 5621-5629.

40. N. Hasegawa, M. Kawasumi, M. Kato, A. Usuki, A. Okada, Preparation and mechanical properties of polypropylene-clay hybrids using a maleic anhydride-modified polypropylene oligomer, Journal of Applied Polymer Science, 67 (1998) 87-92.

41. D.C. Lee, L.W. Jang, Preparation and characterization of PMMA-clay hybrid composite by emulsion polymerization, Journal of Applied Polymer Science, 61 (1996) 1117-1122.

42. M.W. Noh, D.C. Lee, Synthesis and characterization of PS-clay nanocomposite by emulsion polymerization, Polymer Bulletin, 42 (1999) 619-626.

43. Z. Wang, T.J. Pinnavaia, Hybrid organic-inorganic nanocomposites: exfoliation of magadiite nanolayers in an elastomeric epoxy polymer, Chemistry of Materials, 10 (1998) 1820-1826.

44. C. Zilg, R. Mulhaupt, J. Finter, Morphology and toughness/stiffness balance of nanocomposites based upon anhydride-cured epoxy resins and layered silicates, Macromolecular Chemistry and Physics, 200 (1999) 661-670.

45. K. Yano, A. Usuki, A. Okada, T. Kurauchi, O. Kamigato, Synthesis and properties of polyimide-clay hybrid, Journal of Polymer Science Part A: Polymer Chemistry, 31 (1993) 2493-2498.

46. P.B. Messersmith, E.P. Giannelis, Synthesis and characterization of layered silicate-epoxy nanocomposites, Chemistry of Materials, 6 (1994) 1719-1725.

47. L. Chen, S.C. Wong, T. Liu, X. Lu, C. He, Deformation mechanisms of nanoclay-reinforced maleic anhydride-modified polypropylene, Journal of Polymer Science Part B: Polymer Physics, 42 (2004) 2759-2768.

48. K. Wang, L. Chen, J. Wu, M.L. Toh, C. He, A.F. Yee, Epoxy nanocomposites with highly exfoliated clay: mechanical properties and fracture mechanisms, Macromolecules, 38 (2005) 788-800.

49. Y. Kojima, A. Usuki, M. Kawasumi, A. Okada, T. Kurauchi, O. Kamigaito, One–pot synthesis of nylon 6-clay hybrid, Journal of Polymer Science Part A: Polymer Chemistry, 31 (1993) 1755-1758.

50. P. Maiti, M. Okamoto, Crystallization controlled by silicate surfaces in nylon 6-clay nanocomposites, Macromolecular Materials and Engineering, 288 (2003) 440-445.

51. P.H. Nam, P. Maiti, M. Okamoto, T. Kotaka, Foam processing and cellular structure of polypropylene/clay nanocomposites, Proceedings of Nanocomposites 2001, Chicago, Illinois, USA, June 25-27 2001.

52. S.D. Burnside, E.P. Giannelis, Synthesis and properties of new poly(dimethylsiloxane) nanocomposites, Chemistry of Materials, 7 (1995) 1597-1600.

53. Lepoittevin, M. Devalckenaere, N. Pantoustier, M. Alexandre, D. Kubies, C. Calberg, R. Jerome and P. Dubois, Poly(ε-caprolactone)/clay nanocomposites prepared by melt intercalation: mechanical, thermal and rheological properties, Polymer, 43 (2002) 4017–4023.

54. M. Zanetti, G. Camino, R. Thomann, R. Mulhaupt, Synthesis and thermal behavior of layered silicate-EVA nanocomposites, Polymer, 42 (2001) 4501-7.

55. T. Lan, P.D. Kaviratna, T.J. Pinnavaia, On the nature of polyimide-clay hybrid composites, Chemistry of Materials, 6 (1994) 573-575.

56. P.B. Messersmith, E.P. Giannelis, Synthesis and barrier properties of poly(ε-caprolactone)-layered silicate nanocomposites, Journal of Polymer Science Part A: Polymer Chemistry, 33 (1995) 1047-1057.

57. C. Scherer, PA film grade with improved barrier properties for flexible food packaging applications, Proceedings of the New Plastics 1999, London, 2-4 February 1999.

58. D.F. Schmidt, Polysiloxane/layered silicate nanocomposites: synthesis, characterization, and properties, Ph.D. dissertation, Department of Materials Science and Engineering, Cornell University, Ithaca, New York, USA (2003).

59. R.A. Vaia, K.D. Jandt, E.J. Kramer, E.P. Giannelis, Kinetics of polymer melt intercalation, Macromolecules, 28 (1995) 8080-8085.

60. W. Xie, R. Xie, W.P. Pan, D. Hunter, B. Koene, L.S. Tan, R. Vaia, Thermal stability of quaternary phosphonium modified montmorillonites, Chemistry of Materials, 14 (2002) 4837-4845.

61. B.N. Jang, D. Wang, C.A. Wilkie, Relationship between the solubility parameter of polymers and the clay dispersion in polymer/clay nanocomposites and the role of the surfactant, Macromolecules, 38 (2005) 6533-6543.

62. C.M. Koo, H.T. Ham, S.O. Kim, K.H. Wang, I.J. Chung, D.C. Kim, W.C. Zin, Morphology evolution and anisotropic phase formation of the maleated polyethylene-layered silicate nanocomposites, Macromolecules, 35 (2002) 5116-5122.

63. C.M. Koo, S.O. Kim, I.J. Chung, Study on morphology evolution, orientational behavior, and anisotropic phase formation of highly filled polymer-layered silicate nanocomposites, Macromolecules, 36 (2003) 2748-2757.

64. Y. Kojima, A. Usuki, M. Kawasumi, A. Okada, T. Kurauchi, O. Kamigaito, K. Kaji, Novel preferred orientation in injection-molded nylon 6-clay hybrid, Journal of Polymer Science Part B: Polymer Physics, 33 (1995) 1039-1045.

65. T.D. Fornes, D.R. Paul, Modeling properties of nylon 6/clay nanocomposites, Polymer, 44 (2003) 4993-5013.

66. X. Gao, M. Jin, H. Bu, Crystallization of Poly(ethylene 2,6-naphthalate) containing additives, Journal of Polymer Science Part B: Polymer Physics, 38 (2000) 3285-3288.

67. W. Lee (TA Instruments, Singapore), personal communications November 2005 - March 2006.

68. B.B. Sauer, W.G. Kampert, E. Neal Blanchard, S.A. Threefoot, B.S. Hsiao, Temperature modulated DSC studies of melting and recrystallization in polymers exhibiting multiple endotherms, Polymer, 41 (2000) 1099-1108.

69. E.M. Shabana, R.H. Olley, D.C. Bassett, H.G. Zachmann, On crystallization and phase separation phenomena in PEN/PHBA copolyesters, Journal of Macromolecular Science Part B: Physics, 35 (1996) 691-708.

70. L.E. Nielsen, Mechanical properties of polymer and composites, Marcel Dekker, New York (1974) Vol. 2.

71. J.C. Matayabas, S.R. Turner, Nanocomposite technology for enhancing the gas barrier of polyethylene terephthalate, Polymer-Clay Nanocomposites, John Wiley and Sons (2000) 207-226.

72. M. Ito, K. Honda, T. Kanamoto, Two-stage drawing of poly(ethylene 2,6-naphthalate), Journal of Applied Polymer Science, 46 (1992) 1013-1023.

73. V. Kovačević, S. Lučić, M. Leskovac, Morphology and failure in nanocomposites. Part I: Structural and mechanical properties, Journal of Adhesion Science and Technology, 16 (2002) 1343 – 1365.

74. M. Okamoto, S. Morita, H. Taguchi, Y.H. Kim, T. Kotaka, H. Tateyama, Synthesis and structure of smectic clay/poly(methyl methacrylate) and clay/polystyrene nanocomposites via in situ intercalative polymerization, Polymer, 41 (2000) 3887-3890.

75. D. Mckie, C. Mckie, Essentials of Crystallography, Blackwell Scientific Publications, Oxford (1986) 252-264.

76. P. Maiti, P.H. Nam, M. Okamoto, N. Hasegawa, A. Usuki, Influence of crystallization on intercalation, morphology, and mechanical properties of polypropylene/clay nanocomposites, Macromolecules, 35 (2002) 2042-2049.

77. H.G. Haubruge, R. Daussin, A.M. Jonas, R. Legras, Morphological study of melt-crystallized poly(ethylene terephthalate): B. Thin films, Polymer, 44 (2003) 8053-8059.

78. T.N. Blanton, An x-ray diffraction study of poly(ethylene-2,6-naphthalate), Powder Diffraction, 17 (2002) 125-131.

79. Y.H. Ha, Y. Kwon, T. Breiner, E.P. Chan, T. Tzianetopoulou, R.E. Cohen, M.C. Boyce, E.L. Thomas, An orientationally ordered hierarchical exfoliated clay-block copolymer nanocomposite, Macromolecules, 38 (2005) 5170-5179.

80. Y. Kojima, A. Usuki, M. Kawasumi, A. Okada, T. Kurauchi, O. Kamigaito, K. Kaji, Fine structure of nylon-6-clay hybrid, Journal of Polymer Science Part B: Polymer Physics, 32 (1994) 625-630.

81. J.I. Weon, Z. Y. Xia, H. J. Sue, Morphological characterization of nylon-6 nanocomposite following a large-scale simple shear process, Journal of Polymer Science Part B: Polymer Physics, 43 (2005) 3555-3566.

82. N. Sheng, M.C. Boyce, D.M. Parks, G.C. Rutledge, J.I. Abes, R.E. Cohen, Multiscale micromechanical modeling of polymer/clay nanocomposites and the effective clay particle, Polymer, 45 (2004) 487-506.

83. S.S. Ray, P. Maiti, M. Okamoto, K. Yamada, K. Ueda, New polylactide/layered silicate nanocomposites. 1. Preparation, characterization and properties, Macromolecules, 35 (2002) 3104-3110.

84. J. Xiao, Y. Hu, Z. Wang, Y. Tang, Z. Chen, W. Fan, Preparation and characterization of poly(butylene terephthalate) nanocomposites from thermally stable organic-modified montmorillonite, European Polymer Journal, 41 (2005) 1030-1035.

85. N. Vasanthan, D.R. Salem, Structural and conformational characterization of poly(ethylene-2,6-naphthalate) by infrared spectroscopy, Macromolecules, 32 (1999) 6319-6325.

86. Z. Mencik, Crystal structure of polycondensate of naphthalene-2,6-dicarboxylic acid with ethylene glycol, Chemicky Prumysl, 17(1967) 78-83.

87. C.J.M. van den Heuvel, E.A. Klop, Relations between spinning, molecular structure and end-use properties of polyethylene naphthalate tyre yarns, Polymer, 41 (2000) 4249-4266.

88. S. Buchner, D. Wiswe, H.G. Zachmann, Kinetics of crystallization and melting behavior of poly(ethylene-2,6-naphthalenedicarboxylate), Polymer, 30 (1989) 480-488.

89. Y.S. Hu, M. Rugonova, D.A. Schiraldi, A. Hiltner, E. Baer, Crystallization kinetics and crystalline morphology of poly(ethylene naphthalate) and poly(ethylene terephthalate-co-bibenzoate), Journal of Applied Polymer Science, 86 (2002) 98-115.

90. T.M. Wu, C.Y. Liu, Effect of thermal history on the polymorphic behavior of poly(ethylene naphthalate)/clay nanocomposites, Journal of Macromolecular Science – Physics, B43 (2004) 1171-1182.

91. L.J. Mathias, R.D. Davis, W.L. Jarrett, Observation of α and γ crystal forms and amorphous regions of nylon 6-clay nanocomposites using solid-state ^{15}N nuclear magnetic resonance, Macromolecules, 32 (1999) 7958-7960.

92. D.L. VanderHart, A. Asano, J.W. Gilman, Solid-state NMR investigation of paramagnetic nylon-6 clay nanocomposites. 1. Crystallinity, morphology, and the direct influence of Fe^{3+} on nuclear spins, Chemistry of Materials, 13 (2001) 3781-3795.

93. D.M. Lincoln, R.A. Vaia, Z.G. Wang, B.S. Hsiao, Secondary structure and elevated temperature crystallite morphology of nylon-6/layered silicate nanocomposites, Polymer, 42 (2001) 1621-1631.

94. D.M. Lincoln, R.A. Vaia, Z.G. Wang, B.S. Hsiao, R. Krishnamoorti, Temperature dependence of polymer crystallite morphology in nylon-6/montmorillonite nanocomposites, Polymer, 42 (2001) 9975-9985.

95. Q. Wu, X. Liu, L.A. Berglund, FT-IR spectroscopic study of hydrogen bonding in PA6/clay nanocomposites, Polymer, 43 (2002) 2445-2449.

96. D. M. Lincoln, R. A. Vaia, Isothermal crystallization of nylon-6/montmorillonite nanocomposites, Macromolecules, 37 (2004) 4554-4561.

97. T.D. Fornes, D.R. Paul, Crystallization behavior of nylon 6 nanocomposites, Polymer, 44 (2003) 3945-3961.

98. S.S. Nair, C. Ramesh, Studies on the crystallization behavior of nylon-6 in the presence of layered silicates using variable temperature WAXS and FTIR, Macromolecules, 38 (2005) 454-462.

99. H.-D. Wu, C.-R. Tseng, F.-C. Chang, Chain conformation and crystallization behavior of the syndiotactic polystyrene nanocomposites studied using Fourier Transform infrared analysis, Macromolecules, 34, (2001) 2992–2999.

100. I. Ouchi, M. Shimotsuma, Infrared spectra of poly(ethylene 2,6-naphthalate) and some related polyesters, Journal of Applied Polymer Science, 21 (1977) 3445-3456.

101. Y. Shimizu, Y. Ohte, Y. Yamamura, K. Saito, T. Atake, Low-temperature heat capacity of room-temperature ionic liquid, 1-hexyl-3-methylimidazolium bis(trifluoromethylsulfonyl)imide, Journal of Physical Chemistry B, 110 (2006) 13970-13975.

102. X. Gao, R. Liu, Y. Yu, M. Jin, H. Bu, Influence of additives on the crystal structure and melting behavior of poly(ethylene 2,6-naphthalene dicarboxylate), Journal of Polymer Science Part B: Polymer Physics, 42 (2004) 296-301.

103. S.K. Mallapragadan, B. Narasimhan, Infrared Spectroscopy in Analysis of Polymer Crystallinity, Encyclopedia of Analytical Chemistry, John Wiley & Sons (2000) 7644-7658.

104. V. Krikorian, D.J. Pochan, Crystallization behavior of poly(L-lactic acid) nanocomposites: nucleation and growth probed by infrared spectroscopy, Macromolecules, 38 (2005) 6520-6527.

105. R.A. Vaia, R.K. Teukolsky, E.P. Giannelis, Interlayer structure and molecular environment of alkylammonium layered silicates, Chemistry of Materials, 6 (1994) 1017-1022.

106. R.G. Snyder, H.L. Strauss, C.A. Elliger, Carbon-hydrogen stretching modes and the structure of n-alkyl chains. 1. Long, disordered chains, Journal of Physical Chemistry, 86 (1982) 5145-5150.

107. M. Gelfer, C. Burger, A. Fadeev, I. Sics, B. Chu, B.S. Hsiao, A. Heintz, K. Kojo, S.-L. Hsu, M. Si, M. Rafailovich, Thermally induced phase transitions and morphological changes in organoclays, Langmuir, 20 (2004) 3746-3758.

108. Y.C. Chua, X. Lu, T. Wan, Journal of Polymer Science Part B: Polymer Physics, 44 (2006) 1040-1049.

109. P.H. Nam, P. Maiti, M. Okamoto, T. Kotaka, N. Hasegawa, A. Usuki, A hierarchical structure and properties of intercalated polypropylene/clay nanocomposites, Polymer, 42 (2001) 9633-9640.

110. H.G. Haubruge, A.M. Jonas, R. Legras, Staining of poly(ethylene terephthalate) by ruthenium tetroxide, Polymer, 44 (2003) 3229-3234.

APPENDIX A

List of Publications

1. **Yang Choo Chua**, Xuehong Lu, Tong Wan, Polymorphism Behavior of Poly(ethylene naphthalate)/Clay Nanocomposites, Journal of Polymer Science Part B: Polymer Physics, 44 (2006) 1040-1049.
2. **Yang Choo Chua**, Xuehong Lu, Shucheng Wu, Poly(ethylene naphthalate) (PEN)/Clay Nanocomposites Based on Thermally Stable Trialkylimidazolium-Treated Montmorillonite (MMT): Thermal and Dynamic Mechanical Properties, Journal of Nanoscience and Nanotechnology, 6 (2006) 3985-3988.
3. **Yang Choo Chua**, Xuehong Lu, Polymorphism Behavior of Poly(ethylene naphthalate)/Clay Nanocomposites: The Role of Clay Surface Modification, accepted by *Langmuir*.
4. **Yang Choo Chua**, Shucheng Wu, Xuehong Lu, Lin Li, Atomic Force Microscopic Observations on the Crystalline Morphology of Poly(ethylene naphthalate)/Clay Nanocomposites, submitted.
5. Tong Wan, Ling Chen, **Yang Choo Chua**, Xuehong Lu, Crystalline Morphology and Isothermal Crystallization Kinetics of Poly(ethylene terephthalate)/Clay Nanocomposites, Journal of Applied Polymer Science, 94 (2004) 1381-1388.
6. Jiyuan Hao, Xuehong Lu, Songlin Liu, Soo Khim Lau, **Yang Choo Chua**, Synthesis of Poly(ethylene terephthalate)/Clay Nanocomposites Using Aminododecanoic Acid-Modified Clay and a Bifunctional Compatibilizer, Journal of Applied Polymer Science, 101 (2006) 1057-1064.

7. Jiyuan Hao, Xuehong Lu, Songlin Liu, **Yang Choo Chua**, Poly(ethylene terephthalate)/Clay Nanocomposites Based on Aminododecanoic Acid-Modified Clay: Effect of Compatibilizer Reactivity on Clay Dispersion, Journal of Nanoscience and Nanotechnology, 6 (2006) 3981-3984.